Competitive Transport, Extraction and Coordination Chemistry of a Number of Ligands with Selected Transition and Post-Transition Metal Ions

by

Xia Sheng

Thesis submitted in fulfillment of the requirement for the degree of Masters of Science at Stellenbosch University

Supervisor: Robert Luckay

Co-supervisor: Prof. H.G. Raubenheimer

Date: December 2008

Declaration

By submitting this thesis electronically, I declare that the entirety of the work contained therein is my own, original work, that I am the owner of the copyright thereof (unless to the extent explicitly otherwise stated) and that I have not previously in its entirety or in part submitted it for obtaining any qualification.

Date: September 2008

Acknowledgements

Firstly, my deepest appreciation goes to my supervisor, Dr. R. C. Luckay. He gave his endless and willing guidance, advise, support and encouragement not only to my work, but has also helped me to survive in South Africa. I am also very grateful to my co-supervisor Prof. H. G. Raubenheimer for his important discussions, support and financial input.

A special acknowledgement goes to Christoph Strasser, Dr. J. Gertenbach and Dr. L. Dobrzanska for their endless patience in solving some of the difficult crystal structures for me.

I would like to thank every person in the Luckay and Raubenheimer research groups for their company and friendship throughout my stay in Stellenbosch. A special thanks to Dr. S. Cronje, Leigh-Anne de Jongh, Bertie Barnard and Jimmy Sumani for their heart warming friendship and always making me feel at home.

Special thanks to the chemistry department for financial support.

Last but not least, to all my family members for their encouragement and endless love. I would like to express my special gratitude to my parents for their support and encouragement to do my studies in South Africa.

Abstract

The competitive transport, extraction, and coordination chemistry for a series of N-(thio)phosphorylated (thio)amide and N-(thio)phosphorylated (thio)urea ligands were investigated with the seven transition and post-transition metal ions Co(II), Ni(II), Cu(II), Zn(II), Ag(I), Cd(II) and Pb(II). Three N-benzylated derivatives of 1,4,7,10-tetraazacyclododecane (cyclen) were synthesized and a similar study carried out with the same metal ions and the deprotonated precursors. The ligands were all potential specific carriers (ionophores) in the organic phase. The seven metal ions had equal concentrations in the source phase.

The experimental arrangement for the transport studies employed a set-up involving three phases: a source phase and a receiving phase (both aqueous), separated by a chloroform membrane (organic phase). Competitive metal ion solvent extraction involved two phases: an aqueous phase and an organic phase. Similar conditions were used in transport and extraction studies. The metal ion concentrations in the aqueous phases were analyzed by atomic absorption spectroscopy (AAS).

The transport results of deprotonated *N*-(thio)phosphorylated (thio)amides and *N*-(thio)phosphoryated (thio)ureas showed that PhC(S)NPO(OPr*i*)$_2$ (**L1**), BrPhC(S)NPO-(OPr*i*)$_2$ (**L11**) and Pr^{i}NHC(S)NPO(OPr*i*)$_2$ (**L16**) transported Ag(I) into the receiving phase. Under these experimental conditions, **L1** had the highest Ag(I) transport efficiency, at 36.3%, while **L11** only transported one metal ion, viz. Ag(I). With $NH_2C(S)NP(S)(OPr{i})_2$ (**L4**), 94.6% of Ag(I) remained in the membrane phase. Thus **L4** appeared to have the highest formation constant with Ag(I). A small amount of Cu(II) was also transported by **L1**, $NH_2C(S)NP(O)(OPr{i})_2$ (**L9**), **L16** and Bu^{t}NHC(S)-NPO(OPr*i*)$_2$ (**L20**). **L20** had the highest selectivity for Cu(II).

Results of competitive metal ion extraction studies revealed that most ligands extracted up to 100% Ag(I), except **L1** and morpholine substituted ligands (**L7**, **L17**) . The formation constant of **L1** effects a subtle balance between metal uptake and metal loss into and out of the respective membrane phase. **HL7** and **HL17** had low solubility in chloroform. **L4** extracted the highest percentage of Cu(II) (49%).

Two neutral ligands, PhCONHPO(OPr*i*)$_2$ (**1**) and BrPhCONHPO(OPr*i*)$_2$ (**2**) were isolated and their molecular structure determined. They had monoclinic unit cells in

the space groups *C*2/c and $P2_1/n$, respectively. An unprecedented octanuclear $[Ag(I)(\mathbf{L4}\text{-}S,N)]_8$ (**3**) complex was also crystallized. The extended structure showed three different cavities alternating with two unique 16-membered rings, creating a novel AgS_2N_2 cage. Two polynuclear Cu(I) chelates with deprotonated **L4** and **L6** (*t*BuNHC(S)NP(S)(OPr*i*)$_2$) were isolated by the same crystallization method. The complex $[Cu(I)(\mathbf{L4}\text{–}S,S)]_9$ (**4**) consisted of a hexagonal-prismatic hexamer, which exhibited an unusual and unprecedented supramolecular "honeycomb" packing. The trinuclear $[Cu(I)(\mathbf{L6}\text{–}S,S)]_3$ (**5**) consisted of a 6-membered Cu_3S_3 ring attached to a hydroxy tetrahydrofuran molecule.

Di-, tri- and tetra-benzyl-1,4,7,10-tetraazacyclododecane (cyclen) was synthesized, and characterized. None of these compounds was effective in metal transport under these experimental conditions. Nevertheless, Tetra-benzyl cyclen showed the highest extraction efficiency for Ag(I), at 100%, and the highest selectivity for Ag(I) extraction, compared to Cu(II).

An intermediate of dibenzyl cyclen compound dibenzylated dioxocyclen (**6**) was crystallized and found a host THF molecule in the lattice. The crystal and molecular structure confirmed the *cis*-configuration. The X-ray structure of the Cu(II) complex with dibenzylated cyclen (**7**) was determined for the first time. It was found to have an ideal square pyramidal coordination geometry around the central metal ion.

A serendipitous organic compound of isopropylammonium(isopropylamino)-oxoacetate mono-hydrate (**8**) was crystallized. The crystal was held together by inter-molecular hydrogen bonds, which lead to two-dimensional layers with hydrophobic interactions.

Different aspects of the work in this study have been presented in the form of:

Publication:

X. Sheng, C. E. Strasser, H. G Raubenheimer, R. C Luckay – Isopropylammonium (Isopropylamino)oxoacetate monohydrate, *Acta Crys. (2007)*, E63, o4361.

Poster:

Poster presentations by the author at a South African Chemical Institute (SACI) conferences: in July 2007, Inorgic 007, Langebaan (Club Mykonos), South Africa, entitled “Transport, extraction and crystal structures of *N*-thioacylamido(thio) phosphate ligands with metal ions”

List of Abbreviations

Å	Angstrom, 10^{-10} metres
AAS	Atomic Absorption Spectroscopy
BLM	Bulk liquid membrane
Bu	Butyl
Cbz	Benzyl chloroformate
CCDC	Cambridge crystallographic database
$CDCl_3$	Deuterated chloroform
CD_2Cl_2	Deuterated Dichloromethane
CO_2Bn	Benzyloxycarbonyl
CSIRO	Commonwealth Science and Industry Research Organization
D_2O	Deuterium oxide
DOTA	1,4,7,10-tetraazacyclododecane-1,4,7,10- tetraacetic acid
DO3A	Tris N-carboxymethyl-1,4,7,10-tetraazacyclododecane
EDG	Electron donating group
ED-XRF	Energy dispersive X-ray fluorescence
EWG	Electron withdrawing group
ELM	Emulsion liquid membrane
Et	Ethyl
HL	Thiourea ligand
HSAB	Pearson's hard-soft-acid-base principle
ICP-OES	Inductively Coupled Plasma-Optical Emission
Spectroscopy	
IR: *m*	Medium
s	Strong
sh	Shoulder
w	Weak
L	Deprotonated thiourea ligand
M	Metal
MTT	Marine Turbine Technologies
Mp	Melting point
N	Free ligand of benzyl *N*-substitution of cyclen
NMR	Nuclear Magnetic Resonance spectroscopy
NMR: δ	NMR chemical shift in parts per million (ppm)
s	Singlet

	m	Multiplet
	d	Doublet
	br.	Broad
	sept	Septuplet
	ppm	Parts per million
SLM		Supported liquid membrane
TEBA		Triethylbenzylammonium
THF		Tetrahydrofuran
Pr^i		Isopropyl

Contents

Chapter 1

Introduction and objectives

1.1 Membranes

1.1.1 Introduction

A membrane is termed a selectively semi-permeable membrane, when it will allow certain metal ions to pass through it across two phases by a concentration gradient. The membrane contains a suitable ligand (ionophore) to act as the metal ion transporter. There are two generic types of membrane: polymeric membranes and liquid membranes.

Liquid membranes have been widely used in the separation sciences. They are highly selective and with the use of carriers for the transport mechanism, specific metal ion separation can be achieved. The simultaneous extraction and stripping operation is very attractive, because metal ion(s) of interest can be selectively transported from a higher concentration solution to a lower concentration solution by the use of a suitable carrier[1].

Polymeric membranes are membranes that take the form of polymeric interphases, which can selectively transfer certain chemical species over others. Compared to polymeric membranes, liquid membranes produce higher flux and selectivity. The effectiveness of membrane transport is determined by the flux of species through the membrane and by the selectivity of the membrane. This study focuses only on the use of liquid membranes.

There are three types of liquid membranes that are generally employed in the transport of metal ions. These are: bulk liquid membranes, emulsion liquid membranes and supported liquid membranes. Here is a brief overview of the design and set up of these membranes.

Liquid membranes are relatively efficient and as such are being looked into for potential industrial applications in the recovery of metal ions from dilute samples as well as in the treatment of wastewater. Besides these potential applications, there is also a promising avenue for the use of liquid membranes in the biochemical and

biological fields. The use of carriers utilizing proteins, antibiotics, or other molecules naturally found in cell membranes provides a wide area of study for the researcher.

1.1.2 Liquid membranes

1.1.2.1 Bulk liquid membrane

The metal ion transport in the bulk liquid membrane (BLM) systems involves three phases: source phase, receiving phase and membrane phase. The source phase and receiving phase are aqueous phases, which are separated by the organic membrane phase. The ligand is dissolved in a suitable organic solvent, such as chloroform, dichloromethane or a solvent that is denser than water. The cell design and set up employed is the same as that used by Lindoy[2], and is shown in **Figure 1.1**.

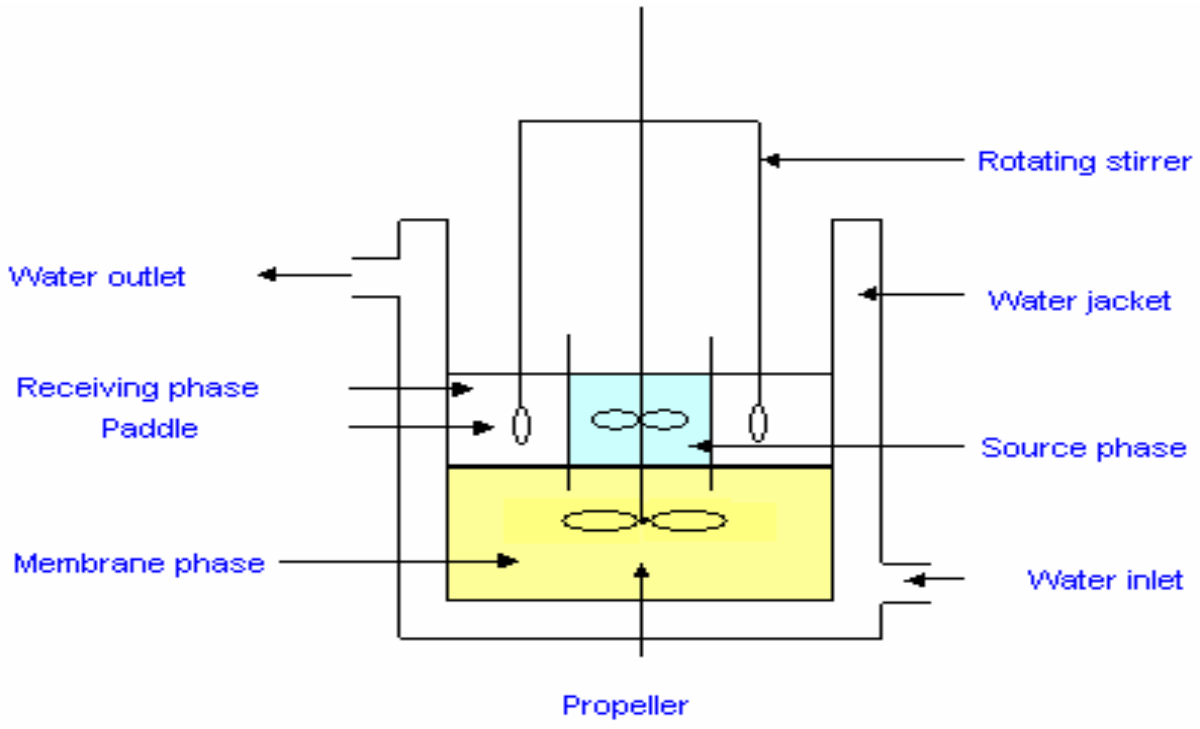

Figure 1.1 Cell diagram for bulk liquid membrane transport setup.

The source phase is placed in the inner concentric cell and the receiving phase surrounds it, with the source phase on top of the membrane phase. The three phases are stirred separately at a low speed (10 rpm in most cases) and this

maintains the stability of the membrane. The concentration of the metal ions transported from the source phase into the receiving phase is determined by spectrometric techniques like inductive coupled plasma (ICP) or atomic absorption spectroscopy (AAS).

The BLMs are used in basic laboratory experiments to indicate potential for separation. The organic (like $CHCl_3$, CH_2Cl_2, etc.) layer is a thick layer of immiscible liquid separating the source and receiving phase. Due to the thick membrane phase, the transport rate is very low, and it is difficult to sort out surface effects in this system. Because of this BLM is not commercially viable and also relatively large standard deviations in data are observed. BLMs are however useful in indicating potential for separation.

1.1.2.2 Emulsion liquid membrane

Emulsion liquid membranes (ELMs) are prepared by dispersing an inner receiving phase in an immiscible liquid membrane phase to form an emulsion. These membranes are also called surfactant liquid membranes. They are very thin and have a large surface area per unit source phase volume, hence, the transport rate is enhanced. Concentrations in the receiving phase are increased significantly, due to the ratio of source phase volume to receiving phase volume, which occurs whenever the organic phase emulsion is added to an even larger quantity of source phase. **Figure 1.2** shows a schematic representation of carrier mediated transport across emulsion liquid membranes.

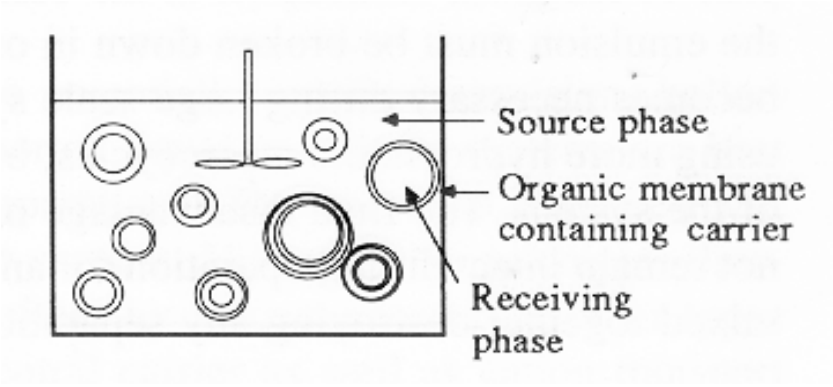

Figure 1.2 Carrier mediated transport across emulsion liquid membranes.

ELM technology refers to the simultaneous extraction, stripping and carrier-mediated transport. The stripping agent is emulsified in the form of fine droplets, with the help of a suitable surfactant, into the membrane phase consisting of a carrier (extractant).

This emulsion is dispersed in the source phase. Metallic elements also dissolve in the source phase and form a complex with the ligand at the interface of the emulsion globule and in the source phase. Afterwards the complex transfers through the organic membrane phase to the membrane-stripping interface and from there it is stripped into the bulk of the encapsulated strip phase. Emulsion stability is maintained by using a moderately hydrophobic membrane solvent and carrier molecules. Furthermore, the ionic strength and pH of the aqueous phases require close monitoring.

The liquid emulsion membrane process is a conventional process. It is a simple operation, has a high efficiency, and a larger interfacial area and scope of continuous operation. However, there are certain industrial disadvantages, all related to the formation of the emulsion.

- Emulsion stability must be controlled, i.e. ionic strength, pH, etc.
- If for any reason the membrane does not remain intact during operation, then the separation achieved to that point is destroyed.
- In order to recover the receiving phase and replenish the carrier phase the emulsion has to be broken. This is a difficult task, since it is already difficult to prepare an emulsion that is stable for storage, furthermore, when working with the emulsion, it must be unstable so that it breaks easily.

1.1.2.3 Supported liquid membrane

Supported liquid membranes (SLMs) are used for the extraction of charged and ionizable compounds. The development of SLMs has reached significant importance for use in separation, purification or analytical applications in areas such as biomedical technology or water treatment[3-6]. SLMs consist of an organic carrier solution immobilized in a thin macroporous polymer film separating two aqueous phases. The organic layer, which plays the role of a membrane, is held in the micropores of a porous membrane by capillary forces and surface tension. The water sample on the donor side of the membrane is maintained at a certain pH, such that the analytes are in their uncharged molecular form and can be extracted into the membrane liquid. On the accepter side is an aqueous solution at a different pH, into which the analytes are extracted.

SLMs show a high efficiency for cation separation owing to molecular recognition processes and they require only a small amount of solubilized organic carriers. This technique offers high analyte enrichment, excellent selectivity, and has been used in large-scale separations. However, for industrial applications, the SLM presents some associated difficulties: e.g. low fluxes, poor mechanical properties and leaching of carriers at membrane interfaces limit the long term stability of the SLM[7,8]. These problems as well as others have until now prevented large-scale applications of liquid membranes in industrial separations.

1.2 Carrier mediated liquid membrane transport and extraction studies using synthetic ionophores

In the past years, a wide range of studies on the selective transport of metal cations through liquid membranes using synthetic ionophores have been carried out. Such ionophores include macrocyclic[9-11] as well as open chain (acyclic) derivatives[12-15] of varying structure and donor atoms. Macrocyclic ligands have been of particular interest to many researchers due to their unique properties such as their capacity to bind selectively to a particular metal ion[16,17] as well as their tendency to form both kinetically and thermodynamically stable metal complexes[18,19]. These studies have employed a systematic variation of the macrocyclic ring size, the donor atoms present, and/or the degree of substitution of the parent ring structure to tune the affinity of these ligands for the specific metal ion(s) of interest[19,20]. For example, macrocyclic crown[21], aza-crown ethers[22] and *N*-benzylated derivatives of cyclam[16] have been extensively used as carriers for the selective transport of transition metal ions as well as heavy metal ions in liquid membranes. However, the complexing ability of crown ethers towards soft heavy metal ions is quite low[23] and therefore, in order to circumvent this problem, some of the oxygen atoms of the crown ethers have been substituted by sulphur atoms. This approach resulted in a high increase in the transport rate of soft metal ions such as Ag(I) and Hg(II). Sulphur containing crown ethers (thiacrown ethers) are hydrophobic and they have high bonding affinities to soft metal ions[24]. Thus, in recent years, some thiacrown ethers have been commonly used as carriers in liquid membrane transport and extraction studies[23,25-27].

Liquid membrane transport and selective extraction of Ag(I) from a mixture of metal ions has also been a subject of interest in the last few years due to the widespread use of silver in different areas of technology and because of its toxicity[28-30]. The

results obtained in such studies vary with the type of ligands and experimental conditions employed. A facilitated counter-transport of Ag(I) and Cu(II) ions, both in acidic thiourea medium across a supported liquid membrane, using di-(2-ethylhexyl)phosphoric acid as carrier, has been investigated[31]. Recently, a study of bulk liquid membrane transport with *N,N*-diethyl-*N'*-camphanyl thiourea[32] and a series of acylthiourea ligands[33] has been published. Ag(I) metal ions are well transported by thiourea ligands.

The fundamental parameters influencing the transport of metal ions include: concentration of ionophore in the membrane phase, pH of the source phase, pH of the receiving phase, metal ion concentration in the source phase, temperature of the system and membrane support characteristics. According to these studies, thiourea can form complexes with Ag(I) and Cu(I) ions which are less mobile than the free metal ions. However, by taking advantage of the optimisation of the different parameters, separation of Ag(I) and Cu(II) in the presence of thiourea can be achieved[33].

1.3 Atomic absorption spectroscopy

1.3.1. Introduction

Atomic absorption spectroscopy (AAS) is an analytical technique used to measure a wide range of elements in materials such as metals, pottery and glass. AAS actually dates back to the nineteenth century, the modern form was largely developed during the 1950s by a team of Australian chemists. They were led by Walsh and worked at the CSIRO (Commonwealth Science and Industry Research Organization) Division of Chemical Physics in Melbourne, Australia[34]. Since then, AAS has become a universal analytical technique for the determination of metallic elements or ions in various applications, such as mining, pharmaceuticals, industry, clinical analysis, environmental analysis and related applications[34].

Although it is a destructive technique (unlike ED-XRF), the sample size needed is very small (typically about 10 mg) and its removal causes little damage. The technique is very sensitive and accurate, and trace elements can be observed down to the parts-per-million level, and the concentration of over 62 different metals in solution can be determined. The technique makes use of the wavelengths of light specifically absorbed by an element. This corresponds to the energies needed to promote electrons from one energy level to another higher energy level. Ions in a sample must undergo three steps to become an atomic gas before analysis:

- Desolvation – the liquid solvent is evaporated, and the dry sample remains.
- Vaporization – the solid sample vaporizes to a gas.
- Volatilization – the compounds constituting the sample are broken into free atoms.

Based on the methods of vaporizing the sample, the technique typically makes use of a flame to atomize the sample, but other atomizers such as a graphite furnace are also used.

Graphite furnace atomic absorption spectroscopy uses a graphite tube with a strong electric current to vaporize the sample. Samples are placed directly into the graphite furnace and the furnace is then heated electrically, in several steps, to dry the sample and then vaporize the analytic atoms or ions in the sample. The graphite furnace has several advantages over a flame. It is a much more efficient atomizer than a flame, and it can directly accept very small absolute quantities of sample. It also provides a reducing environment for easily oxidized elements.

1.3.2 Flame atomic absorption spectroscopy

Flame AAS uses a slot type burner to increase the path length, and therefore to increase the total absorbance according to the Beer-Lambert law (*eq. 1.1*). Sample solutions are usually aspirated with the gas flow into a nebulizing/mixing chamber, to form small droplets before entering the flame. The atomic absorption spectrometer has five major parts: source, collimator, flame, monochromator and detector (**Figure 1.3**).

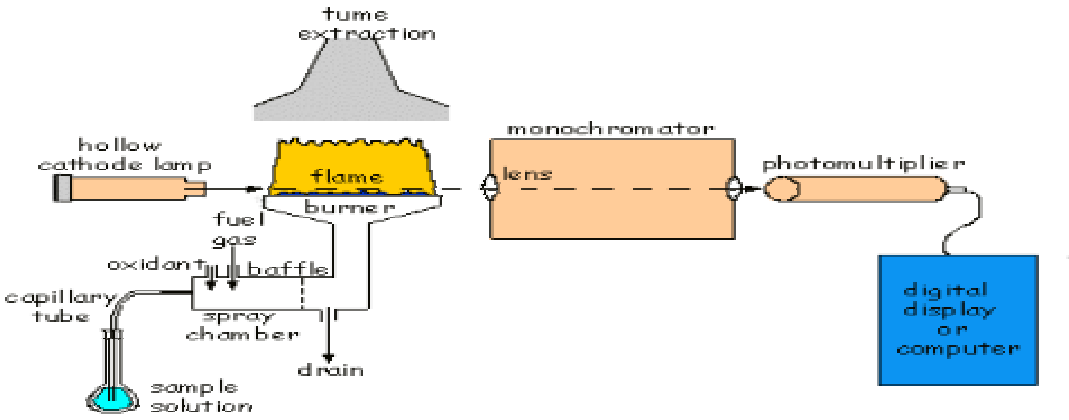

Figure 1.3 Diagram of an atomic absorption spectrophotometer [34].

Different wavelengths absorb at their characteristic wavelength of light. In a typical instrument, several lamps for different atoms are housed in a rotating turret, and the required lamp can be selected. The test sample is dissolved, often in strong acid. The test solution is sprayed into the flame and atomized. The flame is the thermal energy source, which causes the atoms to be energized from the ground state to the first excited state. When the atoms undergo their transition, they absorb some of the light from the beam. So the absorbed light is proportional to the concentration of the atoms in the solution. On the other side, the detector measures the intensity of the light after it has passed through the flame and sample vapour. This difference of intensity to the original light is an indication of the number of light-absorbing atoms in the sample. Measurements are made separately, for each element of interest, to achieve a complete analysis of a sample, and thus the technique is a relatively slow one.

Using the Beer-Lambert law, the AAS analysis curve is plotted as absorbance versus the concentration of standard solution to determine the concentration of metal in the sample. Beer's law states that for a parallel beam of monochromatic radiation passing through homogeneous solutions of equal pathlength the absorbance is proportional to the concentration[34]. As given in equation 1.1:

$$A = \alpha bc \qquad \textit{(eq. 1.1)}$$

Where: A is the absorbance, α is the molar absorptivity, b is the internal cell length and c is the molarity.

1.3.3 Assessment of errors in experimental data

Two types of errors can affect the precision and accuracy of a measured quantity, namely, determinate errors and indeterminate errors.

1.3.3.1 Determinate errors

Determinate errors have a definite source that can usually be identified. They cause all the results from replicate measurements to be either high or low. They are unidirectional, hence, determinate errors are also called systematic errors. The effect of such type of errors may be either constant or proportional. The magnitude of a constant error does not depend on the size of the quantity measured. However, proportional errors increase or decrease in proportion to the size of the sample taken for analysis. The main cause of proportional errors is the presence of interfering contaminants in the sample.

These are three types of determinate error:

- Human errors are the most serious errors for an analyst. Such errors result from the carelessness, inattention, or personal limitations of the experimenter.
- Systematic instrument errors are caused by imperfections in measuring devices and instabilities in their power supplies.
- Method errors arise from non-ideal chemical or physical behaviour of analytical systems.

1.3.3.2 Indeterminate errors

Indeterminate errors, also called random errors, arise when a system of measurement is extended to its maximum sensitivity. They are caused by the many uncontrollable variables that are an inevitable part in every physical or chemical measurement. There are many sources of indeterminate errors, but none can be positively identified or measured because most of them are so small that they are undetectable. The cumulative effect of the individual indeterminate errors, however, causes the data from a set of replicate measurements to fluctuate randomly around the mean of the set.

1.4 The chemistry of *N*-(thio)phosphorylated (thio)amides and *N*-(thio)- phosphorylated (thio)urea ligands

1.4.1 Introduction

N-(thio)phosphorylated (thio)amides (1) and *N*-(thio)phosphorylated (thio)ureas (2) are typical representatives of these general compounds as **HL** (see **Scheme 1.1**). They are attractive compounds because of their ability to form stable chelates with d-group and f-group cations. Some of these complexes possess antiviral and anticancer activity, and show nonlinear optical properties[35]. The ligands and their complexes can be used as extractants, analytical reagents and structural fragments for construction of metal containing macrocycles and polycrown-compunds[36]. *N*-thiophosphoryl thiourea, especially, forms stable chelate complex compounds with soft metal ions and can be used in the development of ion-selective electrodes[39].

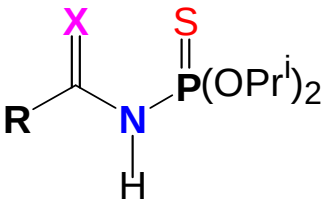

(1)

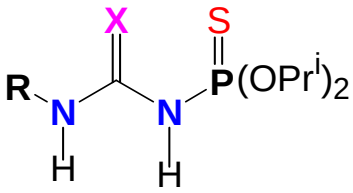

(2)

R = NH_2, C_6H_5, C_4H_8NO, C_5H_5N or alkyl groups, X = S, O

N-(thio)phosphorylated (thio)amides (**HL**) *N*-(thio)phosphorylated (thio)ureas (**HL**)

Scheme 1.1 General structures of the free ligands, **HL**.

1.4.2 Ligand synthesis, properties and conformation

The chemistry of phosphane derivatives of urea and thiourea was first studied during the 1960s[38]. Subsequently, the related bidentate organophosphorus ligand systems were developed to form $R^1C(X)NHPR^2$ and their derivatives[36]. Different $R^1C(X)NHP(Y)R^2R^3$ ligands (R^1 = R-NH or NZ_2 with Z = H, alkyl or aryl; R^2, R^3 = alkyl, aryl, alkoxy or aryloxy; X, Y = O, S or Se) have been reported[39]. Despite the different tautomeric forms that exist infrared studies on some of them support the presence of structures in which two double bonds, C=S and P=S, are present[38]. Delocalization within the C-NH-P unit has been found as more representative of the bonding in the crystal structures[38,39]. It is known that *N*-(thio)phosphoryl thioureas in aqueous alcohol medium are weak acids. The acid dissociation constants (pK_a) have been reported to be in the range 6.9–10.8[40,41].

The interaction between phosphorus(IV)dithio acid partial esters and thiocyanates proceeds with initial formation of addition products to the C=N bond. These adducts are either split by the second molecule of a dithio acid to S-alkyl dithiocarbamates and tetraalkyl trithiopyrophosphates or rearranged into dialkyl *N*-thiophosphoryldithiocarbamates. The latter easily split off the thiols and convert to isothiocyanatothiophosphates. A number of thiophosphorylated and diphosphorylated thioureas have been synthesized by the reaction of isothiocyanatothiophosphates with amines and α-aminoalkylphosphonates[42].

According to the literature, all these ligands have been synthesized by the Russian group of Zabirov and coworkers[42,43]. Dialkyl esters of isothiocyanatothiophoric acid were added with amines, including α-aminophosphonates, yielding thiophosphorylthioureas which are readily identified.

1.4.3 Coordination chemistry of these ligands

N-(thio)phosphorylated (thio)amides and *N*-(thio)phosphorylated (thio)ureas have been widely applied in coordination chemistry. Some close analogues of these ligands are also known to form complexes with a variety of transition metals, both soft and hard, and alkaline and alkaline-earth metals[44]. The ligands used include anionic mixed-donor acyclic compounds, oxygen-nitrogen donors and thioether donors. The bidentate six-membered chelate ring is formed through the partial conjugate system of S(or O)-P-N-C-S(or O), as is shown in **Scheme 1.2**.

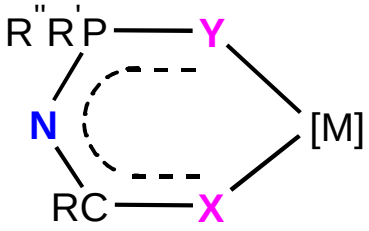

R, R', R''= NH_2, C_6H_5, C_4H_8NO, C_5H_5N or OPr^i; X, Y = S, O; [M] = Ni, Co, Pt, Pd, Zn, Cd.

Scheme 1.2

The crystal structures were reported with Co(II)[35],Cu(I) [44], Ni(II), Zn(II), Cd(II), Pb(II)[38], Ag(I) and Au(III)[39], as well as for K and Na[45]. Mononuclear hexacoordinate compounds have also been prepared from the reactions of different ligands with $SnCl_4$, although the geometries were not confirmed by X-ray studies[38]. Such stoichiometry is the most common among the transition metal complexes described to date[39].

Herrmann *et al.*[46] reported a crystal study of the complex $\{Cu(I)[(C_6H_5O)_2P(S)NC(S)N\text{-}(C_2H_5)_2]\}_3$ in which the metal has trigonal planar geometry. In their preparation Cu(II) is reduced to Cu(I). This trinuclear structure forms a $[Cu_3S_3]$ six-membered ring. In 1999, Birdsall and coworkers[38] reported the first example of a six-membered covalent "true" heterocyclic structure, $Cu(O)C(Ph)NP(S)Ph_2)PPh_2$. The chelate ring occurred in a non-planar pseudo boat conformation ring.

Other representative compounds include the potassium complexes in which the metal atoms are bonded to the sulphur atoms of $(OiPr)_2P(S)NHC(S)Ph$. The potassium atom can be in the centre of a diaza-18-crown-6 cycle, or as part of a more complicated structure[43]. These ligands chelate to transition metal ions through

both phosphorus and chalcogen donor atoms. They are bipodal (thio)phosphorylated thioureas $[(i\text{PrO})_2\text{P(X)NHC(S)NH}]_2$, X=O,S.

The chemistry of chelating ligands attached to metal centers through sulphur atoms has been investigated extensively[39]. The interest in these compounds was stimulated by the promotion of unusual coordination at the metal and/or the interesting stereochemistry of the chelate ring. Deprotonated thiophosphinyl thioureas, $R_2P(S)NC(S)NR'R''$, hold an intermediate position by forming chelate rings with five different atoms in the six-membered carbon-free chelate ring[38-47].

1.4.4 Applications of these ligands

N-(thio)phosphorylated (thio)amides and *N*-(thio)phosphorylated (thio)ureas are known to form complexes with a variety of metals, both soft and hard. Many complexes of transition and alkaline metals with these types of ligands have been reported[44]. Among them, the coordination chemistry of *N*-(thiophosphoryl) thioamides or *N*-(thiophosphoryl)thioureas has been studied and extraction of metals using *N*-[bis(isopropoxy)thiophosphoryl]thiobenzamide has been reported[48]. A liquid ion-selective electrode for the determination of mercury has been used these ligands[39]. *N*,*N*-dialkyl-*N'*-aroylthioureas have been exploited for the convenient HPLC determination of platinum group metals (PGMs), and they have been used to transport Ag(I)[32]. Crown-ethers and azamacrocycles modified by exocyclic groups are widely applied as complexing agents, that are selective for cations of alkaline, alkaline-earth, d-metals, lanthanides and actinides, as well as Tl(I)[44]. They have unusually high redox stability and favourable toxicological properties, which make them important for industrial applications[38]. Some of these applications include: the removal of harmful toxic compounds from organisms and for the detoxification of waste waters containing heavy metals. These ligands also find potential applications in the solvent extraction[39] and chromatographic separation of PGMs, as well as several 'soft' transition metal ions, notably Cu(I), Hg(II) and Au(III)[50].

1.5 The chemistry of benzylated *N*-substitution of 1,4,7,10-tetraazacyclo-dodecane (cyclen) ligands

1.5.1 Introduction

The synthesis of structurally reinforced macrocyclic polyamines and their metal complexes has recently been studied in areas such as molecular recognition and bio-inorganic chemistry[51]. Numerous structurally reinforced macrocyclic polyamines have been studied, but backbone carbon functionalized versions are less common[52]. Macrocyclic polyamines and their metal complexes containing axial ligands have attracted considerable attention because of their structures and chemical properties, which are often quite different from those of uncoordinated axial ligands. One of the most important ligands is 1,4,7,10-tetraazacyclododecane (cyclen), which is used as a model for protein-metal binding sites in biological systems, and as a selective complexing agent for metal ions[53].

1.5.2 Ligand synthesis, properties and conformation

Mixing different pendent groups, especially hydrophilic and hydrophobic groups, to give hetero-substituted cyclen derivatives would be advantageous for fine-tuning the compound's physical properties, for specific applications[54,55]. Structure–activity relationships (SARs) based on the selective modification of structure is well known to be a powerful strategy in new drug development. With coordination complexes of cyclen, the number of acetate groups (CH_2CO_2) introduced onto the nitrogen atoms has a huge effect on the coordination geometry and final formal charge under physiological conditions; it affects both the thermodynamic stability and kinetic inertness[56]. Small changes in the structure can result in huge differences in physiological properties of medicinal agents. The potential and versatile applications have stimulated research into the synthesis of novel cyclen-based ligands with varying types and numbers of pendent arms in attempts to find new ligands that have different chemical, biological or catalytic applications.

A selective method for the *N*-substitution of cyclen is a crucial step in most syntheses of cyclen-based ligands and bifunctional chelating agents. To obtain different substitution patterns, generally a strategy of regioselective protection/1st alkylation/deprotection/2nd alkylation is utilized. Direct functionalization and cyclization of *N*-alkylated precursors can be applied in some instances, but generally a protection/ functionalization/ deprotection method is more reliable and efficient[57].

The protecting groups used are required to be introduced regioselectively among the four identical nitrogen atoms of cyclen in high yield, and easily cleaved in mild reaction conditions without attacking other functional groups[58]. A tri-protected cyclen compound has been reported by Yoo *et al.*[59] which is prepared by the reaction of cyclen and a higher excess of chloral hydrate without difficulties. The benzyl chloroformate (Cbz) protection group has been introduced to tri-alkylated cyclen derivatives[59]. In basic environment the stability of Cbz is different than of the chloral hydrate protection group. Hence it could be deprotected step-by-step. Two disubstituted cyclen isomers, *cis*- and *trans*-dialkylated cyclen derivatives, were successfully prepared in high yield using diethyl oxlate[60].

N-Benzylated cyclen derivatives have the benzyl electron withdrawing group (EWG). They change the electronic structure of the cyclen ring. Mono-, di-, tri- and tetra-*N*-substituted cyclen compounds decrease the proton density. Hence, the different selectivity with metal ions will be studied here.

1.5.3 Applications of these ligands

Current interest in the regioselective *N*-functionalization of 1,4,7,10-tetraazacyclododecane (cyclen) stems mainly from their complexes with radioactive metals for applications in diagnostic medicine (^{64}Cu, ^{111}In, ^{67}Ga) and therapeutic (^{90}Y) medicine[61]. Since the discovery of the Gd(III) complex of 1,4,7,10-tetraazacyclododecane-1,4,7,10-tetraacetic acid (DOTA) and a growing interest in macrocyclic heptacoordinate Ln^{3+} complexes, especially the tris *N*-carboxymethyl-1,4,7,10-tetraazacyclododecane (DO_3A) derivatives, as efficient contrast agents (CAs) for magnetic resonance imaging (MRI)[62]. Most recently, tetraazamacrocycles have found applications as NMR shift and relaxation reagents[62,63] and as RNA cleavage catalysts[63-65] in medicine for anti-tumor[66] and anti-HIV agents[67]. Kong *et al.*[53] describe the synthesis of a new type of cyclen-based ligand with four benzyl groups at the N atoms. Its Co(II), Ni (II) and Cu(II) complexes show high anti-tumor activities in an MTT assay HL-60 tumor cell lines[53].

1.6 Objectives

Metal ion transport and extraction using macrocyclic and open-chain polydentate ligands have attracted interest in recent years. Selective metal ion extraction is a topic of wide commercial interest. Industries require selective and efficient transporting/extracting agents for the recovery of precious and toxic metal ions from industrial effluents. There is published literature on studies of bulk liquid membrane (BLM) transport and extraction of some transition and post transition metal ions using certain ligands as carriers (ionophores) in the membrane phase. This project focuses on the examination of such ionophores including the series of *N*-(thio)phosphorylated (thio)amide and *N*-(thio)phosphorylated (thio)urea, and the synthesis of benzyl *N*-substituted cyclen ligands. It was envisaged that results of this study would contribute towards the design and synthesis of more efficient, selective and commercially viable ligands that will meet the demands of industry.

In the first part of the study, we will investigate the transport, extraction efficiency and selectivity of a series of ligands. Twenty-six *N*-(thio)phosphorylated (thio)amide and *N*-(thio)phosphorylated (thio)urea ligands were to be used as ionophores in the BLM. We preferred these ligands mostly because of their interactions with Ag(I) or Cu(II). The transport efficiency and selectivity of these ligands were examined using a source phase at pH 5.5 and a receiving phase at pH 1.0. Furthermore, competitive solvent extraction involving these ligands will be studied, in order to confirm the selectivity and efficiency with metal ions. A comparison of the transport and extraction results with similar substituted groups will be done, in order to determine the effect of the different constituent functional groups on the transport and extraction behaviour.

In the second part of the study, the X-ray structures of the Ag(I) and Cu(II) complexes will be determined and discussed, in order to further understand the coordination chemistry with these ligands. We planned to grow crystals of the neutral ligands, so that they could be compared with the metal complex structures.

In the third part of the study, di-, tri-, and tetra-benzyl-1,4,7,10-tetraazacyclo-dodecane (cyclen) will be synthesized and characterized by ^{1}H and ^{13}C NMR spectroscopy, and mass spectrometry. The transport and extraction behaviour of these ligands with Ag(I) and Cu(II) were to be determined. Finally, an attempt to investigate the coordination chemistry of these ligands by using crystal structures of some of the intermediates and metal complexes will be determined.

Chapter 2

Experimental

2.1 Competitive transport and extraction

2.1.1 Reagents

Reagent grade $AgNO_3$, $Cu(NO_3)_2 \cdot 3H_2O$, $Cd(NO_3)_2 \cdot 4H_2O$, $Zn(NO_3)_2 \cdot 6H_2O$, $Co(NO_3)_2 \cdot 6H_2O$, $Ni(NO_3)_2 \cdot 6H_2O$ and $Pb(NO_3)_2$ salts were all obtained from Merck and used without further purification. Analytically pure (AR-grade) chloroform (Merck) was used in all transport and extraction experiments. AR-grade HNO_3 (55% w/v) after proper diluting, was used as a receiving (stripping) solution in the transport experiments. Reagent grade acetic acid and sodium acetate were used in the preparation of buffer solutions. All aqueous solutions were prepared using deionized water.

2.1.2 Preparation of solutions

The source phase buffer solution (pH = 5.5) was prepared using CH_3COOH/CH_3COONa, at 25 ^oC:

$$pH = pK_a + \log([CH_3COONa] / [CH_3COOH]) \qquad pK_a = 4.74 \qquad \text{(eq. 2.1)}$$

From eq. 2.1, if 13.91 x 10^{-3} mol (1.8915 g) sodium acetate was required, 2.42 x 10^{-3} mol acetic acid was required to prepare the buffer solution in 100 ml distilled water. The metal ions solution was prepared by using the nitrate salts of the seven metal ions (see **Section 2.1.1**) in the buffer solution (pH 5.5, 100 ml). The final concentration of each metal ion was $1x10^{-2}$ mol dm^{-3}. These solutions were used as source phases in the transport and extraction experiments.

The aqueous receiving phase used in the transport experiments was a solution of 0.1 mol dm^{-3} HNO_3 diluted from 1 mol dm^{-3} HNO_3 with deionized water in a 1 L volumetric flask. The concentration was confirmed using a Corning 425 pH meter.

The chloroform membrane in the transport experiments contained 2 x 10^{-3} mol dm^{-3} ligand and 4 x 10^{-3} mol dm^{-3} palmitic acid. This comprised the organic phase in the transport and extraction experiments.

A Corning 425 pH meter with a combination glass electrode was used to measure the pH values of the buffer solutions. It was calibrated before use by using pH 4.0 and pH 7.0 standard buffer solutions.

2.1.3 Bulk liquid membrane transport experiments

Brief mention was made of bulk liquid membrane (BLM) transport in **Section 1.1.2.1** and the setup shown schematically in **Figure 1.1**. The metal ion transport experiment is a convenient and efficient way of assessing ionophores capability within a series of ligands.

The transport cell was first soaked in concentrated HNO_3 overnight, rinsed with distilled water, dried with acetone, and covered. A volume of organic membrane phase (50 ml) was gently transferred into the bottom of the cell. A volume of source phase solution (10 ml) was thereafter transferred into the central cell. Finally 30 ml aqueous receiving phase was gently placed on the outside of the central cell. Under these conditions, the interfaces between the organic membrane and the two aqueous phases remained flat and well defined. The cell was covered with cover slips to prevent evaporation and obstructions from surrounding dust. The whole system was entirely covered by aluminium foil in order to prevent the light-induced reduction of Ag(I) in the aqueous solution. The experimental temperature was kept at 25 ℃ using a combination water bath pump. All the phases were stirred at 10 rpm by a coupled single geared synchronous motor. The transport experiment runs were terminated after 24 h and the amount of metal ion transported to the receiving phase determined. The amount that remained in the source phase over this period was determined by AAS. Each experiment was done in duplicate and run in parallel. Aqueous solution samples (1 ml) were diluted with 0.1 mol dm^{-3} HNO_3 in a 100 ml volumetric flask. The standards were prepared using the same method as described for diluting the source phase, which is the same as described in **Section 2.1.2**.

The average flux rate, J (mol/h), for each transport experiment was calculated based on the quantity of metal ions transported into the receiving phase in a 24-hour period. The transport results are quoted as the average values obtained from the duplicate runs in all cases. J values equal to or less than 2.2×10^{-8} mol/24 h were assumed to be within experimental error of zero and have been ignored in the analysis of the results.

2.1.4 Competitive metal ion extraction

The chemical reagents of liquid-liquid extraction were identical with those used in the transport experiments above. The source phase contained the seven metal ions Co(II), Ni(II), Cu(II), Zn(II), Ag(I), Cd(II) and Pb(II) as their nitrate salts. Each metal ion was present in an equi-molar concentration of 0.01 mol dm^{-3} in a CH_3COOH/CH_3COONa buffer of pH 5.5. The organic phase contained 2×10^{-3} mol dm^{-3} ligands in chloroform. The chloroform membrane (15 ml) was placed in a polytop, and to this was added aqueous metal ion phase (3 ml) on the top. According to the extraction procedure metal ions are competitively extracted from the aqueous phase into an organic membrane phase. The vial was capped tightly and wrapped with parafilm. Each experiment was done in triplicate, in different polytops. All the polytops were covered with aluminium foil to prevent light-induced reduction of Ag(I). The vials were shaken at 120 cycles per minute for 24 h on a Labcon oscillating shaker at 25 ℃. AAS was used to analy ze the metal ions in the aqueous phase after shaking. The results were quoted as the average value from the three sample vials.

2.2 Synthesis of Ag (I) and Cu(I) complexes

All reagents were commercially available and used without further purification. Melting points were determined using a Gallenkamp melting point apparatus in open capillaries. All ^{1}H and ^{13}C nuclear magnetic resonance spectra were measured at 25 ^{o}C in 5 mm NMR tubes in $CDCl_3$ solution. The chemical shifts (δ) were referenced to tetramethylsilane (TMS) as an internal standard. The instruments used were a Varian Unity 300 and INOVA 600 spectrometer operating at 300 MHz and 600 MHz for proton spectra or at 75 and 150 MHz for ^{13}C spectra. Their purity were checked using melting point determination, ^{1}H and ^{13}C NMR spectroscopy, and mass spectrometry.

2.2.1 Preparation of $[Ag(I)(L4\text{-}S,N)]_8$ (3)

The first step involves the formation of a complex of potassium salt with **L4**. To a solution of **L4** (0.034 g, 0.20 mmol) in THF (5 ml) was added KOtBu (0.74 g, 0.66 mmol). After stirring overnight, the solution was filtered through celite, and then reduced to dryness to yield a white powder, K**L4**. A solution of $AgNO_3$ (0.067 g, 0.20 mmol) in distilled water was added dropwise to K**L4** in CH_2Cl_2 (5 ml). After 1 h stirring, the solution was filtered through celite and reduced to dryness. The complex

was recrystallised fromTHF/pentane (1:1) to yield 0.073 mg product, 96%. The colourless crystals were grown by slow evaporation in a closed bottom glass pipette at 4 ℃ (refrigerator) for one month. Mp: 121–123 ℃.

2.2.2 Preparation of [Cu(I)(L4-*S,S*)]$_9$ (4)

Compound 4 was prepared by mixing a suspension of **L4** (0.026 g, 0.10 mmol) in aqueous ethanol (15 ml), then mixed with an ethanol solution of potassium hydroxide (0.0084 g, 0.15 mmol) and stirring for 1 h. A solution of $CuNO_3 \cdot 6H_2O$ (0.019 g, 0.060 mmol) in water (5 ml) was added dropwise, whilst stirring. The mixture was stirred at room temperature for 6 h and left overnight. The resulting complex was extracted with CH_2Cl_2 and dried over anhydrous $MgSO_4$. The solvent was removed under vacuum. A residue of colourless, needle-shaped crystals was obtained. Yield: 80%. Mp: 181–182 ℃.

2.2.3 Preparation of [Cu(I)(L6-*S,S*)]$_3$ (5)

This complex was prepared according to the method described above for the Cu**L4**, using the following reagents: **L6** (0.31 g, 0.10 mmol), potassium hydroxide (0.0084 g, 0.15 mmol) and $CuNO_3 \cdot 6H_2O$ (0.019 g, 0.060 mmol). The colourless, flat crystals were obtained from a THF solution after it stood for one month. Yield: 82%. Mp: 53–54 ℃

2.3 Synthesis of three *N*-benzylated cyclen derivatives and Cu(II) complexes

All reagents were commercially available and used without further purification. Melting points were determined using a Gallenkamp melting point apparatus in open capillaries. All ^{1}H and ^{13}C nuclear magnetic resonance spectra were measured at 25 ^{o}C in 5 mm NMR tubes in $CDCl_3$ solution. The chemical shifts (δ) were referenced to tetramethylsilane (TMS) as an internal standard. The instruments used were a Varian Unity 300 and INOVA 600 spectrometer operating at 300 MHz and 600 MHz for proton spectra or at 75 and 150 MHz for ^{13}C spectra. Although *N*-benzylated cyclen derivatives have been previously characterized, however, their purity were checked using melting point determination, ^{1}H and ^{13}C NMR spectroscopy, and mass spectrometry.

2.3.1 Preparation of 1,4-dibenzyl-1,4,7,10-tetraazacyclododecane (N2)

Cyclen (1.7 g, 10 mmol) was dissolved in 10 ml dry ethanol, and diethyl oxalate (4.2 g, 20 mmol) was added. The reaction mixture was stirred for 48 h. Thin layer chromatography (TLC) was used to follow the reaction so as to indicate whether the reaction was complete ($CHCl_3$: isopropylamine, 5:1). A white solid was formed (yield 85.6%), R_f: 0.2. The ^1H and ^{13}C NMR spectra confirmed the results which are the same as those previously published[60].

Cyclenoxamide (2.1 g, 8.0 mmol) in 10 ml DMF was treated in the presence of Na_2CO_3 (1.9 g, 18 mmol) and benzyl chloride (2.3 g, 18 mmol). The reaction mixture was stirred for 6 h at 100 ℃. After removal of the solvent under reduced pressure, the residue was dissolved in dichloromethane and filtered to yield a yellowish white solid (yield 98%). The ^1H and ^{13}C NMR spectra confirmed the results which are the same as those previously published[60].

Disubstituted cyclenoxamide was dissolved in distilled water (5 ml) and NaOH (10 mol dm^{-3}, 5ml) was added. The reaction mixture was stirred at 90 ℃ overnight. The product was extracted with dichloromethane. The solvent was removed under reduced pressure to yield a white solid (yield 88%). The products were confirmed by NMR and MS.

2.3.2 Preparation of 1,4,7-Tris(benzyl)-1,4,7,10-tetraazacyclododecane (N3)

A mixture of cyclen (1.7 g, 10 mmol) and chloral hydrate (9.9 g, 60 mmol) was dissolved in ethanol (30 ml) with stirring at 60 ^oC for 4 h. The solution was thereafter dissolved in 30 ml distilled water, and the pH was measured at approximately 9 by using pH paper. Benzyl chloroformate (1 ml) was added under nitrogen and the reaction was stirred for 1 h. The pH was adjusted to 10 from 4 by using saturated Na_2CO_3 solution. A second portion of benzyl chloroformate (1 ml) was then added under nitrogen. After 1 h of stirring, the reaction solution was adjusted to pH 10 again and the third 1 ml portion of benzyl chloroformate added. The reaction was left to stir overnight. The aqueous solution was extracted with methylene chloride (4×20 ml). The combined organic layer was washed with saturated $NaHCO_3$ and dried over anhydrous $MgSO_4$. This was concentrated under vacuum to give a clear light yellow oil. The ^1H and ^{13}C NMR spectra confirmed the results which are the same as those previously published[59].

1-(Benzyloxycarbonyl)-1,4,7,10-tetraazacyclododecane·3HCl: 1,4,7-triformyl-10-(benzyloxy-carbonyl)-1,4,7,10-tetraazacyclododecane (0.731 g, 1.87 mmol) was dissolved in HCl (40 ml, 1 mol dm^{-3}) solution and the solution was stirred in a closed round bottom flask at 50 ℃ for 5 h. The solvent was evaporated completely under vacuum at 60 ℃ to give a white solid. The crude product was refluxed in ethanol (20 ml), cooled to room temperature, filtered, washed with ether (5 ml), and dried in air. Excess ether was added to the ethanol filtrate until the solution became cloudy. The precipitated white powder was collected, washed with a small amount of ether, and dried in air as a second crop (yield 90%). The ^{1}H and ^{13}C NMR spectra confirmed the results which are the same as those previously published[59].

1-(Benzyloxycarbonyl)-4,7,10-tris(benzyl)-1,4,7,10-tetraazacyclododecane: N,N-diisopropyl-ethylamine (5.9 ml, 33.6 mmol) was added to 1-(Benzyloxycarbonyl)-1,4,7,10-tetraazacyclo-dodecane·3HCl in 40 ml chloroform. Benzyl bromide (5.8 g 34 mmol) was added to the solution dropwise at room temperature. The reaction mixture was slowly heated to 60 ℃ with stirring and allowed to react for 15 h. The solvent was removed under vacuum. The crude product was dissolved in toluene (5 ml) and excess hexane was added to form a white precipitate, which was washed with ether to give an 80% yield of white powder. The ^{1}H and ^{13}C NMR spectra confirmed the results which are the same as those previously published[59].

In a three-necked round bottom flask, to a solution of 1-(Benzyloxycarbonyl)-4,7,10-tris (benzyl)-1,4,7,10-tetraazacyclododecane in 30 ml of absolute ethanol was added 10% Pd/C (0.25 g, 87%). The reaction mixture was stirred under hydrogen gas at atmospheric pressure for 24h. The Pd catalyst was filtered off using celite and the filtrate was concentrated under vacuum to give a white solid product (yield 87%). The products were confirmed by NMR and MS[59].

2.3.3 Preparation of 1,4,7,10-tetrabenzyl-1,4,7,10-tetraazacyclododecane (N4)

Cyclen (0.17 g, 1.0 mmol) was suspended in CH_2Cl_2 (5 cm^3). $PhCH_2Cl$ (0.51 g, 4.0 mmol) was added dropwise to a solution of excess NaOH (0.32 g, 8.0 mmol) at room temperature. To the stirred solution was added TEBA (0.23 g, 1.0 mmol) as catalyst in water (6 cm^3) as catalyst. The reaction was monitored by TLC until the $PhCH_2Cl$ disappeared after 4 days. The resulting solution was extracted with CH_2Cl_2 (3 × 5 cm^3), and the combined CH_2Cl_2 extracts were dried with anhydrous Na_2SO_4. After filtration the filtrate was evaporated to dryness and a white solid was obtained. The

crude product was recrystallized from CH_2Cl_2–EtOH (3:5) to give white crystals (yield 54%.) m.p. 149-150 ℃. The products were confirmed by NMR and MS.

2.3.4 Preparation of dibenzylated cyclen Cu(II) compound (7)

A methanol solution of $Cu(ClO_4)_2 \cdot 6H_2O$ (0.037 g, 0.10 mmol) was added to a methanol solution (3 ml) of the ligand **N2** (0.035 g, 0.10 mmol). The mixture was refluxed for 1 h. After cooling, the precipitate was recrystallized in CH_3CN (yield 75%). Blue, flat crystals were obtained. m.p: 108-109 ℃.

2.4 X-ray structure determinations

Crystal data collection and refinement details of compound **6**, **7** and **8** are summariesed in **Table 6.9**. Data sets were collected on Bruker SMART Apex CCD diffractometer with graphite monochromated MoKα radiation (λ = 0.71073 Å)[68]. Data reduction was carried out with standard methods using the software package Bruker SAINT and data were treated with SADABS[69–71]. All the structures were solved using direct methods or interpretation of a Ptterson synthesis, which yielded the position of the metal atoms, and conventional difference Fourier methods. All non-hydrogen atoms were refined anisotropically by full-matrix least square calculation on F^2 using SHELX-97[72] within an X-seed environment [73,74]. They hydrogen atoms were fixed in calculated positions. Figures were generated with X-seed[73] and POV Ray for Windows, with the displacement ellipsoids at 50% probability level unless stated otherwise.

Chapter 3

Competitive metal ion bulk membrane transport studies involving *N*-(thio)phosphorylated (thio)amide and *N*-(thio)phosphorylated (thio)urea ligands

3.1 Introduction

The *N*-(thio)phosphorylated (thio)amide and *N*-(thio)phosphorylated (thio)urea (**HL**) ligands (**Appendix 1**) were supplied by the Russian group of Zabirov. They had been fully characterized and the pure samples were supplied to us. Recently these ligands have been extensively used for coordination chemistry, because the bidentate chelates with the '*S,S*', '*S,O*' or '*O,O*' donor atoms, form especially stable chelate complex compounds with soft metal ions and can be used in the development of ion-selective electrodes. The substituted groups with thiourea affect the chemical properties of the ligands, and hence they have been employed to study the bulk liquid membrane transport and solvent extraction. The properties, conformations, coordination and some applications of these ligands were described in **Section 1.4**.

In this chapter, a comparative study of the transport properties of various thiourea ligands (**Appendix 1**) with a number of transition and post transition metal ions is presented. The seven metal ions in solution are Co(II), Ni(II), Cu(II), Zn(II), Ag(I), Cd(II) and Pb(II), as their nitrate salts.

The ligands are grouped into seven sections according to their structural similarities. The results and discussion of the results obtained for each group of ligands is presented after each section. Finally, conclusions are drawn concerning the overall transport results that are obtained.

3.1.1 Theoretical background

A schematic illustration of the mechanism of bulk membrane transport is shown in **Scheme 3.1**. A source phase pH of 5.5 and a receiving phase pH of 1.0 are adopted as optimum conditions with the ligand concentration at 2×10^{-3} mol dm^{-3}. These are the same conditions as used for similar ligands by Habtu *et al.*[33] At the interface of the source phase / organic phase, the metal in the source phase is in contact with the ligand in the organic phase. The deprotonated ligand combines with the metal ion to

form a neutral complex at the surface. The metal-ligand complex diffuses into the organic phase, until it comes to the membrane/ receiving phase interface. Because the receiving phase is more acidic, the ligand is now protonated and the metal ions are released into the receiving phase. This process is called "stripping". The protonated ligands then diffuse back across the membrane to the source phase / membrane phase interface to repeat the cycle. The direction of the proton transport is in the opposite direction to that of the metal ions. Palmitic acid (4×10^{-3} mol dm^{-3}) has also been used to perform two important roles: keeping a lipophilic counter ion in the organic phase for charge neutraliszation of the metal cation being transported; preventing hydrophilic nitrate anions into the organic phase. However, metal ion transport can be driven past the 50% mark by maintaining the required pH gradient between the source phase and the receiving phase[2].

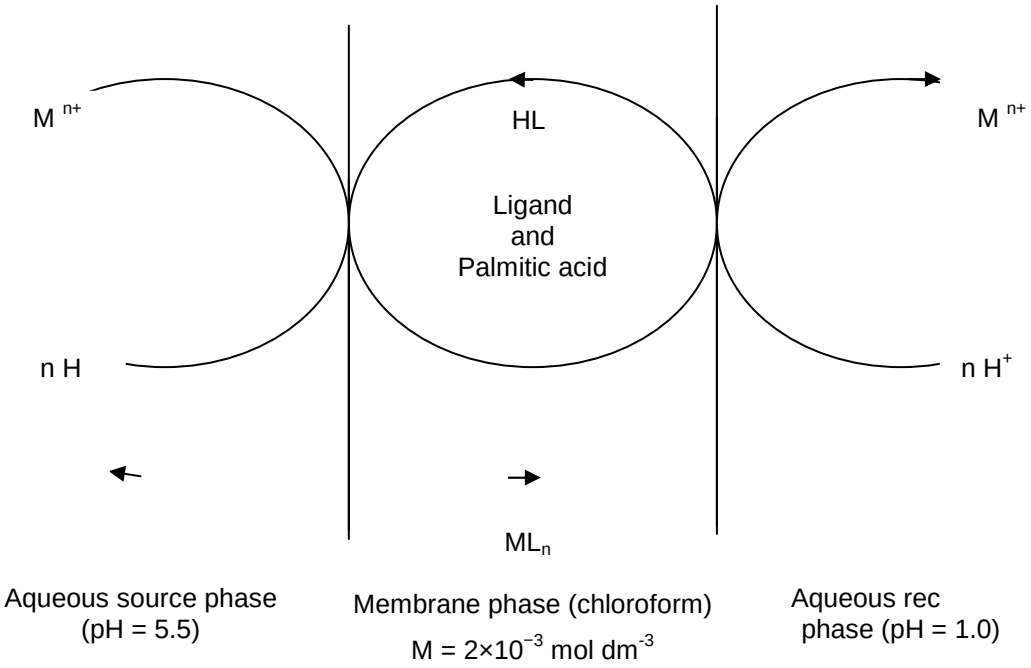

Scheme 3.1 A schematic representation of the mechanism of transport of a metal ion across a chloroform membrane.

In a liquid membrane system, if a ligand is to qualify as a suitable metal ion carrier, it should fulfil certain conditions. These conditions are:

- It should be selective.
- It should display rapid metal exchange kinetics.
- It should be sufficiently lipophilic[15] (and preferentially of low molecular weight) to avoid leaching into the aqueous source and receiving phases.
- It has to have a moderately high formation constant with the target metal ion to be transported[2].

In general, ligands of the type **HL** that are derived from benzoyl chloride are very stable and relatively hydrophobic[75]. This property makes these ligands suitable for transport and extraction studies.

In the presence of certain acceptors, the charge on the sulphur donor atom of these ligands can be increased by means of resonance effects. The combination of high charge density at the donor atoms with a relatively high NH acidity has the effect that almost all complexes of these ligands are formed in acidic media[76]. In acidic conditions it is only the platinum group metals, gold, silver and mercury that are complexed as a result of their specific acceptor properties[76]. Therefore, it is possible to carry out separations within this group of thiophilic elements by adjusting the acid concentration, the ligand dose, and by exploiting kinetic effects.

There have been two publications of the transport of transition and post-transition metal ions through bulk liquid membranes using thiourea ligands as carriers (ionophores). There is one report which illustrates the highly selective Ag(I) bulk liquid membrane transport using these ligands, i.e. *N*,*N*-diethyl-*N*'-camphanylthiourea[32,33].

According to Pearson's hard–soft–acid–base (HSAB) principle[77], soft metal ions prefer ligands with soft donor atoms, and hard metal ions prefer ligands with harder donor atoms. Ag(I) and Pb(II) are classified as soft acids whereas Co(II), Ni(II), Cu(II), Zn(II) and Cd(II) are classified as borderline acids. The soft acids are the electronegative metals. They are characterized by quite high Pauling electronegativities for metals, generally in the range of 1.9 to 2.54. Gold is the most electronegative metal and hence the softest. Therefore, according to this principle, Ag(I) is softer than Pb(II) because the electronegativity of Ag(I) (1.93) is higher than that of Pb(II) (1.87). The HSAB principle can be restated as: Softer Lewis bases tend to combine with softer Lewis acids[78]. Since the donor atoms of the most common Lewis bases have electronegativities increasing in the order S < Br < N < Cl < O < F, Ag(I) should be transported with sulphur-containing ligands better than any of the other six metal ions. Similarly, ligands containing oxygen or nitrogen as their donor atoms tend to combine with the harder metal ions as both the oxygen and nitrogen atoms are harder compared to sulphur. Therefore, the presence of the sulphur donor atom in the *N*-(thio)phosphorylated (thio)amide and *N*-(thio)phosphorylated (thio)urea ligands could make these ligands selective for Ag(I).

3.1.2 Calculations

The conditions used for the transport experiments are described in **Section 2.1.2**. All three phases (source phase, membrane phase and receiving phase) were stirred separately for 24 h at 25 ℃, at a speed of 10 rpm. The average cation flux rate is given by J-values, which are based on the quantity of metal ion transported into the receiving phase, see equation 3.1.

$$J = \frac{C_{(receiving)} \quad x \quad V}{t} \qquad \text{(eq. 3.1)}$$

where: $C_{(receiving)}$ is the concentration of the cation in the receiving phase (mol dm^{-3}).
V is the volume of the receiving phase (30 cm^3).
t is the transport time (24 h).
In this study, the concentration of metal ion remaining in the aqueous source phase and transported to the aqueous receiving phase was measured by AAS. The transport results were given as the average values obtained from duplicate runs, carried out in parallel. J-values equal to or less than 2.2×10^{-8} mol per 24 h assumed to be within experimental error of zero, and were ignored in the analysis of the results.

The percentage of metal ion(s) transported from the aqueous source phase to the aqueous receiving phase (T%) is calculated using eq. 3.2:

$$(T\%) = (n_r / n_i) \times 100 \qquad \text{(eq. 3.2)}$$

where n_r and n_i represent the number of moles of the metal ion transported into the receiving phase and the initial number of moles of the metal ion in the source phase, respectively.

A blank experiment was carried out for the transport studies in which the membrane phase contained palmitic acid (4×10^{-3} mol dm^{-3}) without the carrier (ligand). No transport of cation(s) from the source phase into the organic phase was observed. The transport experiments were carried out in duplicate to check reproducibility. All duplicate runs were within 1-2% of one another. Errors (both determinate and indeterminate) that were introduced throughout the experiments were assumed to be within ± 5% of the results.

Throughout this chapter, the term '% metal transported' refers to the percentage of the metal ion transported from the aqueous source phase to the aqueous receiving phase. The following abbreviations are also used:

$^{Ag}T_r\%$ = Percentage of Ag (I) transported into the receiving phase.

$^{Ag}T_m$%= Percentage of Ag (I) transported into the membrane phase.

$^{Cu}T_r$% = Percentage of Cu (II) transported into the receiving phase.

$^{Cu}T_m$%= Percentage of Cu (II) transported into the membrane phase.

In the context of transport behaviour, 'efficiency' is synonymous with high mass transfer of the species being transported. The efficiency of the transport set up shown in **Figure 1.1** is determined by two physical parameters. These are the physical dimension of the transport cell and the rate of stirring of the solutions. Efficiency can be enhanced by increasing the interfacial contact area between the membrane and the aqueous phases. However, stirring the organic and aqueous phases at a higher rate (>10 rpm) is not recommended as it may cause complete mixing of the two phases.

Another important term is 'selectivity'. In the context of transport, 'selective' means that the ligand selects one metal over the others by a relatively large percentage difference. A parameter called 'selectivity factor of Ag(I) to Cu(II)', η (Ag(I)/Cu(II)), has also been defined for comparing the selectivity of a specific ligand for Ag(I) over that for Cu(II) as follows:

$$\eta\ ((Ag(I)/Cu(II)) = \frac{^{Ag}T_r\ \%}{^{Cu}T_r\ \%}$$

3.2 Results and discussion

The fundamental parameters that influence the competitive transport of the metal ions are: concentration of ligand, pH of source phase, pH of receiving phase (strippant) and the use of hexadecanoic (palmitic) acid. All the experimental parameters used in this study were identical, and defined in the previous experimental work (see **Chapter 2**). The structure of the various ligands was the major difference evaluating the competitive metal ion bulk membrane transport studies described. The series of *N*-(thio)phosphorylated (thio)ureas and *N*-(thio)phosphoryl-ated (thio)amide ligands had the different substituted functional groups. We systematically grouped the ligands into seven groups. Each group had a similar substituent with slight variation in the structure, and the transport results obtained under the same conditions are compared.

3.2.1 Comparison of metal ion transport by HL7 and HL17

In this section, **HL7** and **HL17** are grouped together. Both compounds contain a morpholine group, but they differ at the phosphorus end, with a P=S unit for **HL7** and a P=O unit for **HL17**. Competitive metal ion transport experiments involving these ligands are conducted and the results are summarized in **Table 3.1**.

Table 3.1 J-values for the competitive metal ion transport by **HL7**and **HL17** (data includes ± 5% experimental error).

	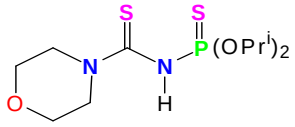 **HL7**	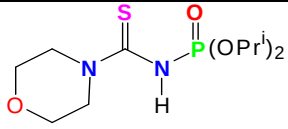 **HL17**
Metal ion transport: J values (mol/h x 10^{-7})		
	HL7	**HL17**
Ag(I)	–	–
Cu(II)	–	–
Cd(II)	–	–
Co(II)	–	–
Ni(II)	–	–
Pb(II)	–	0.28
Zn(II)	–	–
$^{Ag}T_r$%	–	–
$^{Ag}T_m$%	32	32
$^{Cu}T_r$%	–	–
$^{Cu}T_m$%	42	–
η(Ag(I) / Cu(II))	–	–

The experimental conditions are: pH of source phase = 5.5, pH of receiving phase = 1.0 and concentration of ligand = 2.0×10^{-3} mol dm^{-3}.

The effect of a morpholine group attached to these *N*-(thio)phosphorylated (thio)amide ligands is investigated by studying the coordination of **HL7** and **HL17** with metal ions. Most of the metal ions remaine in the membrane phase, and no metal ions are transported to the receiving phase. The percentages of Ag(I) and Cu(II) transported into the receiving phase ($^{Ag}T_r$% and $^{Cu}T_r$%) are both zero (**Table 3.1**). The most likely reason for this is the lower solubility of the morpholine substituted **HL** ligands than the rest of the **HL** ligands in chloroform. The other possibility is that morpholine as an organic heterocyclic group, features both amine and ether functional groups. Because of the amine, morpholine is a Lewis base and an electron donor group.

Ag(I) is a soft metal ion, and obviously is easily coordinated with soft S donor atoms containing deprotonated ligands. The percentages of Ag(I) that remain in the membrane phase ($^{Ag}T_m$%) in experiments with these two ligands are both about 32%. This shows that Ag(I) has a lower formation constant with morpholine substituted

ligands, because of the harder donor atoms of O and N present in the morpholine ring. On the other hand, the hard Cu(II) metal ion complexes are more favourable with these ligands.

Comparison of the percentage Ag(I) transported into the membrane phase of **HL7** and **HL17** at a ligand concentration of 2×10^{-3} mol dm^{-3} (See **Table 3.1**) shows that the Ag(I) transport is not affected with these ligands.

3.2.2 Comparison of metal ion transport by HL15 and HL18

These *N*-(thio)phosphorylated (thio)urea ligands **HL15** and **HL18**, both contain a pyridine group, but the position of the N differs in the pyridine group. It is either the *o*-unsaturated nitrogen donor (**HL15**) or the *m*-unsaturated nitrogen donor (**HL18**). Results of metal ion transport experiments involving these ligands are tabulated in **Table 3.2**.

Table 3.2 J-values for the competitive metal ion transport by **HL15** and **HL18** (data includes ± 5% experimental error).

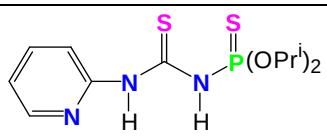

HL15

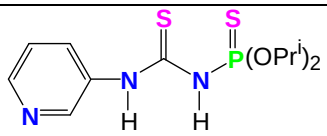

HL18

Metal ion transport: J values (mol/h x 10^{-7})		
	HL15	**HL18**
Ag(I)	–	–
Cu(II)	–	–
Cd(II)	–	–
Co(II)	–	–
Ni(II)	–	–
Pb(II)	–	–
Zn(II)	–	–
$^{Ag}T_r$%	–	–
$^{Ag}T_m$%	85	93
$^{Cu}T_r$%	–	–
$^{Cu}T_m$%	70	–
η(Ag(I) / Cu(II))	–	–

The experimental conditions are: pH of source phase = 5.5, pH of receiving phase = 1.0 and concentration of ligand = 2.0×10^{-3} mol dm^{-3}.

In aqueous solution, pyridine is a weaker base than the other saturated nitrogen donors. The lone pair of electrons is not delocalized into the aromatic *pi*-system. The nitrogen is sp^2 hybridized in pyridine, which leads to a greater s character in the orbital used for bonding to the metal ion, and hence more covalent bonding occurs. Pyridine ligand is normally used as in coordination chemisty. When nitrogen donor atoms are part of the imine moiety, the group has the possibility of increasing in

softness, similar to the case of P donor. The results of the $^{Ag}T_m$% have a relatively great value for both ligands, since Ag(I) probably has a high formation constant, due to contribution by the pyridine substituent.

Table 3.2 shows that Cu(II) ions neither remained in the membrane phase nor are transported by **HL18**, but 70% Cu(II) metal ions remained in the membrane phase by **HL15**. Another possibility is that they may form complexes, which is shown in **Scheme 3.2**. The deprotonated pyridine substituted ligand (**HL15**) with an *o*-unsaturated nitrogen is a good ligand for coordinating with Cu(II) ions. The Cu(II) ion is a hard metal ion, and it may not coordinate with the main body of the *N*-(thio)phosphorylated (thio)amide ligand to form the six-membered chelate ring of S-C-N-P-S-M.

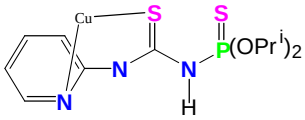

HL15

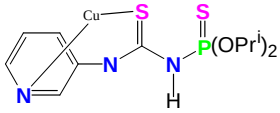

HL18

Scheme 3.2

The **HL15** forms a six-membered chelate ring, whereas **HL18** forms a seven-membered chelate ring. The seven-membered ring is not as stable as the five- or six-membered chelate rings. According to the transport results with **HL15** and **HL18**, the Cu (II) ion is not transported to the receiving phase by **HL18**. It is more difficult for **HL18** to complex to metal ions compared to **HL15** due to steric hindrance at the pyridine *N*-donor atom.

In this group, the Ag(I) ion is good at coordinating with deprotonated **HL15** and **HL18**, but is not easily stripped to the receiving phase in the bulk membrane transport experiment. These results indicate that **HL15** and **HL18** do not qualify for transport of Ag(I) metal ions. The *o*-unsaturated nitrogen ligand has a possibility for increasing the formation constant with Cu(II) than the *m*-unsaturated nitrogen ligand.

3.2.3 Comparison of metal ion transport by HL3, HL4, HL9 and HL21

Competitive metal ion transport experiments involving **HL3**, **HL4**, **HL9** and **HL21** as ionophores have been conducted. This group can be simplified as *N*-(thio)phosphorylated (thio)amide (**HL3** and **HL21**) and as *N*-(thio)phosphorylated (thio)urea (**HL4** and **HL9**) ligands. **HL3** and **HL9** have an O bonded to P, whereas **HL4** and **HL21** have an S bonded to P. The results are presented in **Table 3.3**.

Table 3.3 J-values for the competitive metal ion transport by **HL3**, **HL4**, **HL9** and **HL21** (data includes ± 5% experimental error).

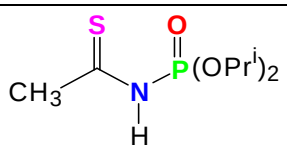

HL3

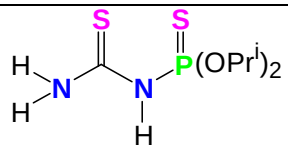

HL4

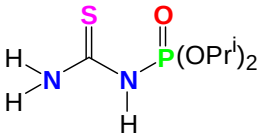

HL9

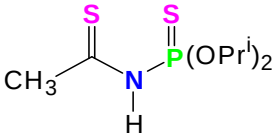

HL21

Metal ion transport: J values (mol/h x 10^{-7})				
	HL3	**HL4**	**HL9**	**HL21**
Ag(I)	–	0.63	–	–
Cu(II)	–	1.3	1.4	–
Cd(II)	–	–	–	–
Co(II)	–	–	–	–
Ni(II)	–	–	–	–
Pb(II)	–	–	–	–
Zn(II)	–	–	–	–
$^{Ag}T_r$%	–	–	–	–
$^{Ag}T_m$%	75	95	91	86
$^{Cu}T_r$%	–	2.0	2.2	–
$^{Cu}T_m$%	33	37	40	13
η(Ag(I) / Cu(II))	–	–	–	–

The experimental conditions are: pH of source phase = 5.5, pH of receiving phase = 1.0 and concentration of ligand = 2.0×10^{-3} mol dm^{-3}.

All transport results depend on the different electron densities of the amide and methyl groups. N is an electron donor atom, which is an important factor in coordination chemistry.

The J values in **Table 3.3** shows that **HL4** is the only one which has transport values for both Cu(II) and Ag(I). **HL4** not only has two thio-groups, but also the terminal amide functional group, hence the deprotonated **HL4** possibly forms complexes with the harder metal Cu(II) and soft metal Ag(I). S donates better for the softer Ag(I) metal ion than the O-donor. The complex stabilities of such systems are most likely dominated by the favourable enthalpy contribution arising from the formation of the Ag–S bond relative to the Ag–O bond [15]. From **Table 3.3**, the sum of the percentages of Ag(I) transported into the receiving phase ($^{Ag}T_r$%) and percentages of Ag(I) remained in the membrane phase ($^{Ag}T_m$%) shows that **HL4** and **HL9** probably have a relatively high formation constant. **HL4** and **HL9** was taking metal ion into the organic phase but not releasing it into the receiving phase. It can be explained by the two possible sites of coordination with the metal ion. One coordination forms a

six-membered ring with the (*S,S*) chelate ligand. The other coordination possibility is the amide being converted to a nitrile group by losing the S of C=S, and the N of the nitrile group coordinates with the metal ion. The synthesized compound [Ag(I)(**L4**-*S,N*)]$_8$ that shows these different coordination modes will be discussed further in **Section 5.3**. X-ray crystal structures can be used to provide evidence of Cu(I) and Ag(I) coordination with **L4**. **HL9** is a good Cu(II) transport agent. In **Table 3.3**, **HL9** is only selective for Cu(II) in the receiving phase, albeit low at 2.2%.

The amide substituent on **HL** ligand did not have influence much on the bulk membrane transport with metal ions. Deprotonated *N*-(thio)phosphorylated (thio)urea (**HL4** and **HL9**) most likely have a high formation constant with Ag(I).

3.2. 4 Comparison of metal ion transport by HL11, HL19 and HL26

The results of the competitive metal ion transport experiments involving **HL11**, **HL19** and **HL26** are summarized in **Table 3.4**. This group of compounds has a substituent in the p-position on the aromatic ring. For the purpose of comparison, these three ligands are studied to determine the effect of transport with EWG (**HL11** and **HL19**) and EDG (**HL26**) substituted on the aromatic ring.

Table 3.4 J-values for the competitive metal ion transport by **HL11**, **HL19** and **HL26** (data includes ± 5% experimental error).

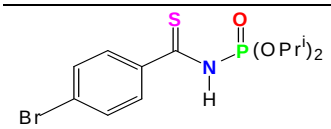 **HL11**	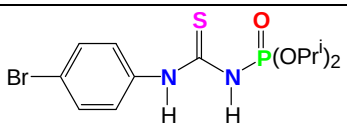 **HL19**	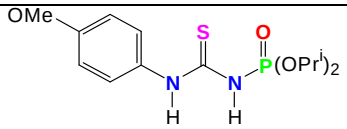 **HL26**
Metal ion transport: J values (mol/h x 10^{-7})		
	HL11	**HL19**	**HL26**
Ag(I)	2.2	–	–
Cu(II)	–	–	–
Cd(II)	–	–	–
Co(II)	–	–	–
Ni(II)	–	–	–
Pb(II)	–	–	–
Zn(II)	–	–	–
$^{Ag}T_r$%	5.1	–	–
$^{Ag}T_m$%	60	89	79
$^{Cu}T_r$%	–	–	–
$^{Cu}T_m$%	40	13	–
η(Ag(I) / Cu(II))	η→∞	–	–

The experimental conditions are: pH of source phase = 5.5, pH of receiving phase = 1.0 and concentration of ligand = 2.0 × 10^{-3} mol dm^{-3}.

HL11 and **HL19** have the same substituted group, which is a *p*-bromo substituted aromatic ring, while **HL19** is a (thio)urea ligand, and **HL11** is a (thio)amide ligand. The competitive transport of metal ions is zero for **HL19**. A lone pair of electrons on the nitrogen as thiourea fragment of **HL19** possibly enhances the coordination with the metal ions: 89% of Ag(I) ions remained in the membrane phase without stripping to the receiving phase. **HL11** does not coordinate easily with Ag(I): only 60% of Ag(I) remained in the membrane phase, however it is slightly easier to strip the metal ion to the receiving phase. **HL11** exhibits good transport of Ag(I) ($^{Ag}T_i$% 5.1%). Attempts were tried to grow crystals of the Ag(I) with deprotonated **HL11** to investigate the coordination structure, using three different deprotonation reagents such as NaOAc, NaH and KOH, were success.

HL19 and **HL26** were compared: the **HL19** with the electron withdrawing Br atom substituted on the aromatic ring and **HL26** with the electron donating methoxy group on the *p*-position of the aromatic ring. In **HL26**, the methoxy group donates electrons to the aromatic ring, which increases the electron density of the coordination HN-C(S)-N-P(O) moiety in **HL26**. Whereas **HL19** with electron withdrawing substitution perhaps decreases the electron density, but with Br^- it is not such a strong EWG, it does not significantly increase the Ag(I) metal ion binding. The percentage of Ag(I) that remains in the membrane phase in **HL19** is 89%, which is slightly higher than in **HL26**. The higher electron density of **HL26** does not improve the Cu(II) metal ion transport either. The lowest electron density **HL11** yields the best Cu(II) transport result.

Under the same experimental conditions, the highest η-value is exhibited here by **HL11**, hence, **HL11** has the highest selectivity with Ag(I). Ag(I) most likely has high formation constants with deprotonated thiourea ligands, compared to with deprotonated thioamide ligands.

3.2.5 Comparison of metal ion transport by HL6, HL8, HL16 and HL20

The comparison of **HL6** with **HL20** and **HL8** with **HL16** is quite similar to the comparison of **HL3** with **HL21** (**Section 3.2.3**). All these four ligands have a bulky alkyl substituent group with thioamide and thiourea ligands. The two alkyl groups are tertiary butyl (**HL6** and **HL20**) and isopropyl (**HL8** and **HL16**). The results for the competitive metal ion transport experiments for this group are shown in **Table 3.5**.

Table 3.5 J-values for the competitive metal ion transport by **HL6**, **HL8**, **HL16** and **HL20** (data includes ± 5% experimental error).

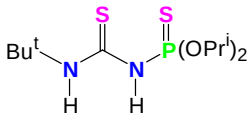 **HL6**	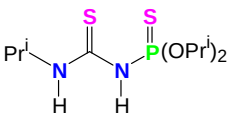 **HL8**	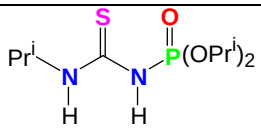 **HL16**	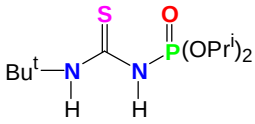 **HL20**

Metal ion transport: J values (mol/h x 10^{-7})

	HL6	**HL8**	HL16	**HL20**
Ag(I)	–	–	1.3	0.42
Cu(II)	–	–	1.4	3.8
Cd(II)	–	–	–	–
Co(II)	–	–	–	–
Ni(II)	–	–	–	–
Pb(II)	–	–	–	–
Zn(II)	–	–	–	–
$^{Ag}T_r$%	–	–	3.0	–
$^{Ag}T_m$%	41	69	86	84
$^{Cu}T_r$%	–	–	2.2	6.0
$^{Cu}T_m$%	38	39	9.0	19
η(Ag(I) / Cu(II))	–	–	η→1.4	–

The experimental conditions are: pH of source phase = 5.5, pH of receiving phase = 1.0 and concentration of ligand = 2.0×10^{-3} mol dm^{-3}.

The isopropyl group is not as bulky as the tertiary butyl group, since bulky groups hinder the metal ion complexation with phosphorylated thioureas. This is the reason for (*S,S*) donor set **HL8** has a higher formation constant than **HL6** with Ag(I) metal ions. Similarly, the same can be said for (*S,O*) donor set **HL16** compared to **HL20**. This Ag(I) transport result is due to the fact that the longer alkyl substituents (propyl groups) in **HL16** make the ligand more lipophilic compared to **HL20** with the butyl substituents, and hence **HL16** transports better than **HL20**. **Table 3.5** shows that **HL16** and **HL20** have more Ag(I)% metal ions present in the membrane phase. The η-value of **HL16** is 1.4, which means it has a better selectivity for Ag(I) metal ions compared to Cu(II) metal ions. **HL20** has a greater ability to transport Cu(II) into receiving phase, at 6.0%. When certain metal ions are transported to the receiving phase, it means a better potential balance for coordinating and releasing that metal.

Comparison of the percentage of Ag(I) remaining in the membrane phase ($^{Ag}T_m$%) in the case of **HL6**, **HL8**, **HL16** and **HL20**, under the same experimental condition, shows that the ligands with isopropyl substituent groups are most likely to form stable complexes with metal ions. This analysis shows how steric hindrance can play a role in metal ion binding. **HL16** and **HL20** with (*S,O*) donor sets transport Cu(II) and Ag(I) metal ions, and **HL20** has a high selectivity for transport of Cu(II).

3.2.6 Comparison of metal ion transport by HL1, HL2, HL5, HL10, HL12, HL13 and HL14

All the *N*-(thio)phosphorylated thioamides and *N*-(thio)phosphorylated thiourea ligands possess an aromatic ring as the substituent group and thus they are grouped together. The transport results are presented in **Table 3.6**.

The highest η-value and Ag(I) J-value are recorded for **HL1**. It means that ligand **HL1** has the best moderate stability constant with Ag (I). **HL1** has the highest transport efficiency for Ag(I) and it is very selective for Ag(I) compared to any of the other ligands. In **HL1** there are fewer donor atoms in the substituent group, which decreases metal ion coordination but makes the ligand more lipophilic.

The steric effects of the benzo groups together with electronic effects are most likely the factors preventing the other ligands from transporting Ag(I).

Table 3.6 J-values for the competitive metal ion transport by **HL1**, **HL2**, **HL5**, **HL10**, **HL12**, **HL13** and **HL14** (data includes ± 5% experimental error).

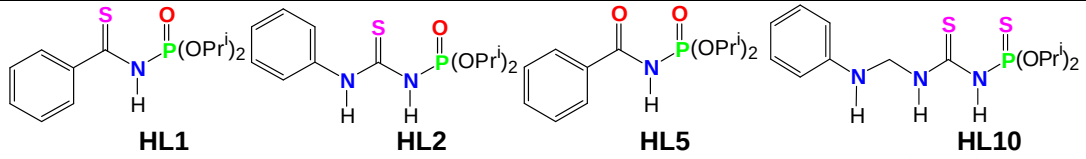

Metal ion transport: J values (mol/h x 10^{-7})							
	HL1	**HL2**	**HL5**	**HL10**	**HL12**	**HL13**	**HL14**
Ag(I)	8.3	–	–	–	–	–	–
Cu(II)	4.2	–	–	–	–	–	–
Cd(II)	–	–	–	–	–	–	–
Co(II)	–	–	–	–	–	–	–
Ni(II)	–	–	–	–	–	–	–
Pb(II)	–	–	–	–	–	–	–
Zn(II)	–	–	–	–	–	–	–
$^{Ag}T_r$%	36	–	–	–	–	–	–
$^{Ag}T_m$%	70	82	28	38	93	96	41
$^{Cu}T_r$%	6.6	–	–	–	–	–	–
$^{Cu}T_m$%	18	28	54	37	45	62	65
η(Ag(I) / Cu(II))	5.4	–	–	–	–	–	–

The experimental conditions are: pH of source phase = 5.5, pH of receiving phase = 1.0 and concentration of ligand = 2.0×10^{-3} mol dm^{-3}.

3.2.7 Comparison of metal ion transport by HL22, HL23, HL24 and HL25

HL22, **HL23**, **HL24** and **HL25** are grouped together in this section, because these bipodal *N*-phosphorylated thioureas are ligands that have two -P(O)-NH-C(S)- moieties linked to each other, with extended carbon chain and oxygen donor atoms. Results of competitive metal ion transport experiments involving these ligands are summarized in **Table 3.7**.

This ligand group has two sulphur and two oxygen donor atoms. The donor atoms are arranged around the ligand symmetrically. However, although these ligands have two (*S,O*) bonding sites that could potentially complex to two Ag(I) ions, they are less efficient for transporting Ag(I) than the single (*S,O*) donor sites, since all $^{Ag}T_r\%$ are zero. The possible reasons that could contribute to the decrease in the Ag(I) transport by these ligands are:

- Electronic interaction between the two Ag(I) ions makes it difficult for the ligand to carry two Ag(I) ions through its (*S,O*) donor sets as they are in close proximity to one another.

- A conformational change within the ligand, which may not favour the binding of the second Ag(I) ion, may be induced and this decreases the efficiency of the ligand to transport Ag(I).

Table 3.7 J-values for the competitive metal ion transport by **HL22**, **HL23**, **HL24** and **HL25** (data includes ± 5% experimental error).

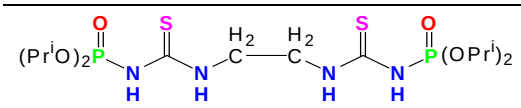

HL22

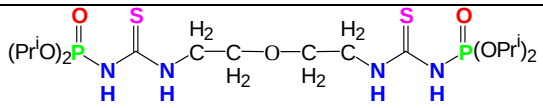

HL23

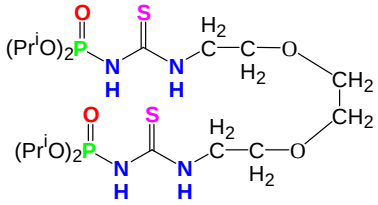

HL24

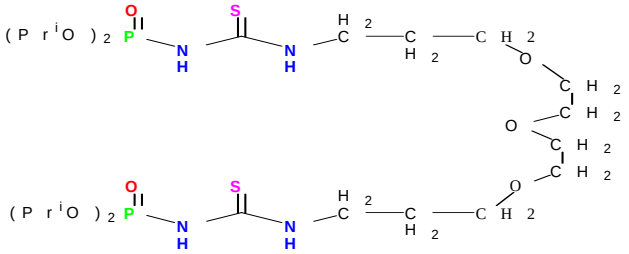

HL25

Metal ion transport: J values (mol/h x 10^{-7})				
	HL22	**HL23**	**HL24**	**HL25**
Ag(I)	0.42	–	–	–
Cu(II)	1.2	–	0.47	0.47
Cd(II)	–	–	–	–
Co(II)	–	–	–	–
Ni(II)	–	–	–	–
Pb(II)	–	–	–	0.42
Zn(II)	–	–	–	–
$^{Ag}T_r$%	–	–	–	–
$^{Ag}T_m$%	77	89	89	93
$^{Cu}T_r$%	–	–	–	–
$^{Cu}T_m$%	4.17	–	17	4.2
η(Ag(I) / Cu(II))	–	–	–	–

The experimental conditions are: pH of source phase = 5.5, pH of receiving phase = 1.0 and concentration of ligand = 2.0×10^{-3} mol dm^{-3}.

HL22 is the only ligand here that does not have any oxygen donor atom in the middle of the large ligand. However, **HL22** has the lower percentage of the Ag(I) remaining in the membrane phase. **HL25** has three extended O donor atoms, and it has the highest Ag(I) metal ion membrane concentration. This is probably because the stability constant of these ligands with Ag(I) is very high. It appears that more donor atoms can enhance the Ag(I) metal ion binding with the ligand, but it is difficult to strip into the receiving phase.

According to the J-values, **HL24** and **HL25** are only slightly selective for the Cu(II) metal ion. Considering that the percentage of Cu(II) that remained in the membrane phase is very low, it is concluded that both ligands do not form ideal complexes with Cu(II), and hence do not transport Cu(II) into the receiving phase.

Two of (*S,O*) chelate donor sets most likely increase the formation constant of Ag(I) with thiourea ligands, and decrease the transport potential of Ag(I). On the other hand, these bipodal *N*-phosphorylated thiourea ligands have a potential possibility to transport Cu(II) metal ions.

3.3 Conclusion

Considering all the transport results, Ag(I) was the best transported metal ion, followed by the Cu(II) metal ion. The other metal ions were affected only slightly, hence only Ag(I) and Cu(II) were studied further.

Figure 3.1 summarizes the transport of Ag(I) into the receiving phase by the 26 ligands under the same experimental conditions. It shows that **HL1** is the most efficient ligand for transport of Ag(I) into the receiving phase; the $^{Ag}T_r$ value is 36% (see **Table 3.4.6**). **HL11** and **HL16** also exhibit Ag(I) transport, but they are not good ligands for transport, because the $^{Ag}T_r$ values are lower than 5%. **HL1**, **HL11** and **HL16** three ligands had the (*S,O*) donor atoms bonding. **Figure 3.2** shows the 26 ligands with the total percentage of metal ion in the membrane and receiving phases. **HL4** has the highest formation constant with Ag(I), because it has the highest percentage of Ag(I) in the membrane phase. **HL4** contains two sulphur donor atoms. The (*S,S*) donor site is good for Ag(I) coordination, but it is difficult to strip Ag(I) into the receiving phase. **HL5** is the only ligand with (*O,O*) donors, and it is the ligand which has the lowest transport of Ag(I). This means the *O,O*-chelating group is not the best for the soft Ag(I) metal ion. The Ag(I) transport efficiency has the following order: *S,S*-chelating > *S,O*-chelating > *O,O*-chelating. The complex stabilities of the systems are likely dominated by the favourable enthalpic contributions arising from formation of the Ag–S bonds relative to the Ag–O bonds [14].

Other low Ag(I) transport ligands are **HL7** and **HL17**, because the morpholine substituent blocks the metal ion transport (see **Section 3.1.4.1**). **Figure 3.2** shows that **HL17** only selects Ag(I), which is transported into the membrane, but not into the receiving phase. Pyridine is a good substituent group for Ag(I) metal ion coordination, especially the electron donor N on the O-position, but Ag(I) transport is very low (see **Section 3.2**). Comparison of the bulky alkyl substituted functional groups indicates that tertiary butyl groups hinders the metal ion forming complexes with the ligand (see **Section 3.1.4.5**). Ligands that have more electron donor atoms of N and O in the extended ligand chain can increase the metal ion coordination, but it is then more difficult to strip the Ag(I) metal ions into the receiving phase (see **Section 3.1.4.4** and

Section 3.1.4.7).

When considering Cu(II) transport by the 26 ligands, **HL20** showed the best selectivity with Cu(II), although transport of Cu(II) (6%) into the receiving phase was still not adequate. **HL1** transported the most Cu(II), but still less than 7% (**Figure 3.1**). **HL15** had 70% of Cu(II) which remained in the membrane phase. **HL15** was the best ligand which coordinates with Cu(II).

Finally, overall transport results were carried out with **HL1** have the highest efficiency for Ag(I) and Cu(II). **HL20** and **HL11** have the best selectivity for the transport of Cu(II) or Ag(I). Liquid membrane separation is far more efficient and selective compared to the classical chloride precipitation technique for separating Ag(I) from other metal ions. In fact, in our case, it would also be difficult to separate Ag(I) from Pb(II) using the chloride precipitation method as chloride would not only precipitate Ag(I) as AgCl but it would also precipitate Pb(II) as $PbCl_2$.

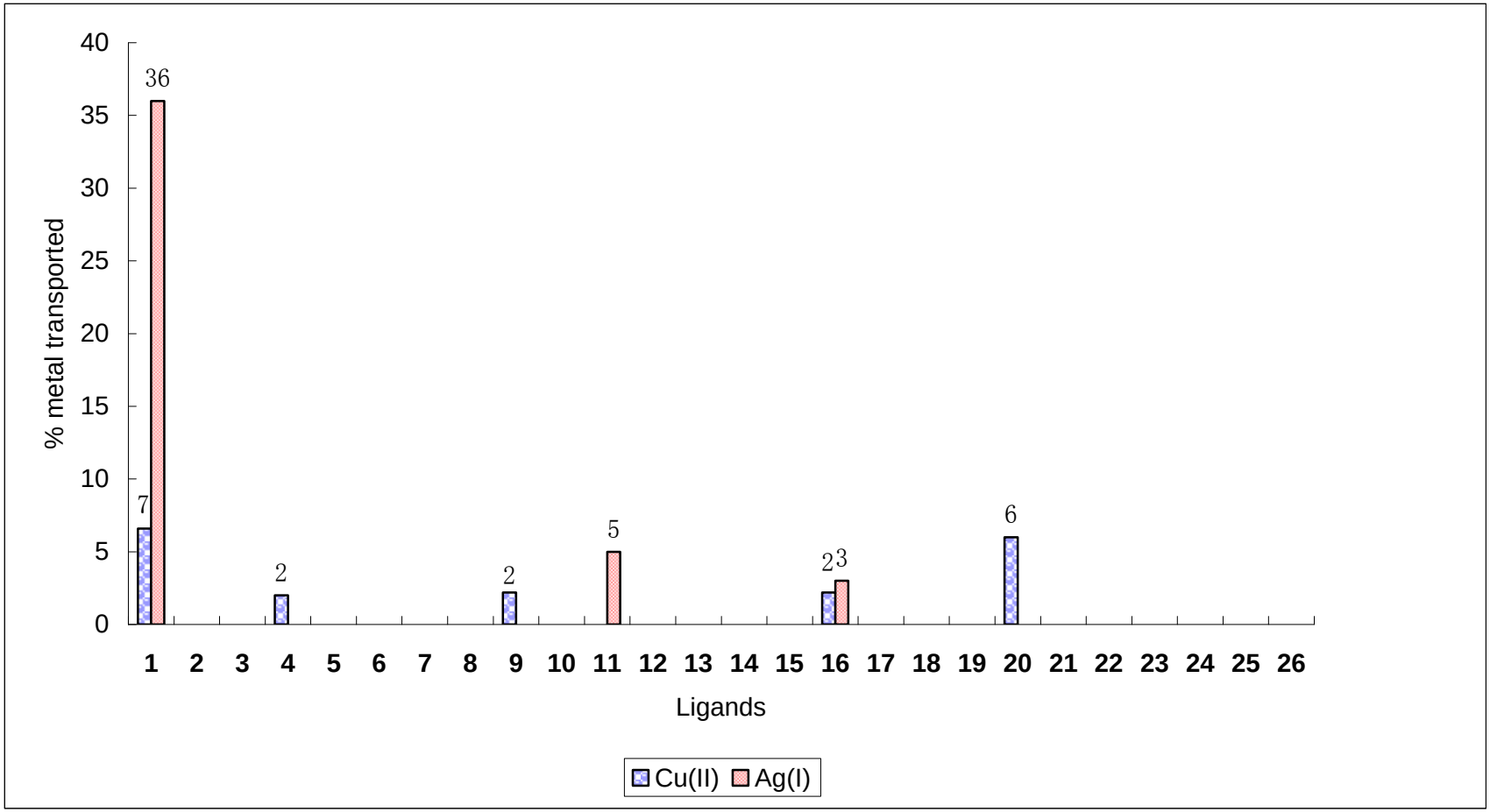

Figure 3.1 Comparison of the percentage transport of Ag(I) and Cu(II) ions in competitive transport studies involving all ligands. **1** represents **HL1**, **2** represents **HL2**, *etc.* The experimental conditions are: **source phase pH = 5.5**, **receiving phase pH = 1.0** and **concentration of ligand** = **2 x 10 $^{-3}$ mol dm^{-3}**.

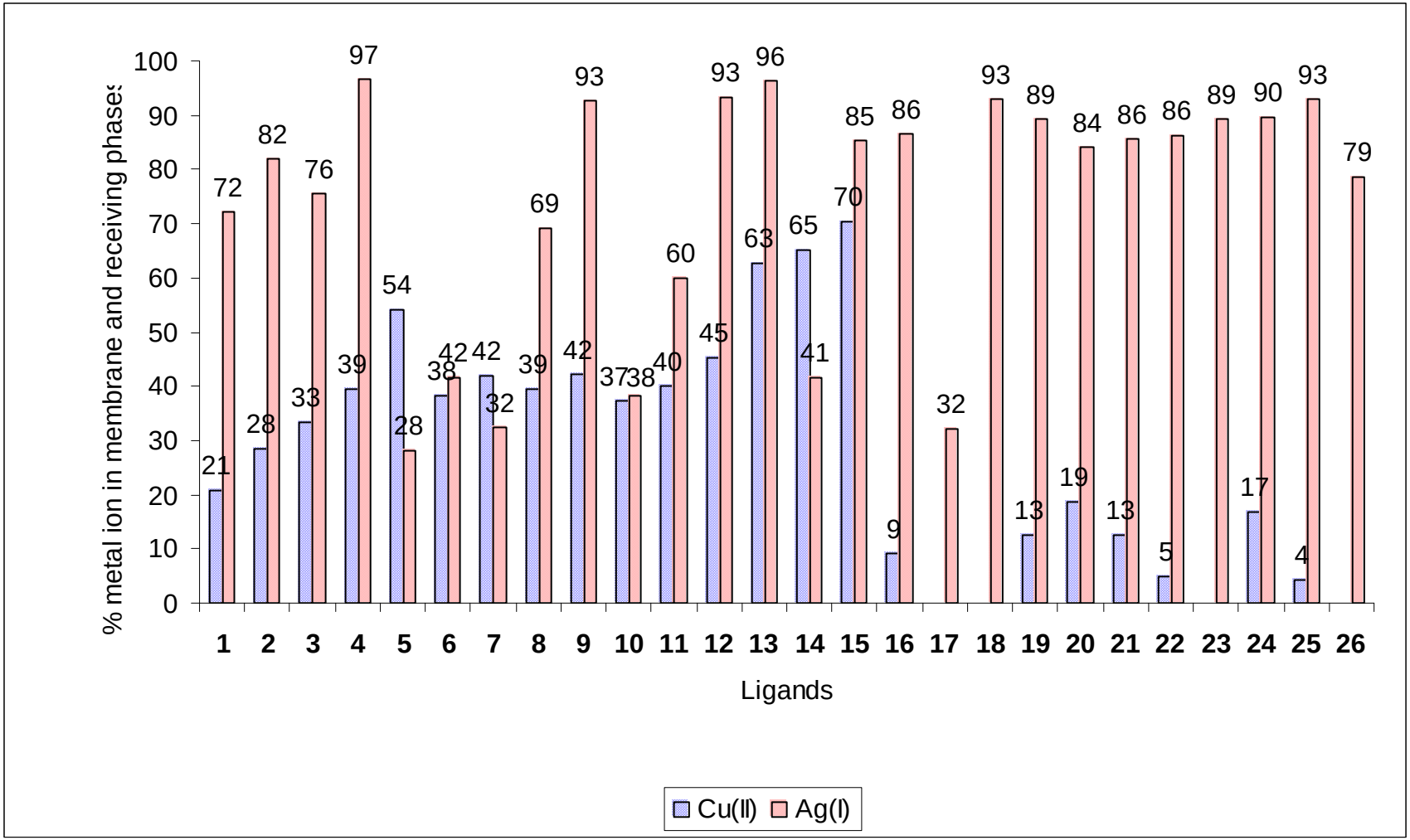

Figure 3.2 Total percentage of Ag(I) and Cu(II) ions ion in the membrane and receiving phase in the competitive transport studies involving all ligands. **1** represents **HL1**, **2** represents **HL2**, *etc.* The experimental conditions are: **source phase pH = 5.5**, **receiving phase pH = 1.0** and **concentration of ligand** = **2 x 10 $^{-3}$ mol dm^{-3}**.

Chapter 4

Competitive metal ion extraction studies involving *N*-(thio) phosphorylated (thio)amide and *N*-(thio)phosphorylated (thio)urea ligands

4.1 Introduction

4.1.1 Introduction

Further efforts to better understand the results of the membrane ion transport further, led us to the competitive study using liquid-liquid extraction. This study involves using the same seven metal ions and the same ligands, under the same experimental conditions of the transport, but with no receiving phase.

There are several important parameters to be considered in metal ion extraction:

- structure of the ligand
- stability of the individual metal / ligand complexes
- type of solvent
- nature of the accompanying anion
- pH of the aqueous phase during extraction.

In this study, the focus was only on the effect of varying the ligand structure on the extraction behaviour of these ligands. The rest of the factors are constant, and the same as those in the membrane transport studies.

Competitive two-phase solvent extraction experiments were carried out as described in **Section 2.2.4**. All the reagents used and the methods of preparation of solutions were as described for the membrane transport experiments in **Section 2.1.1** and **2.1.2**. In the transport experiments, the ratio of the source phase to the transport membrane phase is 1:5. In order to mirror these conditions, the volumes were 3 ml aqueous phase and 15 ml organic phase in the extraction studies. The results of the two-phase solvent extraction experiments are compared with that of the three-phase transport experiments and an attempt is made to logically relate and explain both sets of results.

4.1.2 Theoretical background

Metal ion extraction involves two phases: an aqueous phase and an organic phase. The solvent extraction of a monovalent metal ion (M^+) by the ligands, where the complex extracted has a composition ratio of 1:1 metal ion to ligand, can be shown by the series of equilibrium equations shown in **Scheme 4.1**. There are two formation processes for a metal ion-ligand complex in aqueous and organic phases[79]. These processes are generally competitive and depend on the coordination ability of the ligand in the aqueous phase and its hydrophobicity. Therefore, the species formed in both phases should be carefully considered while evaluating the equilibrium constants[80].

The equilibrium constants can be defined when the aqueous and organic phase volumes are equal, and it is assumed that the metal ion does not dissociate in the non-polar organic solvent.

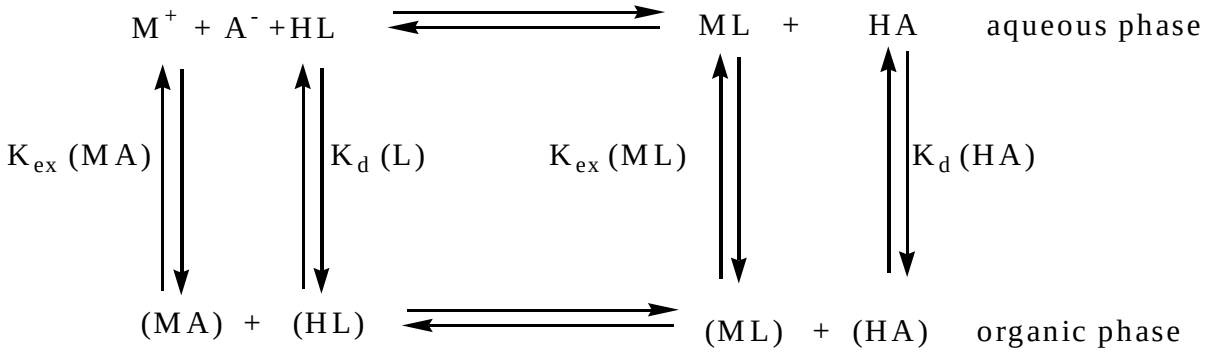

Scheme 4.1 Equilibrium constants for a metal salt two-phase solvent extraction.

$K_{ML} = [ML]_{aq} [HA]_{aq} / [M^+]_{aq} [A^-]_{aq} [HL]_{aq}$

$K_{ex} (MA) = [MA]_o / [M^+]_{aq} [A^-]_{aq}$

$K_d (L) = [HL]_o / [HL]_{aq}$

$K_{ass} = [ML]_o [HA]_o / [MA]_o [HL]_o$

$K_{ex} (ML) = [ML]_o / [ML]_{aq}$

$K_d (HA) = [HA]_o / [HA]_{aq}$

where:

"aq" = aqueous phase; "o" = organic phase; "A^-" = anion of the salt; "M^+" = monovalent metal ion.

K_{ML}: the stability constant of the metal ion-ligand complex in the aqueous phase;

K_{ex} (MA): the distribution constant of the metal salt between the aqueous and organic phases;

K_d (L): the distribution constant of the ligand between the aqueous and organic phase;

K_{ass}: the association constant of the metal salt with the ligand in the organic phase;

K_{ex} (ML): the distribution constant of the complex salt between the aqueous and organic phase;

K_d (HA): the distribution constant of the acid (HA) between the aqueous and organic phases.

The above equilibrium can be summarized as:

$$M^+_{aq} + A^-_{aq} + (HL)_o \rightleftharpoons (ML)_o + (HA)_{aq}$$

$$K_{eq} = \frac{[ML]_o[HA]_{aq}}{[M^+]_{aq}\,[A^-]_{aq}\,[HL]_o} \qquad \text{(eq. 4.1)}$$

Assuming no volume change occurs on mixing the two phases, for a system involving M^{n+}, we can write:

$$M^{n+}_{aq} + nA^-_{aq} + (HL)_o \rightleftharpoons (MLA_{n-1})_o + (HA)_{aq}$$

$$K_{eq} = \frac{[[MLA_{n-1}]_o[HA]_{aq}}{[M^{n+}]_{aq}\,[A^-]^n_{aq}\,[HL]_o} \qquad \text{(eq. 4.2)}$$

A detailed solvent extraction study was not undertaken in this study to establish K_{ex} and K_{eq}. Rather, the overall distribution constant D for the Ag(I) extracted can be measured using the following relationship:

$$D = \frac{\text{Total Ag(I) concentration in the organic phase}}{\text{Total Ag(I) concentration in the aqueous phase}}$$

In the extraction experiments, the source phase and organic phase were shaken for 24 h at a rate of 120 cycles per minute, on a Labcon oscillating shaker. The experiments were all carried out at 25 ^oC and in duplicate. The concentration of the metal ions remaining in the aqueous source phase were measured by AAS. In all cases, the values between any two duplicate runs did not exceed 2%. Any apparent extraction of small amounts of metal ions (< 2%) may be an artifact rather than a true indication towards a particular metal ion and therefore were ignored from the treatment of the data. The sum of all experimental errors involved in all measurements is assumed to be within ± 5%.

The percentage of metal ion extracted was calculated as follows:

$$\% \text{ metal ion extracted} = \frac{n_b - n_a}{n_b} \times 100 \qquad \text{(eq. 4.3)}$$

where:

- n_b refers to the number moles of the metal ion present in the aqueous source phase before the extraction, and
- n_a refers to the number of moles of the metal ion present in the aqueous source phase after the extraction.

Also note that the terms ‘selectivity’ and ‘efficiency’ are used in the same context as defined in **Chapter 3**.

4.2 Results and discussion

4.2.1 Comparison of extraction of metal ions by HL7 and HL17

Structurally, ligands **HL7** and **HL17** have the same substituted morpholine group, but differ in their chelate donor sets (*S,S*) and (*S,O*). The results of the competitive metal ion extraction studies involving the metal ions Co(II), Ni(II), Cu(II), Zn(II), Ag(I), Cd(II) and Pb(II) are summarized in **Figure 4.1**.

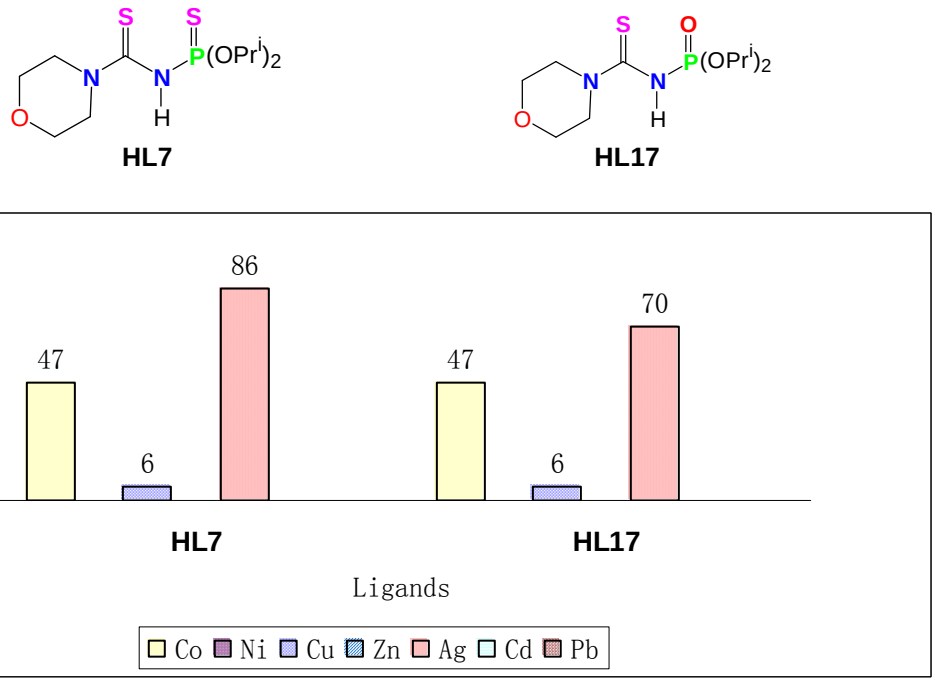

Figure 4.1. Comparison of the percentage extraction of the different metal ions in competitive extraction studies involving **HL7** and **HL17**. **pH of the aqueous phase = 5.5** and the **concentration of the ligand** is **2 x 10^{-3} mol dm^{-3}**.

The percentage extraction of Ag(I) with **HL7** is 86%, but it is lower at 70% for **HL17** (**Figure 4.1**). Accordingly, the difference between these two ligands are the (*S,S*) donor set for **HL7** and the (*S,O*) donor set for **HL17**, which probably explains the difference for extraction with Ag(I).

The morpholine groups appear to cause decreased soft metal ion coordination ability. Most of the other ligands studied extract all the Ag(I) metal ion present in the solution, but the two morpholine substituted ligands extract less than 100%. The lone pair of electrons on the nitrogen of the morpholine group can be protonated. This functional group could perhaps be changing the sulphur atoms electronically, i.e. making it a harder donor atom. Steric effects can also perhaps make it more difficult for the metal ion to coordinate in the presence of this group. However, the most likely reason is the lower solubility of these ligands in the chloroform phase. The difference

in solubility behaviour is directly related to the polarity and lattice energy. Because of the lower solubility in chloroform, the ligand bleeds across the interface into the aqueous phase. Solubility is an important factor determining the extraction efficiency of a ligand. Both ligands have the same extraction values for Co(II) and Cu(II)metal ions at 47% and 6%, respectively (**Figure 4.1**). Hence the harder donor atoms N and O that exist in the morpholine groups tend to coordinate better to hard metal ions.

At a ligand concentration of 2 × 10^{-3} mol dm^{-3}, the extraction efficiency of **HL7** is greater than that of **HL17**. The extraction percentage of Ag(I) is relatively low, which means that the morpholine substituent group is most likely responsible the lower extraction efficiency of these two ligands. The extraction selectivities of **HL7** and **HL17** for Cu(II) and Co(II) is, unusually, exactly the same, indicating that the (*S,S*) and (*S,O*) chelate sets do not affect the hard metal extraction.

4.2.2 Comparison of extraction of metal ions by HL15 and HL18

Both **HL15** and **HL18** are *N*-(thio)phosphorylated (thio)ureas with a pyridine group, but they differ by the pyridine-N being in the *o*-unsaturated (**HL15**) or *p*-unsaturated (**HL18**) position. The results of the competitive metal ion extraction are shown in **Figure 4.2**.

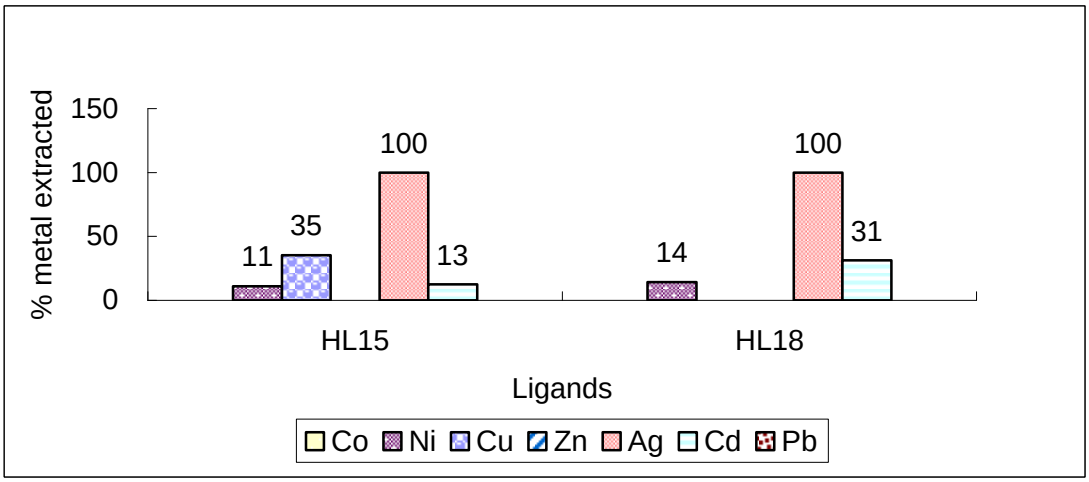

Figure 4.2 Comparison of the percentage extraction of the different metal ions in competitive extraction studies involving **HL15** and **HL18**. **pH of the aqueous phase = 5.5** and the **concentration of the ligand** is **2 x 10^{-3} mol dm^{-3}**.

As there are (*S,S*) coordination sites for soft metal ions, so the percentage extraction of Ag(I) is 100%, and even extracted an amount of the borderline soft metal ion Pb(II).

Pyridine is basic in terms of chemical properties, because the lone pair of electrons is not delocalized into the aromatic pi-system at the nitrogen atom. Pyridine is sometimes used as a coordination ligand, so perhaps coordination may take place at the pyridine-N or the other two N-atoms. Nitrogen donor atoms of the thiourea moiety helps the ligand to complex with harder metal ions. The **HL15** forms a six-membered chelate ring between S and the pyridine-N, whereas **HL18** forms a seven-membered chelate ring (see **Scheme 3.2**). The seven-membered ring is not as stable as the five- or six-membered chelate rings (as discussed in **Section 3.2.2**). This is consistent with the transport result of **HL15** extracting Cu(II) but no extraction with **HL18**. The extraction results for the harder metal ions Cd(II) and Ni(II) are also shown in **Figure 4.2**. The pyridine substituted *N*-(thio)phosphorylated (thio)urea ligands have the possibility of forming a complex with hard metal ions.

Under the same conditions, the extraction efficiency of **HL15** and **HL18** for Ag(I) are 100%, so pyridine substituted **HL** ligand affects the metal ion selectivity. The *m*-unsaturated pyridine substituent group attached to the thiourea ligand did not extract any Cu(II).

4.2.3 Comparison of extraction of metal ions by HL3, HL4, HL9 and HL21

HL3 and **HL21** terminate with a methyl group, while **HL4** and **HL9** terminate with an amine group. These four ligands are the simplest amongst the 26 ligands studied. In **Figure 4.3** the extraction results are shown.

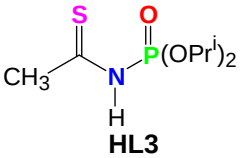

HL3

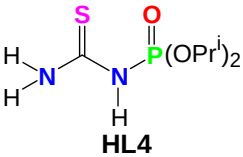

HL4

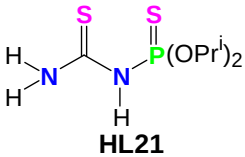

HL21

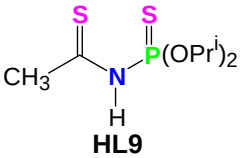

HL9

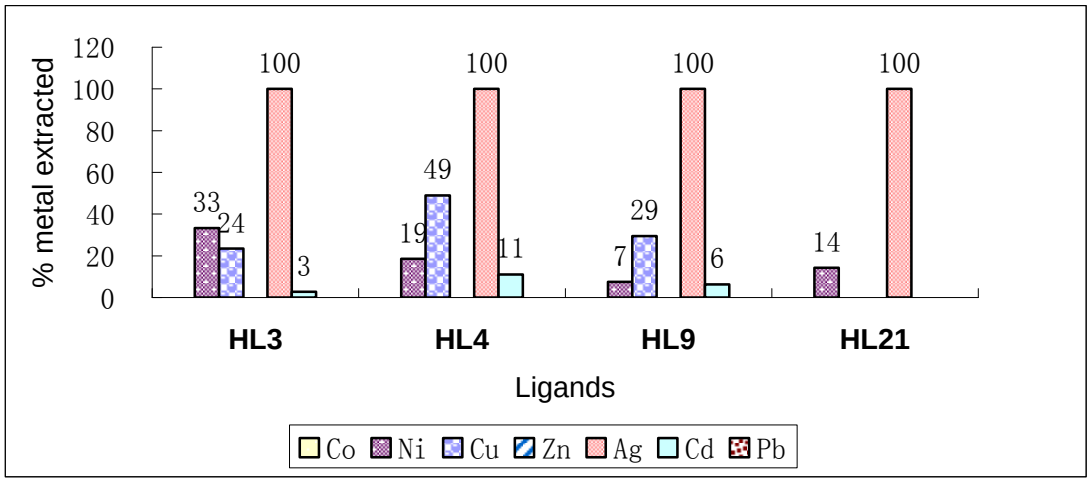

Figure 4.3. Comparison of the percentage extraction of the different metal ions in competitive extraction studies involving **HL3**, **HL4**, **HL9** and **HL21**. **pH of the aqueous phase = 5.5** and the **concentration of the ligand** is **2 x 10^{-3} mol dm^{-3}**.

All four ligands exhibit 100% Ag(I) extraction, which is expected, based on a 1:1 ligand to metal mole ratio. The alkyl substituted ligands with (*S,S*) donor sets (**HL21**) do not extract the harder metal ions, since there are no hard donor atoms to coordinate with hard metal ions. The amine group is capable of coordinating to metal ions like Cu(II). According to the transport results of **HL4** and **HL9** both have a high percentage of Cu(II) stripped in the receiving phase. When comparing the extraction results of all the ligands, **HL4** has the highest extraction percentage for Cu(II), at 49%, and the extraction percentage of **HL9** is 29% (**Figure 4.3**). If the ligand to metal mole ratio is increased to 2:1, then the percentage extraction will also obviously increase.

The harder metal ions, Cd(II) and Ni(II), are also extracted by these ligands. The methyl substituted ligands have a higher selectivity than the amine substituted ligands. **HL3** shows 33% extraction of Ni(II) and 3% extraction of Cd(II), whereas **HL21** only shows 14% extraction of Ni(II), and no Cd(II) or Cu(II) extraction. **HL4** and **HL9** show extraction of four different metal ions. **HL3** has a P=O unit, which can coordinate with harder metal ions, hence the behaviour being better with Ni(II) and Cd(II), whereas **HL21** has a P=S unit, which shows a preference for softer metal ions.

The extraction efficiencies of **HL3**, **HL4**, **HL9** and **HL21** for Ag(I) are all 100% under the same experimental conditions. **HL4** is the best and most successful ligand for Cu(II) here, while the selectivity for Ag(I) compared with the other metal ions indicates that **HL21** is a best choice.

4.2.4 Comparison of extraction of metal ions by HL1, HL2, HL11, HL19 and HL26

The results of the competitive metal ion extraction experiments involving the grouping of the *p*-position substituted aromatic ligands are summarized in **Figure 4.4**.

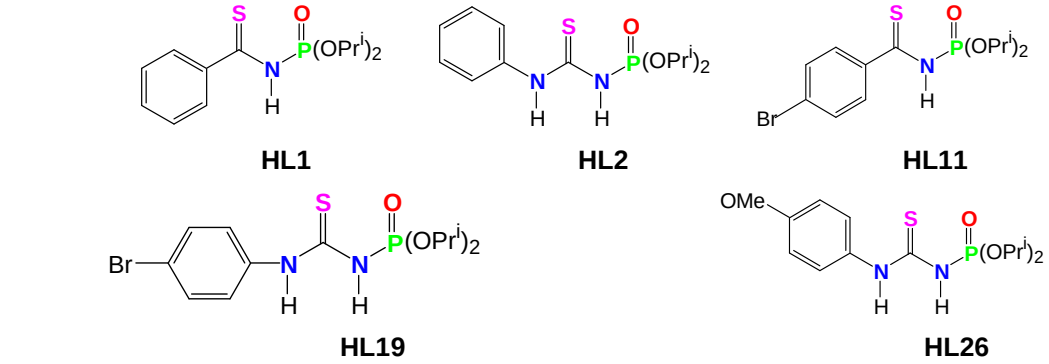

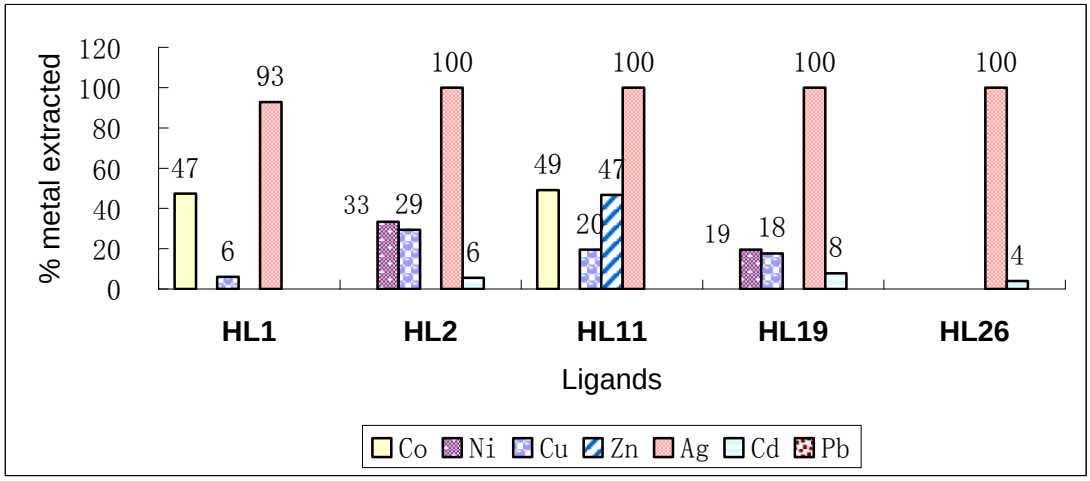

Figure 4.4. Comparison of the percentage extraction of the different metal ions in competitive extraction studies involving **HL1**, **HL2**, **HL11**, **HL19** and **HL26**. **pH of the aqueous phase = 5.5** and the **concentration of the ligand** is **2 x 10^{-3} mol dm^{-3}**.

As can be seen from their structures, both the **HL11** and **HL19** ligands possess electron-withdrawing substituents attached to the benzyl groups. The substituents (Br^-) withdraw electrons from the ring, therefore decreasing the electron density from the carbonyl sulphur of the thiourea moiety, making the sulphur even softer. This helps the ligand to complex with Ag(I) even better. The transport results of **HL2**, **HL11 HL19** and **HL26** show transfer of the Ag(I) metal ion to the membrane phase, but it is not stripped into the receiving phase. **HL1** is the best ligand for Ag(I) transport (**Section 3.2.6**), although it does not extract 100% Ag(I), because of a very likely moderate stability constant with Ag(I). In terms of the structure of **HL1**, there is no donor atom between the sulphur and benzyl group.

The divalent metal ion Cu(II) is extracted by **HL2**, **HL11** and **HL19**, and the percentages are 29%, 20% and 18%, respectively (**Figure 4.4**). **HL1** extracted only 6% Cu(II), which is consistent to the transport results. **HL1** shows the highest Cu(II) transport efficiency. Deprotonated **HL1** does not form a very stable complex with Cu(II), and hence it is easily stripped into the receiving phase.

The harder metal ions Cd(II) and Ni(II) are extracted by the *N*-(thio)phosphorylated(thio)urea ligands (**HL2**, **HL19**, **HL26**), and Co(II) is extracted by *N*-(thio)phosphorylated(thio)amide ligands (**HL1**, **HL11**). The highest extraction percentage of Ni(II) is 33%, exhibited by **HL2**.

Comparison of the Ag(I) metal ion extraction by **HL1**, **HL2**, **HL11 HL19** and **HL26** shows that **HL1** has the lowest extraction efficiency. The highest transport efficiency was shown with **HL1**, since **HL1** has the proper balance of formation and releasing Ag(I). **HL26** has the highest selectivity for Ag(I), compared to all the other metals. The percentage extraction results for these five ligands are very close to one another, which means that the bulky functional groups did not have a considerable discrimination effect on the extraction behaviour of the ligands.

When summarizing all the results of Co(II) extraction (**Figures 4.1** and **4.4**), it is evident that there are four ligands that extract Co(II) metal ions, viz. **HL1**, **HL7**, **HL11** and **HL17**. It is an interesting finding that only thioamide ligands perform this extraction. The thiourea ligands do not extract any Co(II).

4.2.5 Comparison of extraction of metal ions by HL6, HL8, HL16, and HL20

These four ligands (**HL6**, **HL8**, **HL16**, **HL20**) are similar *N*-(thio)phosphorylated(thio)urea ligands with bulky alkyl groups as substituents (Pr^i and Bu^t). Their selectivity and efficiency of extraction of Ag(I) is compared and summarized in **Figure 4.5**.

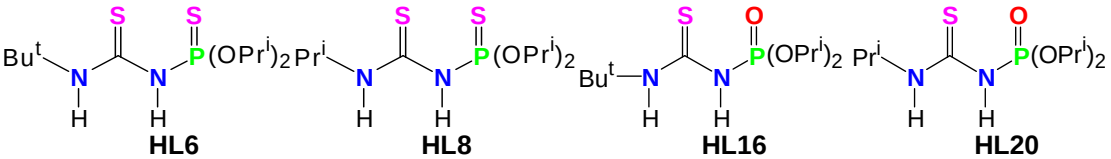

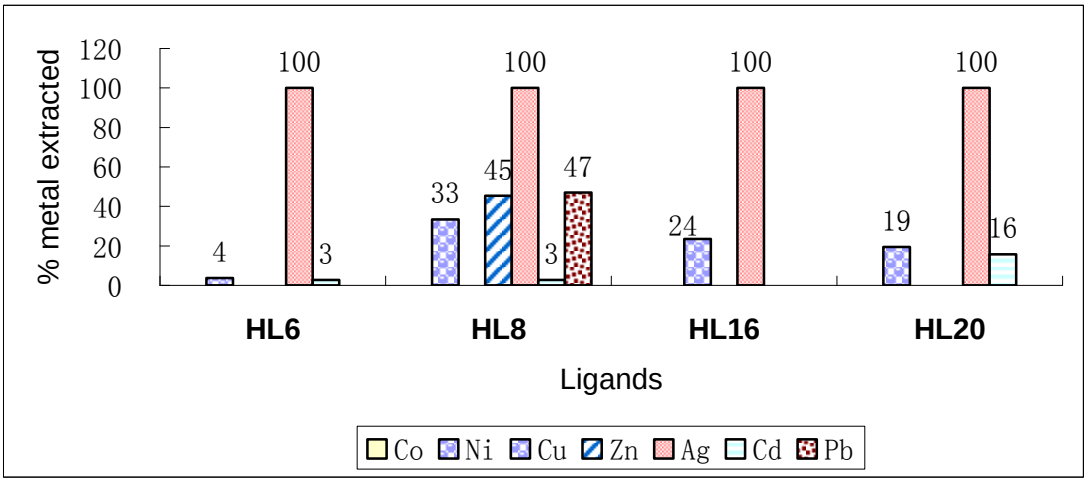

Figure 4.5. Comparison of the percentage extraction of the different metal ions in competitive extraction studies involving **HL6**, **HL8**, **HL16**, and **HL20**. **pH of the aqueous phase = 5.5** and the **concentration of the ligand** is **2 x 10^{-3} mol dm^{-3}**.

These ligands can also be compared with the methyl substituted ligands **HL3** and **HL21**. The extraction percentage of Ag(I) is 100% for all the ligands. The Cu(II) metal ion is only extracted by **HL16**, at 24%. This ligand has a P = O unit instead of a P = S unit.

Summarizing the percentage extraction of Cd(II) and Ni(II), indicates that the most sterically hindered ligands **HL6** and **HL16** have the lowest percentage, and **HL16** does not extract these two metal ions. **HL8** is the only ligand that extracted the widest variety of metal ions into the organic phase, even Zn(II) and Pb(II). **HL8** contains the (*S,S*) soft donor chelate and thiourea moiety, which tends to complex with hard metal ions. It also has the less bulky alkyl substituted functional group. **HL11** also extracts some Zn(II) **(Figure 4.4).**

The extraction efficiency of **HL6**, **HL8**, **HL16**, **HL20 (Figure 4.5**) for Ag(I) are all 100% under the defined experimental conditions. The percentage of Ag(I) extraction for these ligands are very close to one another. This means that the alkyl functional groups do not have a considerable effect in discriminating the Ag(I) extraction behaviour of these ligands.

4.2.6 Comparison of metal ion extraction by HL5, HL14, HL10, HL12 and HL13

In this group, all the ligands have an aromatic ring substituted with the *N*-(thio)phosphoryl-ated(thio)urea and *N*-(thio)phosphorylated(thio)amide ligands. In

Figure 4.6, the results of the competitive metal ion extraction studies involving **HL5**, **HL14**, **HL10**, **HL12** and **HL13** are presented.

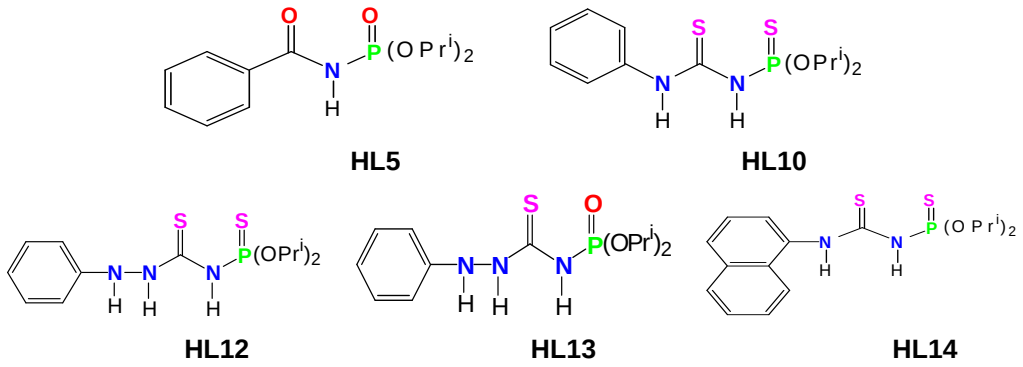

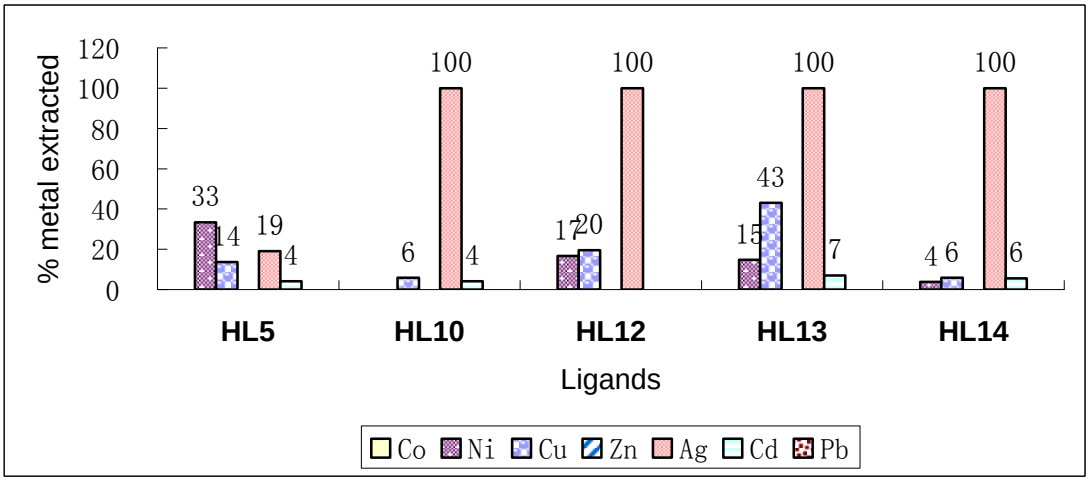

Figure 4.6. Comparison of the percentage extraction of the different metal ions in competitive extraction studies involving **HL6**, **HL8**, **HL16**, and **HL20**. **pH of the aqueous phase = 5.5** and the **concentration of the ligand** is **2 x 10^{-3} mol dm^{-3}**.

Ligand **HL5** is the only ligand with no sulphur atom attached; there is a carbonyl group instead. Only 19% Ag(I) is extracted by **HL5**. This indicates that the S is an important structural feature for forming a complex with the soft metal ion Ag(I). The other ligands of this group all extract 100% of the original Ag(I) metal ion present.

Considering the extraction results of Cu(II), **HL13** shows the highest percentage, at 43%. **HL12** also shows a relatively high Cu(II) extraction, at 20% **(Figure 4.6**). **HL12** and **HL13** have two hard nitrogen donor atoms, which increases the possibility of coordination with hard metal ions. **HL13** has the (*S,O*) chelate bonding set, which is favourable for complex formation with Cu(II). Hence the extraction results of **HL13** for Cu(II) are twice as high as **HL12**.

The extraction efficiency is consistent with the transport results obtained in **Section 3.2.6**: **HL5** was the poorest extractant for Ag(I). The selectivity of the grouped

ligands for Ag(I) compared with Cu(II) is in the order: **HL10** = **HL14** > **HL12** > **HL13** > **HL5**. In this study **HL10** is the only ligand that extracts Cd(II).

4.2.7 Comparison of metal ion extraction by HL22, HL23, HL24 and HL25

In this section, **HL22**, **HL23**, **HL24** and **HL25** are the bipodal *N*-phosphorylated thiourea ligands that have two -P(O)-NH-C(S)- moieties linked to each other, with an extended carbon chain and oxygen donor atoms. Competitive metal ion extraction experiments involving these ligands were conducted and the results are summarized in **Figure 4.7**.

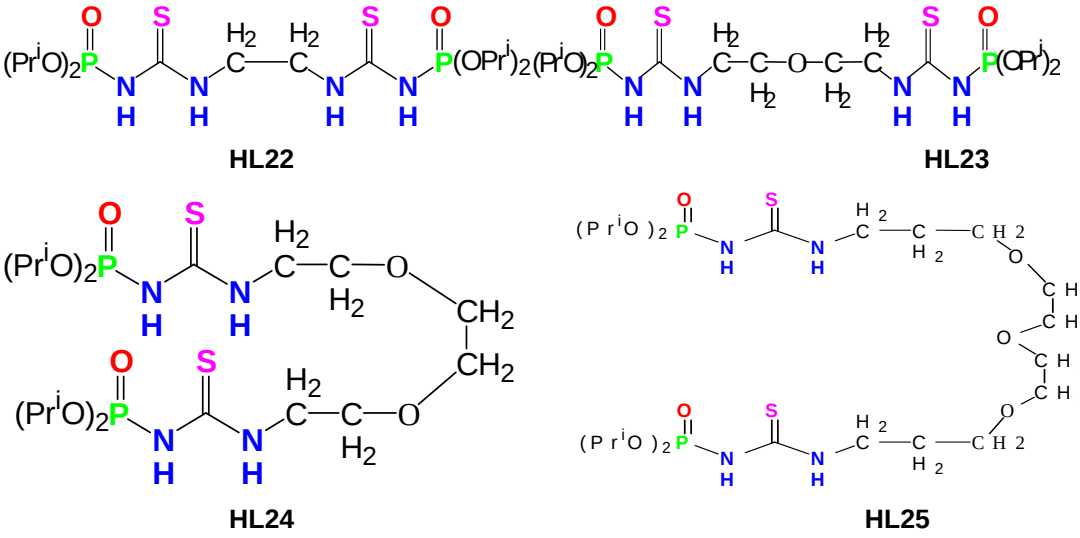

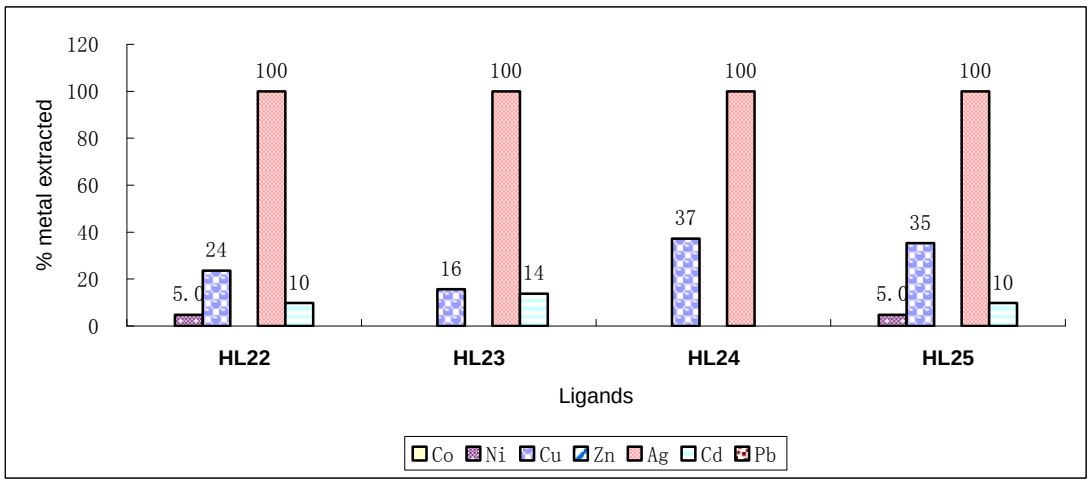

Figure 4.7. Comparison of the percentage extraction of the different metal ions in competitive extraction studies involving **HL22**, **HL23**, **HL24** and **HL25**. **pH of the aqueous phase = 5.5** and the **concentration of the ligand** is **2 x 10^{-3} mol dm^{-3}**.

All the ligands have two (*S,O*) electron donor bonding sites, which are symmetrically placed around the ligand. It seems that the ligand can accommodate two metal ions

thus forming a complex in a 2:1 mole ratio of metal ion to ligand. All these ligands have 100% Ag(I) extraction, based on a 1:1 ligand to metal mole ratio. So the extended (thio)phosphorylated(thio)urea ligands are good for the extraction of Ag(I) metal ions, but they could in future be treated with 2:1 ratio of metal ions with ligands, see if they will extract 100% of Ag(I).

HL24 has the highest extraction percentage for Cu(II) and **HL23** is the lowest, which confirms the transport results (see **Section 3.2.7**). **HL24** does not extract either Cd(II) or Ni(II); **HL23** extracts only Cd(II), and L22 and **HL25** have the same selectivity for these two metal ions.

The extraction efficiencies of **HL22**, **HL23**, **HL24** and **HL25** for Ag(I) are 100%. These ligands select some Cu(II), because of an extended hard donor atom structure. The selectivity for Ag(I) compared with Cu(II) is in the order: **HL23** > **HL22** > **HL25**> **HL24**. The percentages of Ag(I) and Cu(II) extraction for these ligands are very close. This means that the extended alkyl functional groups and oxygen donor atoms do not have a considerable effect in discriminating Ag(I) and Cu(II) extraction behaviour of these ligands.

4.3 Conclusion

Theory does not decree that transport and extraction results should coincide in terms of selectivity and efficiency for a specific metal ion[18]. The competitive metal ion extraction achieved with the series of *N*-(thio)phosphorylated (thio)ureas and *N*-(thio)phosphoryl-ated(thio)amide ligands was fully confirmed here by the results of the membrane transport experiments, so the extraction was worthy of study.

Figure 4.8 shows that most of the ligands studied extract 100% of Ag(I). The ligands which had the poor extraction efficiencies were the same as the transport results, viz. **HL5**, **HL7** and **HL17**. However, **HL1** was the best ligand for transport, but it did not extract all of Ag(I) metal ion into the organic phase. This showed that **HL1** most likely has a moderate stability constant with Ag(I), hence taking it into the organic phase and releasing the metal ion into the receiving phase. **HL26** had the highest selectivity for Ag(I) compared with the other metals. **HL4** extracted the most Cu(II) metal ion. Most of the ligands also extracted with small amount of Ni(II) and Cd(II). **HL2**, **HL3** and **HL5** selected more Ni(II), all at 33%, and **HL18** selected more Cd(II), at 31%. Only four (thio)amide ligands with bulk substituents extracted Co(II), viz. **HL1**, **HL7**, **HL11** and **HL17**. **HL8** was an unusual ligand in that it extracted a variety of metal ions, viz. Ag(I), Co(II), Cd(II), Ni(II), Pb(II) and Zn(II), except Cu(II).

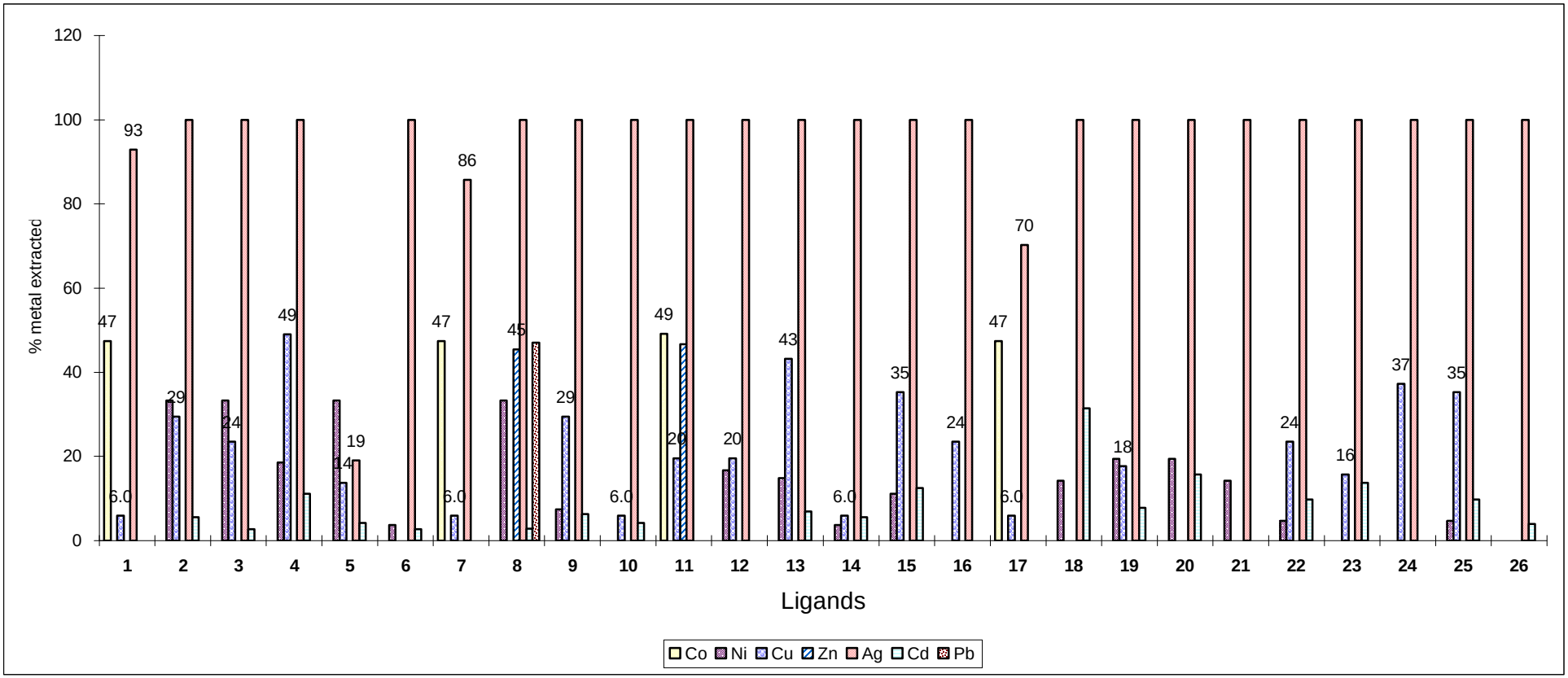

Figure 4.8 Comparison of the competitive extraction studies involving all ligands studied. The experimental conditions were: pH of the source phase =**5.5** and concentration of ligand = **2 x 10 $^{-3}$ mol dm^{-3}**. **1**=**HL1**, **2**=**HL2**, *ect*.

Chapter 5

Studies of Cu(I) and Ag(I) complexes with *N*-(thio)phosphorylated (thio)ureas

5.1 Introduction

As discussed previously, during transport and extraction the metal ions from the aqueous phase are carried to the organic phases dependent upon the coordination abilities and strength of binding exhibited by the *N*-(thio)phosphorylated (thio)amide and *N*-(thio)phosphorylated (thio)urea ligands. Cu(II) and Ag(I) were transported most effectively of the seven chosen metal ions (**Chapter 3**). Hence, the formation of Cu(II) and Ag(I) complexes with the series of *N*-(thio)phosphorylated (thio)amide and *N*-(thio)phosphorylated (thio)urea ligands were investigated. Some crystal structures have been determined and are valuable in the membrane transport studies owing to a clarification of the type of bonding that occurs between metal ions and ligands.

N-(thio)acylamido(thio)phosphates (**Scheme 5.1** (a))[36] are attractive pre-ligands because of their various ways of interaction with d-group and f-group cations upon deprotonation. Therefore, these compounds and their complexes can be used as extractants, analytical reagents[36] and structural fragments for the construction of metal-containing macrocycles and polycrown-compounds[45]. Dithioderivatives of these compounds, N-thioacylamidothio-phosphates (**Scheme 5.1** (b)) or their diphosphorus analogues (**Scheme 5.1** (c)), and their complexes with d-group cations, have been extensively studied. Ligands, as anions, are coordinated bidentately in these compounds, through the donor atoms of the carboryl and phosphoric groups.

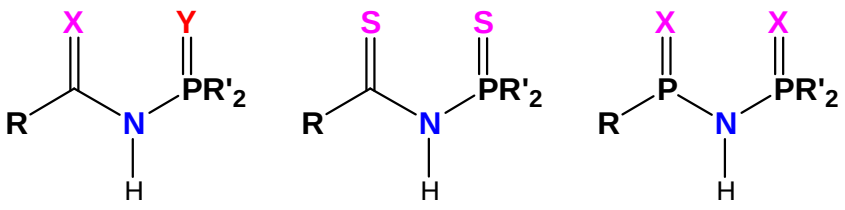

(a) (b) (c)

X, Y = O, S and Se; R=Alk, Ar, ArNH, AlkNH, Alk_2N; R' = OAlk, OAr, Ar

Scheme 5.1 (a) *N*-(thio)acylamido(thio)phosphate, (b) *N*-thioacylamido thiophosphate and (c) *N*-(thio) phosphate.

The present study is aimed at the preparation and full characterization of a number of Cu(I) and Ag(I) complexes with deprotonated *N*-(thio)phosphorylated (thio)urea (**HL**) ligands and also determination of the X-ray structure of *N*-(thio)phosphorylated (thio)amide free ligands for comparative proposes. The (*S,O*)-chelation is easily converted into (*O,O*)-chelation[37], during a typical reaction with alkaline permanganate or alkaline hydrogen peroxide changing thioureas into ureas. However, (*O,O*) donor atoms are not effective for soft Ag(I) metal ion bonding. Another difficulty experienced with Ag(I) is its light sensitively, so that most Ag(I) complexes can normally not be isolated in crystalline form. Yet, in this reaction a rare Ag(I) crystalline complex was obtained and is described below. In these studies, involving copper, a reductive elimination reaction was utilised for the conversion of the alcohol to an aldehyde and reducing Cu(II) to Cu(I). Cu(I) complexes of related ligands have been published by Verat[44], Herrman[46] and Sokolov[48]. All the known compounds have a trigonal planar geometry with S donor atoms. However, in a structure now determined by us, tetrahedral geometry occurred.

5.2 Results and discussion

Section 5.2.1 describes the preparation and isolation of the various Ag(I) and Cu(I) compounds, respectively, while **Section 5.2.2** is devoted to the spectroscopic characterisation of these compounds. In **Section 5.2.3** the crystal structures of two free (thio)amide ligands (PhCONHPO(OPr*i*)$_2$ (**1**) and BrPhCONHPO(OPr*i*)$_2$ (**2**)) are reported. Furthermore, the two Cu(I) complexes, [Cu(I)(**L4**-*S,S*)]$_6$ (**4**) and [Cu(I)(**L6**-*S,S*)]$_3$ (**5**) are obtained in two true polynuclear forms. In addition, the molecular structure of the very unique octanuclear [Ag(I)(**L4**-*S,N*)]$_8$ (**3**) cluster is also discussed.

5.2.1 Preparation of Ag(I) and Cu(I) compounds with *N*-(thio)phosphorylated (thio)urea and *N*-(thio)phosphorylated (thio)amide free ligands

5.2.1.1 Preparation of PhCONHPO(OPri)$_2$ (1) and BrPhCONHPO(OPri)$_2$ (2)

In the synthesis of compounds **1** and **2**, the original aim was to isolate the Ag(I) complex with deprotonated **HL1** and **HL11** (**Appendix 1**), which successfully transported Ag(I) metal ions (see **Section 3.3**). **HL1** and **HL11** were reacted separately in a 30 ml solvent mixture of acetonitrile–water in a volume ratio of (5:1). A solution of $NaOOCCH_3$ in water was used for deprotonation. The resulting reaction mixture was heated to reflux in an oil bath at 50ºC for 1 h. The colourless crystals were crystallized from an acetontrile-chloroform (1:1) solution over a period of ten

days. This basic solution destroyed the C=S bond, causing the ligands to be modified. That is a typical reaction (eq. 5.1), when alkaline permanganate or alkaline hydrogen peroxide converts thiourea into urea[81]:

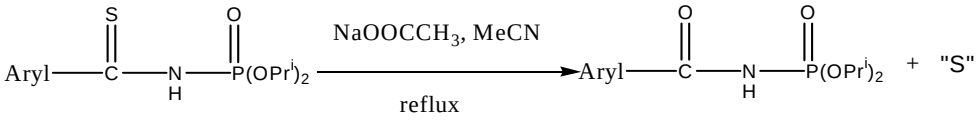

(eq. 5.1)

Thiourea Urea

5.2.1.2 Preparation of [Ag(I)(L4-S,N)]$_8$ (3)

Compound **3** was synthesized by the method described in **Section 2.2.2** using a 1:1 metal to ligand ratio. Single crystals were isolated from THF solvent after a period of one month in a closed thin glass pipette stored at 4 °C.

In this process, some of the $AgNO_3$ was converted into Ag_2O (eq. 5.2). The Ag_2O, similar to HgO, stripped the disubstituted thiourea[82] from sulphur and formed C=N double bonds as seen in eq. 5.3.

$$2AgNO_3 \xrightarrow{light} Ag_2O + N_2O_5$$

(eq. 5.2)

$$RNHC(S)NHR' + Ag_2O \xrightarrow{\Delta} RN{=}C{=}NR' + Ag_2S + H_2O$$

(eq. 5.3)

carbodiimides

R = $(Pr^iO_2)_2P(S)$; R' = H

The carbodiimide has a tautomeric structure in the form of a cyanamide, according to eq. 5.4.

$$RHN\text{-}C{\equiv}N: \rightleftharpoons RN{=}C{=}NH$$

(eq. 5.4)

Raman spectra investigations have shown that two tautomeric forms are present in equilibrium in the solid or fused state, and in solution[82]. In a further reaction the deprotonated ligands were trapped by the metal and formed the octanuclear complex, [Ag(I)(**L4**-*S,N)*]$_8$ (**Scheme 5.2**) (eq. 5.5). The X-ray crystal structure of compound **3** showed the two forms in eq. 5.4 coexisting (**Section 5.2.3.2**). This was confirmed by the ^{13}C **NMR** spectrum (**Table 5.1**: δ 92.4 and δ 74.2).

$$8(Pr^iO)_2P(S)NCNH + 8AgNO_3 \xrightarrow{KOtBu} [AgNCN(S)P(OPr^i)_2]_8 \qquad \text{(eq. 5.5)}$$

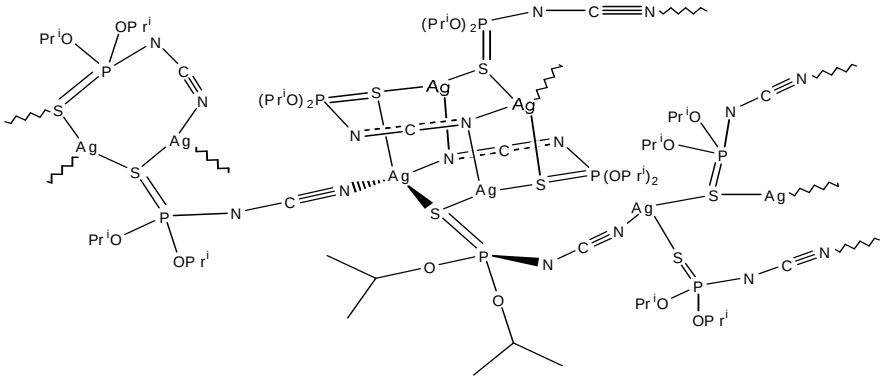

Scheme 5.2

5.2.1.3 Preparation of [Cu(I)(L4-S,S)]$_6$ (4) and [Cu(I)(L6-S,S)]$_3$ (5)

The two Cu(I) complexes were synthesized as described in **Section 2.2.2** and **Section 2.2.3**. Herrmann and co-workers[46] have established the reaction pathways of the N-thiophosphorylthioureas during Cu(I) complex formation. As in our experiments, the *N*-thiophosphorylated thiourea ligand (**HL**) was firstly deprotonated by stirring with KOH for 1 h (eq.5.6). The deprotonated ligand was added to Cu(II) nitrate salt at a ratio of 2:1, and this led to the formation of the unstable [Cu(II)L_2] chelate (eq. 5.7). The ethanol (as solvent) was oxidised by the unstable chelate to acetaldehyde and in turn the unstable [Cu(II)L_2] complex reduced to [Cu(I)L][46] in practically quantitative yield.

$$HL + KOH \rightarrow KL + H_2O \qquad \text{(eq. 5.6)}$$

$$Cu^{2+} + 2KL \rightarrow [CuL_2] + 2K^+ \qquad \text{(eq. 5.7)}$$

$$6[Cu(II)L_2] + 3C_2H_5OH \rightarrow 2[Cu(I)L]_3 + 3CH_3CHO + 6HL \qquad \text{(eq. 5.8)}$$

Crystals were isolated for complex **4** (**Figure 5.9** and **Chart 5.4**) from a 5:1 solvent mixture of acetone/hexane after storing it for one week in a closed thin glass pipette in a refrigerator at 4 ºC. This condition has a less open evaporation surface area, and a low surrounding temperature. It could be that one requires slow evaporation of the solvent, in order to grow good quality crystals. Single crystals of complex **4** were colourless and needle-shaped.

The crystalline complex **5** (**Figure 5.13**) was obtained by the same method as complex **4**, but the colourless, flat crystals were obtained from a THF solution which stood for one month. An accidental chemical reaction occurred between THF and water. An OH-group replaced an α-hydrogen in the THF molecule, and an alcohol

molecule was formed with simultaneous elimination of hydrogen gas (eq. 5.9). At present, the mechanism of this reaction has not been established.

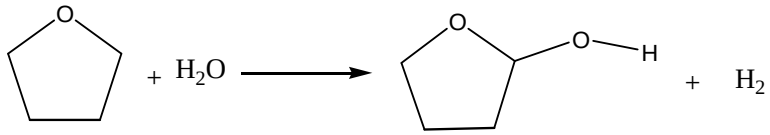

(eq. 5.9)

5.2.2 Spectroscopic characterization of compounds 3, 4 and 5

NMR Spectroscopy

The ^{1}H, ^{13}C and ^{31}P **NMR** data for compounds **3**, **4** and **5** were recorded in $CDCl_3$ and the results are summarized in **Tables 5.1**, **5.2** and **5.3**, respectively**.**

The **^{1}**H signal of the original NHP(S) unit in the N-thiophosphorylthiourea ligands is absent in all the **^{1}**H **NMR** spectra, confirming that deprotonation has occurred.

In all the **^{1}**H **NMR** spectra the isopropyl hydrogen atoms appear at approximately δ 1.30 (CH_3) and δ 5.00 (CH). In compound **3**, the methyl group protons have the same chemical shifts, but for compounds **4** and **5**, there are two chemical shifts. In the **^{1}**H **NMR** spectrum a multiplet at δ 4.72 occurs for H^2 (proton with tertiary carbon of isopropyl group) in compound **3**, but H^2 in compounds **4** and **5** forms doublets of septets, with a coupling constant of ^{3}J = 6.16 Hz, at δ 4.73. These results are consistent with the X-ray structure (see **Section 5.2.3.3**) which shows the N≡C-N combination in a close to linear coordination with Ag(I) metal ion in compound **3** (**Table 5.1**). The linear coordination geometry is more symmetrical than the bidentate chelate ring as a result of the partial conjugate system of S-P-N-C-S with the metal ion in compounds **4** and **5** (**Tables 5.2** and **5.3**). As expected, for complex **3** no NH unit is present, because of the nitrile group formation. As discussed (eq. 5.4), N≡C-NHR exists as a tautomeric structure with HN=C=NR in compound **3**, which is proved by the **^{13}**C **NMR** spectra. Far upfield in the **^{13}**C **NMR** spectra, two carbon peaks occur at δ 92.93 and δ 74.27.

In the ^{1}H **NMR** spectrum of compound **4**, the signals of the two nonequivalent protons of the NH_2 group are observed at δ 6.36 and δ 5.81 (**Table 5.2**). It should be noted that the signals of the H^{5a} and H^{5b} protons of the NH_2 groups have different scalar coupling with the phosphorus atom (**Scheme 5.3**).

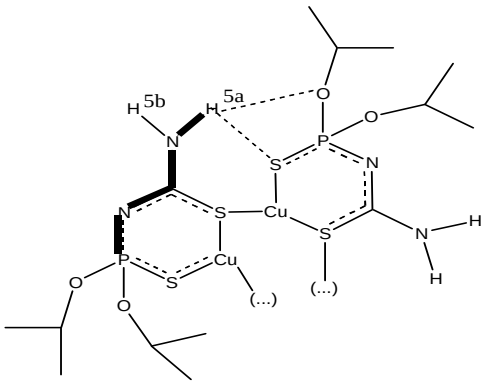

Scheme 5.3

The ^{1}H NMR spectrum of compound **4**, obtained at 25 °C is shown in **Figure 5.1 B**. The downfield resonance H^{5a} of the NH_2 group in compound **4** clearly shows a splitting due to the $^{4}J_{PNCNH}$ spin–spin interaction. The contribution of the observed splitting to the presence of $^{4}J_{PNCNH}$ spin–spin coupling is confirmed unambiguously by recording the ^{1}H **NMR** spectra with ^{31}P decoupling, and $^{4}J_{PNCNH}$ coupling constants are measured for the polynuclear compound (8.60 Hz) by Sokolov *et al.*[45].

For complex **4** in $CDCl_3$, a comparative analysis of ^{1}H **NMR** data gives evidence for the existence of a polynuclear chelate at room temperature. The ^{1}H **NMR** spectrum of H^{5a} and H^{5b} shows two signals of different intensity, corresponding to the two nonequivalent protons of the NH_2 group (**Figure 5.1 B**). This explains the participation of the sulphur atom of the C=S groups in bridging bonds, resulting in a decrease of the electronic density in the conjugated chelate ring. There is thus an increase in the conjugation degree of the lone electron pair of the NH_2 group and an increase of the H_2N-C bond rotation barrier[47].

Variation of the chemical shift for the H^{5a} proton of the NH_2 group in complex **4** could be assigned to the formation of intramolecular hydrogen bonds in molecules of the polynuclear aggregate (**Scheme 5.3**). This is confirmed by the ^{1}H **NMR** spectrum of **4** in d_6-acetone (**Figure 5.1 A**) which shows a weak shift of the H^{5a} resonance ($\Delta\delta_H$ + 0.3), whereas the H^{5b} peak is strongly downfield shifted ($\Delta\delta_H$ + 1.5) due to the formation of hydrogen bonds. Such an interaction could take place with the solvent [$NH^{ab}\cdots O=C(Me)_2$] or with another chelate molecule (**Figure 5.1 A**).

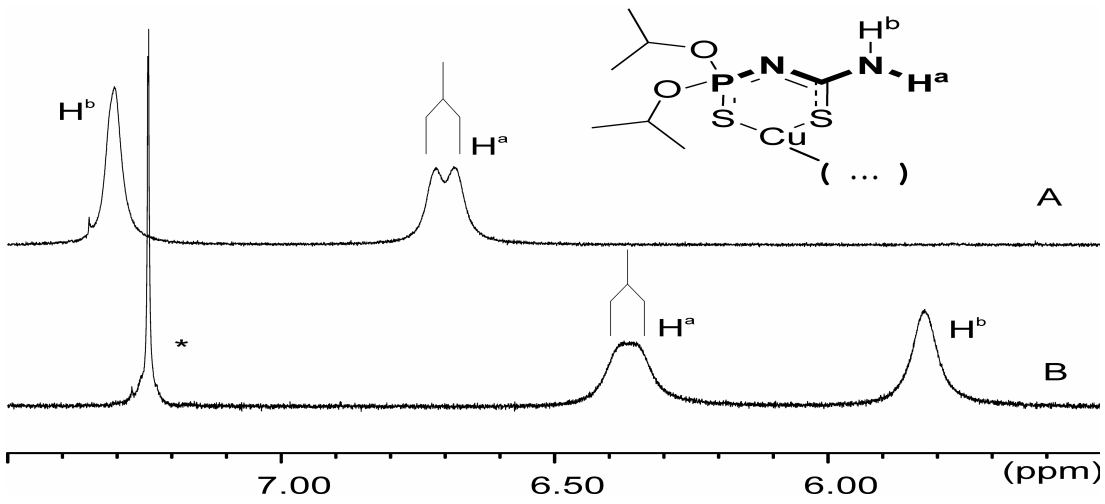

Figure 5.1 Proton resonances of the NH_2 group of complexes $[Cu_nL_n]$ at 25 °C in solvent $(CD_3)_2C=O$ (**A**) and $CDCl_3$ (**B**). The signal of $CDCl_3$ is marked by *****.

Thus, a comparative analysis of the ^1H **NMR** spectra of two nonequivalent protons in the NH_2 group for complex **4** clearly demonstrates the preservation of the bonding between [CuL] units of $[Cu_nL_n]$ aggregates in $CDCl_3$.

As mentioned, compound **5** (**Table 5.3**) consists of a polynuclear Cu(I) complex and an OH group replaced an α-hydrogen in a THF molecule, which modified the ^1H and ^{13}C **NMR** spectra. In THF solvent, multiple peaks of H^{10} occur at δ 1.41, and tertiary butyl groups (H^6) exhibit a singlet at δ 1.38. The methyl group as part of the isopropyl group, resonates at δ 1.35, and forms doublets with a coupling constant of ^3J = 6.16 Hz.

The ^{13}C **NMR** spectra of complexes **4** and **5** in $CDCl_3$ show narrow ($\Delta\delta_H$ = 11 Hz) multiplets at δ 173.9 and δ 168.6 for the thiocarbonyl carbon atom. The CS carbon signal appears as a singlet in the spectra of the free thiourea and thioamide ligands and their mononuclear chelates[83]. Similarly, complex **3** also has multiplet peaks for NCN carbon atoms. The observed splitting of ^{13}C **NMR** peaks is a result of nonequivalence of these carbon atoms, which confirms the existence of the polynuclear structures.

In the ^{31}P **NMR** spectra of the neutral *N*-thiophosphorylated ligands, the chemical shifts occur normally in the range δ 52.8–60.6[50]. However, in compounds **3**, **4** and **5**, all the ^{31}P signals are out of this range. Compound **3** forms an N≡C bond, so an increase of the electron density perhaps causes an upfield shift at δ 63.73 and compounds **4** and **5** resonate downfield at δ 51.23 and δ 49.90, respectively. The

phosphorus proton in ^{31}P **NMR** spectra confirm the presence of deprotonated ligands[50].

Table 5.1 ^{1}H, ^{13}C and ^{31}P **NMR** data for compound **3** in $CDCl_3$.

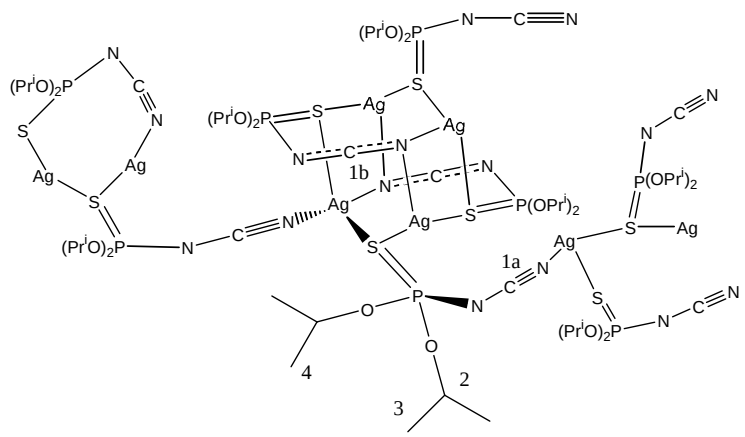

Assignment	**δ**
^{1}H **NMR**	
$H^{3/4}$	1.36 (d, ^{3}J=6.16, 12H)
H^{2}	4.72(m, 2H)
^{13}C **NMR**	
$C^{3/4}$	23.45 (s)
C^{2}	29.68 (s)
C^{1b}	74.27 (m)
C^{1a}	92.39 (m)
^{31}P **NMR**	
P	63.73 (s)

Table 5.2 ^{1}H ^{13}C and ^{31}P **NMR** data for compound **4** in $CDCl_3$.

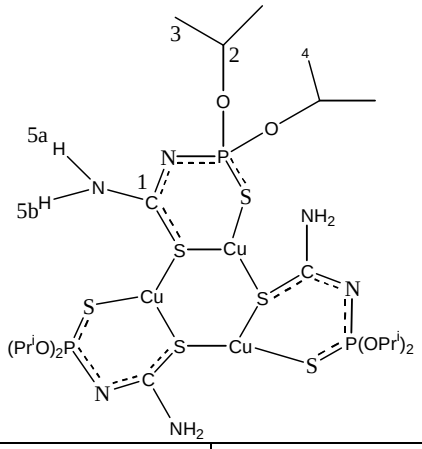

Assignment	**δ**
^{1}H **NMR**	
$H^{3/4}$	1.34 (d, ^{3}J=6.16, 6H)
	1.36 (d, ^{3}J=6.16, 6H)
H^{2}	4.73 (d. sept, ^{3}J=6.16, 2H)
H^{5a}	6.36 (br., 1H)
H^{5b}	5.81 (br., 1H)
^{13}C **NMR**	
$C^{3/4}$	29.67 (s)
	23.45 (s)
C^{2}	72.67 (s)
C^{1}	173.94 (m)
^{31}P **NMR**	
P	51.23 (s)

Table 5.3 ^{1}H ^{13}C and ^{31}P **NMR** data for compound **5** in $CDCl_3$.

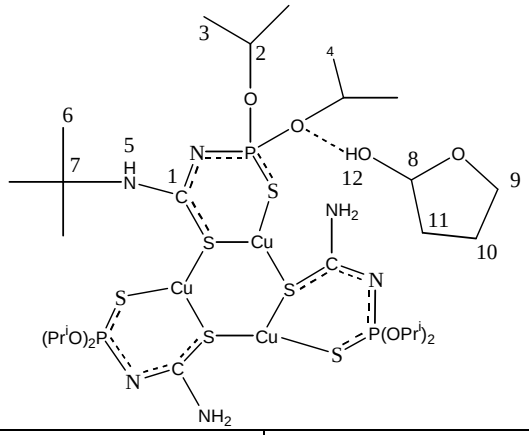

Assignment	**δ**
^{1}H **NMR**	
$H^{3/4}$	1.35 (d, ^{3}J=6.16, 12H)
H^{6}	1.38 (s, ^{3}J=6.16, 9H)
H^{10}	1.41 (m, 2H)
H^{12}	4.24 (q, ^{3}J=7.04, 2H)
H^{9}	4.35 (t, ^{3}J=7.04, 2H)
H^{2}	4.73 (d. sept, ^{3}J=6.16, 1H,)
H^{5}	6.14 (br., H)
H^{8}	6.58 (d, ^{3}J=9.39, 1H)
^{13}C **NMR**	
C^{2}	30.92 (s)
$C^{3/4}$	23.85 (s)
C^{6}	28.39 (s)
C^{7}	54.10 (s)
C^{10}	67.41 (s)
C^{11}	51.23 (s)
C^{9}	72.28 (s)
C^{1}	168.59 (m)
C^{8}	207.03 (s)
^{31}P **NMR**	
P	49.90 (s)

Infrared spectroscopy

The IR spectra of compounds **3** and **4** were analysed using a ZnSe plate. Spectroscopic data are summarized in **Table 5.4**.

Table 5.4 Selected infrared data (cm^{-1}) in compounds **3** and **4**.

	ν_{NH}	$\nu_{C\equiv N}$	ν_{sCN}	ν_{CS}	ν_{PNC}	ν_{POC}
$Ag[NCNP(S)(OPr^i)_2]$ **(3)**		2173 br., s 2128 sh.			748 s	978 s
$Cu[H_2NC(S)NP(S)(OPr^i)_2]$ **(4)**	3291 w		1523 br., s	1621 vs	748 s	991 s

The lowest limit of our IR spectrometer analysing using a ZnSe plate is 650 cm^{-1}, hence, a P=S band is not clearly observed. The P=S group absorption bands for neutral ligands normally appear characteristically in the range 616–640 cm^{-1}, but the deprotonated ligand is down shifted at 604–618 cm^{-1}.[44] In compound **4**, the band for NH_2 clearly exists at 3291 cm^{-1}, which is a unique band assigned. To make these two complexes the same starting ligand ($(Pr^iO)_2P(S)NC(S)NH_2$) was used, but nevertheless, compound **3** formed via a ligand rearrangement reaction (**Section 5.2.1.2**). As expected, compound **3** does not show an NH_2 peak, and the nitrile group occurs as a strong broad peak at 2173 cm^{-1} with a shoulder at 2128 cm^{-1}.[84] Occurrence of the new broad and strong peak at 1460–1568 cm^{-1} shows the presence of the conjugated SCN unit, but probably also the formation of (*S,S*) chelates[48]. The SCN unit is present in compound **4**, but not in compound **3**.

Mass spectrometry

Electrospray ionisation mass spectrometry (ESI-MS) data for compound **3** are summarized in **Table 5.5**. A low intensity peak for the molecular ion is observed at *m/z* 329. The base peak fragment of complex **3** corresponds to the $[Ag(N\equiv C)]^+$ unit. Another diagnostic signal corresponding to $[M + SP]^+$ is present at *m/z* 391. This provides evidence for the polynuclear molecular structure. There is a high intensity peak (80%) for the removed metal at m/z 220.

Table 5.5 ESI-MS data for compound **3**.

m/z	Intensity	Fragment ion
391	28	$[M+ SP]^+$
329	15	$[M]^+$
220	80	$[M-Ag]^+$
133	100	$[Ag(N\Xi C)]^+$

The characteristic fragmentation peaks attained by ESI-MS analysis for complex **4** are listed in **Table 5.6**. The molecular ion of complex **4** is observed at *m/z* 319, and the $3[M]^+$ is observed as a peak at *m/z* 957. Complex **4** is a polynuclear molecule, which was discussed by ^{13}C **NMR** spectra and the X-ray crystal structure will confirm that complex **4** has three nuclear units, which will be described in **Section 5.2.3**. Therefore, two ligands coordinate to the metal ions forms the base peak at *m/z* 575. The fragment at *m/z* 376 corresponds to the mass of the molecular ion with an additional SCN fragment. The most stable fragment occurs as $[CuSPN]^+$ at *m/z* 141.

Table 5.6 ESI-MS data for compound **4**.

m/z	Intensity	Fragment ion
957	10	$3[M]^+$
575	100	$[M+L]^+$
376	45	$[M+ SCN]^+$
319	30	$[M]^+$
141	30	$[CuSPN]^+$

Table 5.7 summarizes the ESI-MS spectrometric data obtained for compound **5**. The base peak corresponds to the molecular ion peak at *m/z* 375, and the other diagnostic peak is observed at *m/z* 419 for the additional CS fragment.

Table 5.7 ESI-MS data for compound **5**.

m/z	Intensity	Fragment ion
419	45	$[MCS]^+$
375	100	$[M]^+$

5.2.3 Structure determination of compounds 1–5

5.2.3.1 Crystal and molecular structures of the two free ligands: PhCONHPO(OPr*i*)$_2$ and BrPhCONHPO(OPr*i*)$_2$

The X-ray diffraction structure of compound **1** is shown in **Figure 5.2**, and the selected bond lengths and angles are given in **Table 5.8**. The structure was solved in the monoclinic space group C_2/c.

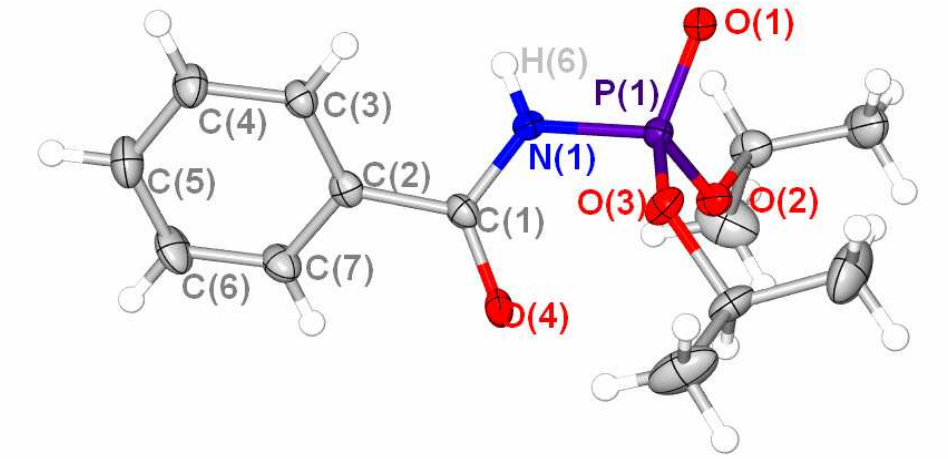

Figure 5.2 Molecular structure of the free ligand PhCONHPO(OPr*i*)$_2$ (compound **1**)showing the atom numbering scheme. Ellipsoids enclose 50% of the electron density.

The structure of compound **1** shows the ligand, which was used to study the metal ion transport and extraction. This is an *N*-oxyphosphorylated oxyamide with a benzyl substituent. The X-ray structure of compound **1** had been published and characterized by Zabirov *et al*.[43]. The crystal structure is briefly described here and compared with previous reports. They have the same crystal system and space group. Compound **1** has slightly shorter a, b and c (22.831(2) Å, 8.831(9) Å and 14.984(2) Å) values compared with Zabirov's structure (22.946(3) Å, 8.950(1) Å, 15.440(1) Å). The angle C(1)-N(1)-P(1) (124.4°) is slightly smaller than in Zabirov's structure (125.5°). The distance of C=O in compoun d **1** is short with a value of 0.075 Å, which is in the range of carbon–oxygen double bond distances. The bond length of P=O is the same (**Table 5.8**); the two isopropyl groups and aromatic ring are similar to those in Zabirov's structure.

The X-ray diffraction structure of compound **2** is shown in **Figure 5.3**, and the selected bond lengths and angles are given in **Table 5.8**. In compound **2** a *p*-

hydrogen has been substituted by Br. The crystal has a monoclinic unit cell, and the space group is $P2_1/n$.

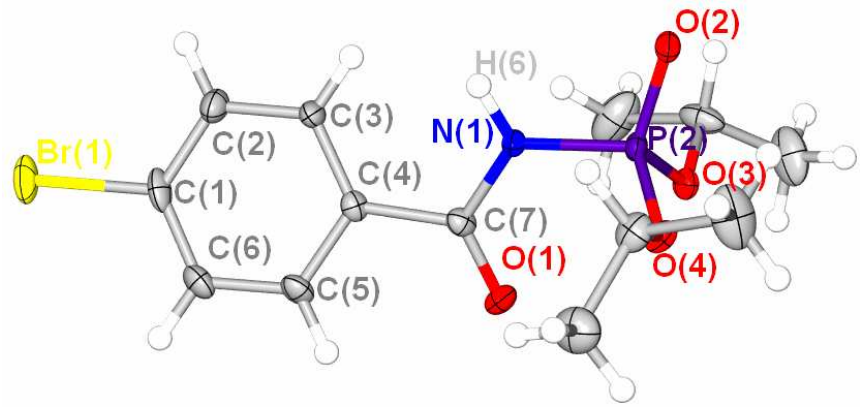

Figure 5.3 Molecular structure of the free ligand BrPhCONHPO(OPr*i*)$_2$ (compound **2**) showing the atom numbering scheme. Ellipsoids enclose 50% of the electron density.

The C=O bond length (1.225(4) Å) is slightly shorter than in compound **1** (1.309(2) Å), but the P=O distance and the angle C(1)-N(1)-P(1) are both identical to those in compound **1** (**Table 5.8**).

Considering the bond lengths in the two OPr^i groups, compound **1** and compound **2** do not differ significantly from one another, but the angles are not the same. The most likely reason is disordering and probably rotation of the isopropyl groups. The O-P-O angle range is from 114.6(8)º to 116.2(1)º, and the P-O-C angle from 119.7(2)º to 121.1(2)º for both compounds.

The packing of compound **1** is shown in **Figure 5.4**, viewed along the b-axis. Each molecule with the aromatic ring along the c-axis is packed back to back.

Figure 5.5 shows the packing of compound **2** along the a-axis. Each identical molecule is packed in a layer along the c-axis. Two layers have the Br atoms pointing in one direction and the next two layers have the Br atoms pointing in the opposite directions.

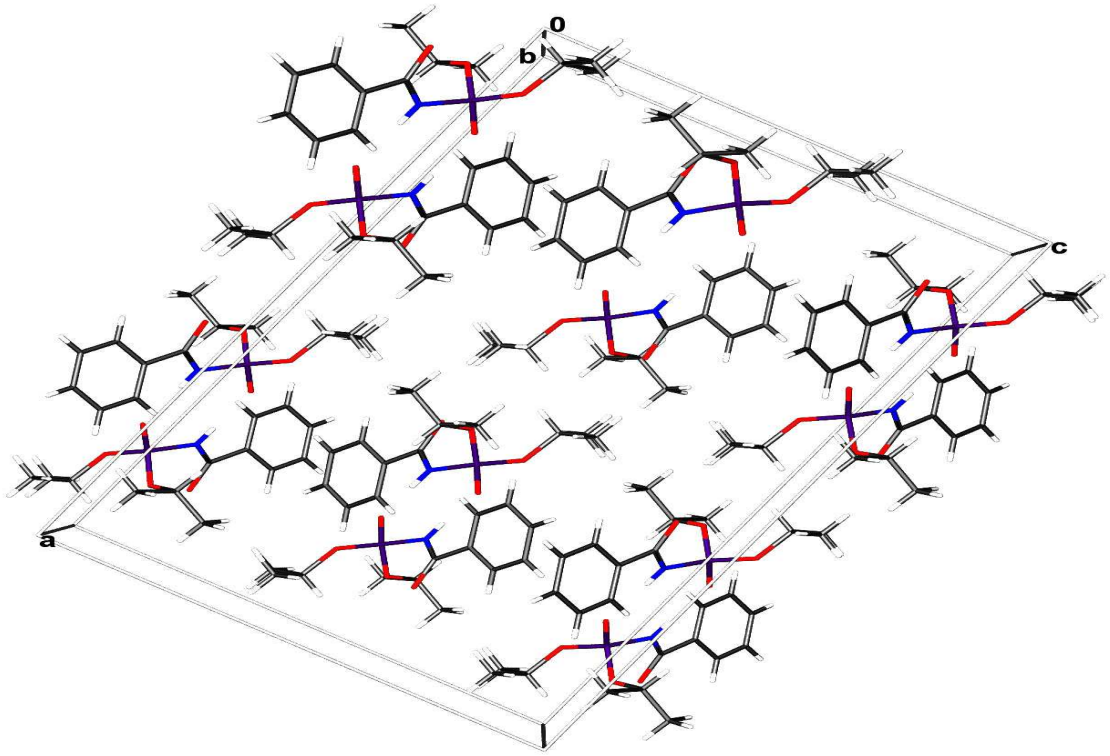

Figure 5.4 Unit cell and packing pattern of compound **1** viewed along the b-axis.

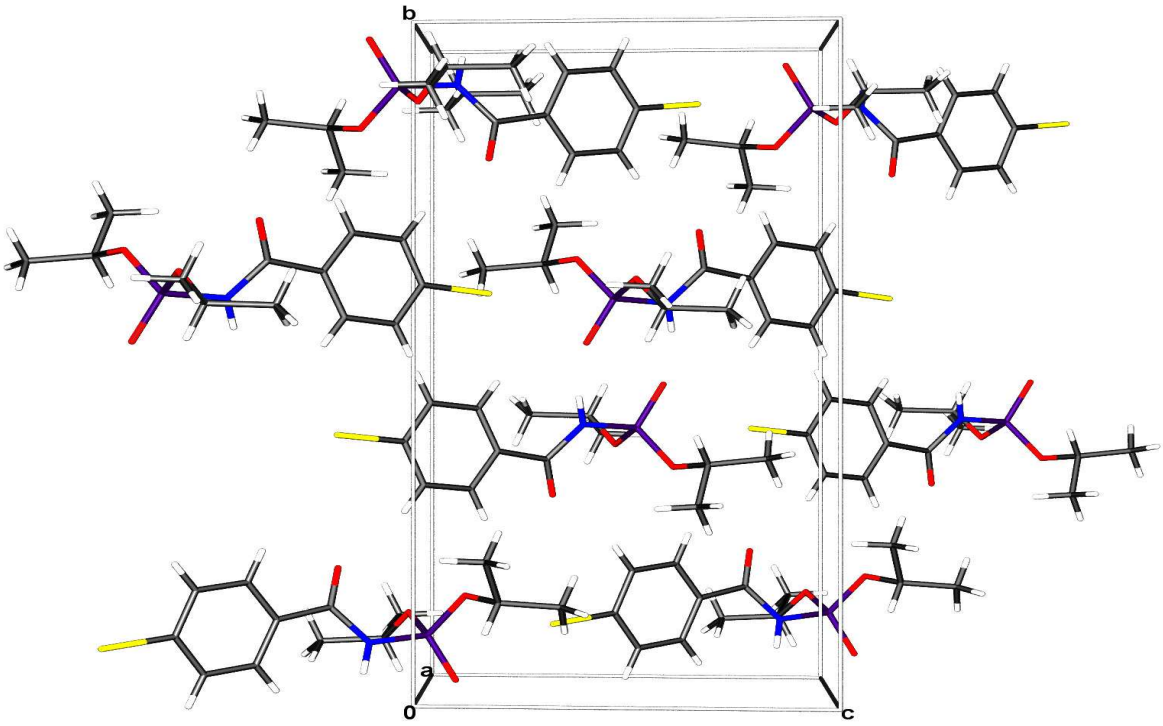

Figure 5.5 Unit cell and packing pattern of compound **2** viewed along the a-axis.

Table 5.8 Selected bond lengths (Å) and angles (º) for compound **1** and **2**.

Compound **1**		Compound **2**	
Bond lengths (Å)			
C1-O4	1.309(2)	Br1-C1	1.903(3)
C1-N1	1.374(3)	P2-O2	1.473(2)
N1-P1	1.663(2)	P2-O3	1.555(2)
N1-H6	0.800(2)	P2-O4	1.558(2)
P1-O1	1.465(2)	P2-N1	1.669(3)
P1-O3	1.553(2)	O1-C7	1.217(4)
P1-O2	1.565(2)	O3-C8	1.466(4)
O2-C8	1.469(2)	O4-C9	1.467(4)
O3-C9	1.466(2)	N1-C7	1.390(4)
		N1-H6	0.910(4)
Bond angles (º)			
O1-P1-O3	115.9(8)	O2-P2-O3	115.9(1)
O1-P1-O2	114.6(8)	O2-P2-O4	116.2(1)
O3-P1-O2	103.5(8)	O3-P2-O4	99.4(1)
O1-P1-N1	108.5(8)	O2-P2-N1	107.7(1)
O3-P1-N1	104.4(8)	O3-P2-N1	108.8(1)
O2-P1-N1	109.3(8)	O4-P2-N1	108.4(1)
C1-N1-P1	124.4(2)	N1-C7-C4	116.8(3)
O4-C1-N1	122.1(2)	C7-N1-P2	123.2(2)
N1-C1-C2	116.6(2)	C8-O3-P2	121.1(2)
C8-O2-P1	120.1(1)	C9-O4-P2	119.7(2)
C9-O3-P1	126.4(1)	C6-C1-Br1	118.6(2)
O2-C8-C10	106.3(2)	C2-C1-Br1	119.0(3)
O2-C8-C11	107.8(2)	O1-C7-N1	121.9(3)

5.2.3.2 Crystal and molecular structure of [Ag(I)(L4-*S*,*N*)]$_8$ (3)

The X-ray diffraction structure of compound **3** is shown in **Figure 5.6** (a), and the selected bond lengths and angles are given in **Table 5.9**. The structure was solved in the monoclinic space group $P2_1/c$.

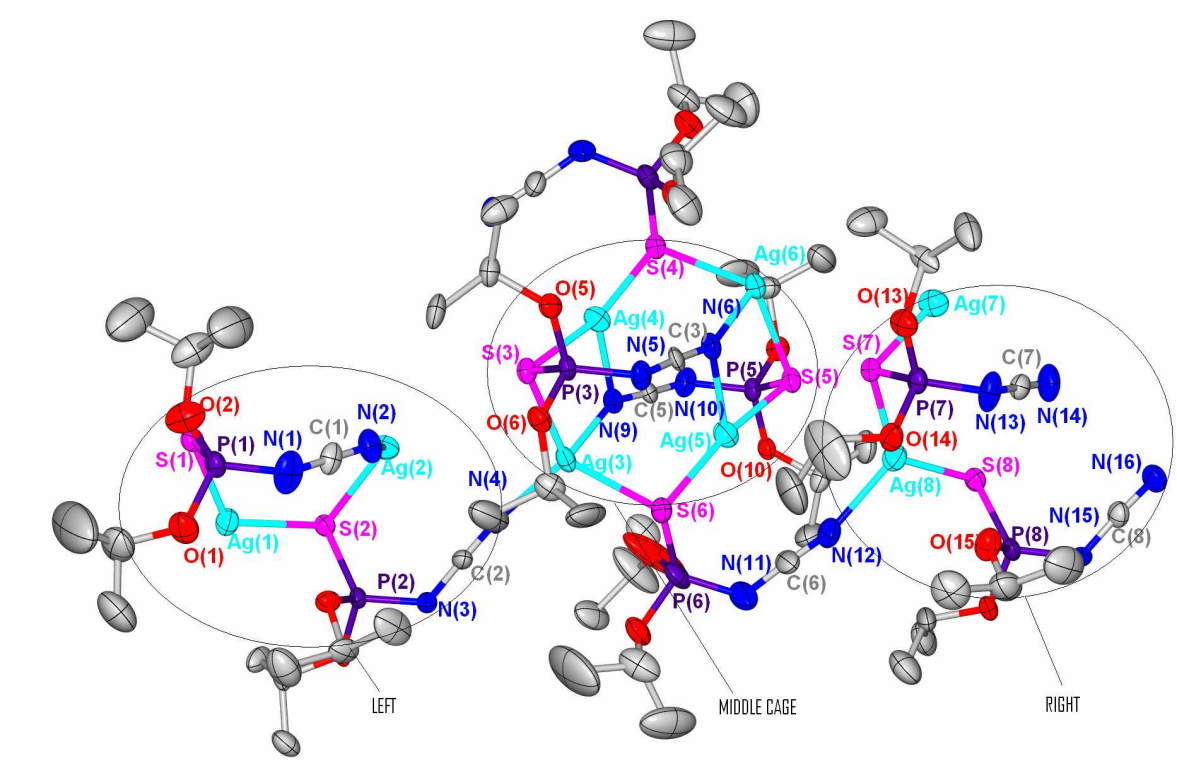

(a)

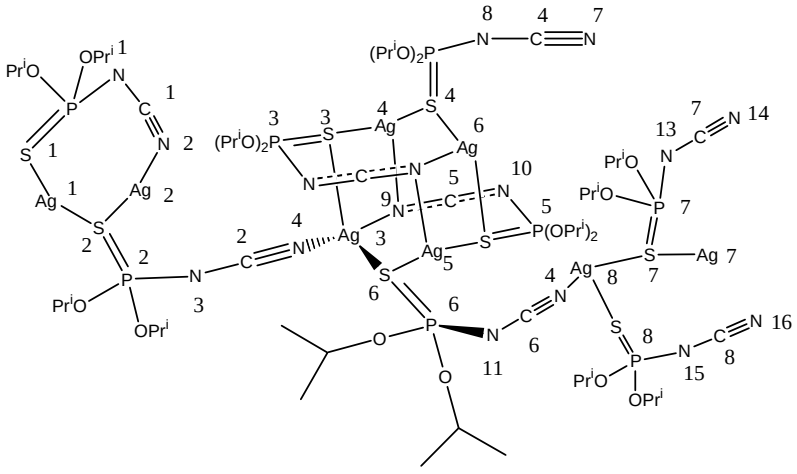

(b)

Figure 5.6 (a) Molecular structure of compound [Ag(**L4**-*S,N*)]$_8$ (compound **3**) showing the atom numbering scheme. Ellipsoids enclose 50% of the electron density. (b) The simplified line diagram of compound **3**.

The simplified line diagram of complex **3** is presented in **Figure 5.6** (b). The structure shows that eight Ag(I) atoms are bonded to eight deprotonated ligands forming a [Ag(L-S,N)]$_8$ cluster. The molecular structure (**Figure 5.6**) can be divided into three different entities: The left section is connected to the middle cage by a tetrahedral Ag(3); the middle cage is connected to the right-hand chain by a sulphur-phosphorus bond (S(6)-P(6)).

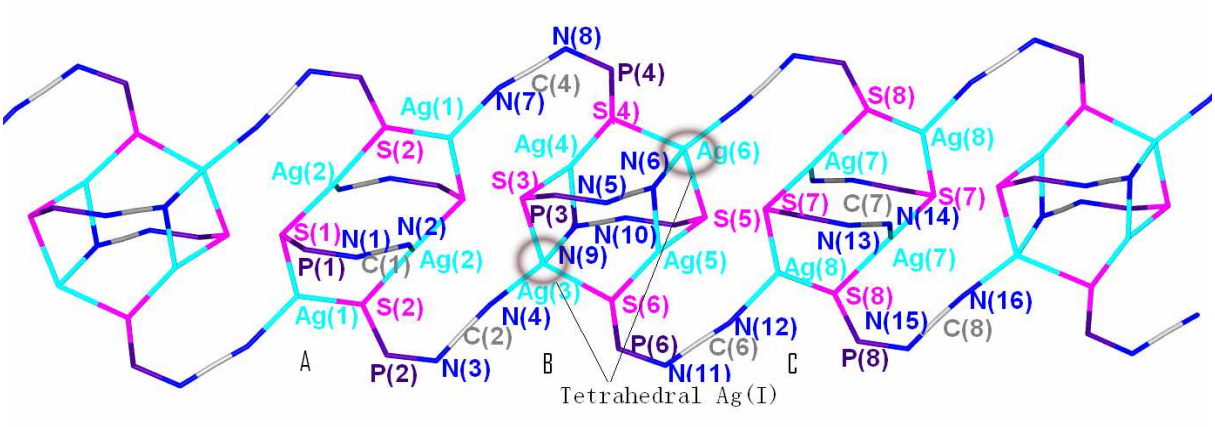

Figure 5.7 Extended structure of compound **3** showing the connection with each section. The isopropyl groups are omitted for clarity.

Figure 5.7 represents the extended structure of compound **3**, showing the connectivity details. It is interesting and worth mentioning that the structure contains three asymmetric cavities (**A**, **B**, **C**). Cavities are connected by two S-P-N-C-N bridges with two Ag-S-Ag units to form 16-membered rings.

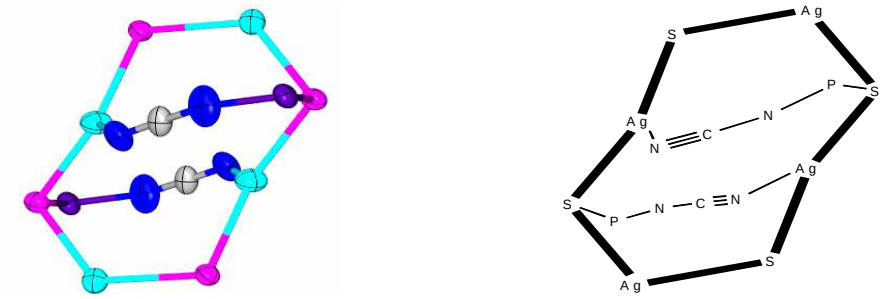

(a) (b)

Chart 5.1 (a) Structure of Ag_4S_4 core of section **A** with thermal ellipsoids at 50% probability level (certain units are omitted from the Ag_4S_4 ring for clarity). (b) Line diagram of section **A** with the bold bonds showing the Ag_4S_4 ring.

Section **A** (**Chart 5.1**) and section **C** are very similar, because they have the same constitution, but slightly different bond lengths and angles. Only two Ag-S-Ag angles are larger than 100.0(3)º. They are the Ag(1)-S(2)-Ag(2) angle at 101.5(2)º and the Ag(8)-S(8)-Ag(7) angle at 100.1(1)º, which are respectively located in the equivalent positions of section **A** and section **C**. All the other Ag-S-Ag angles are around 90.0º. The symmetrical angles of S(2)-Ag(1)-S(1) (**A**) and S(8)-Ag(8)-S(7) (**C**) have a 19.2(1)º difference. The almost linear N(1)-C(1)≡N(2) angle (177.0(2)º) differs by 0.1º from N(13)-C(7)≡N(14) (177.1(2)º). The terminal N donor atoms show a monodentate coordination mode.

All the cavities could be useful for storing gases or solvent of crystallization, especially section **B** (in **Figure 5.7** and simplified in **Chart 5.2**), which is a special cage. A tetranuclear Ag_4S_4 ring entity occurs in this cage. The S donors and N (N(6) and N(9)) donors exhibit μ_2-bridging coordinated modes. It is best named a $Ag_4N_2S_4$ cage, which is unprecedented.

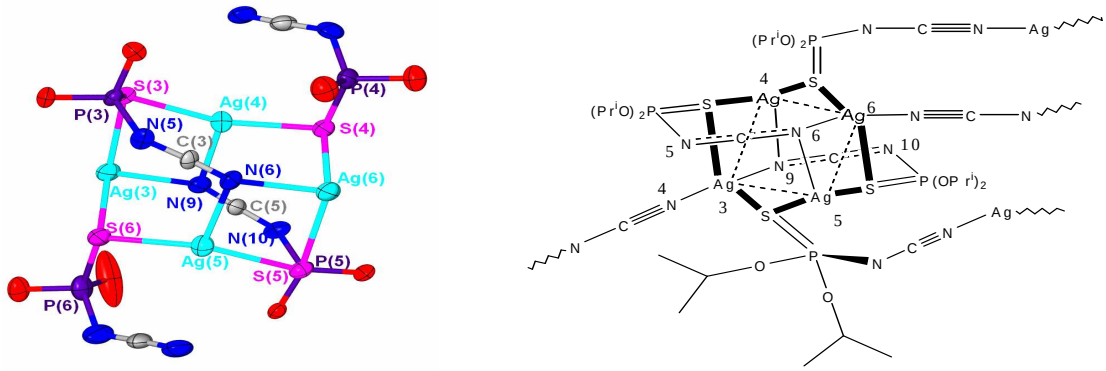

(a) (b)

Chart 5.2 (a) Structure of Ag_4S_4 core of the middle cage unit Ag_4L_4 with thermal ellipsoids at 50% probability level (only the ligand moiety on the upper $Ag_4N_2S_4$ cage is shown for clarity). (b) Line diagram of the $Ag_4N_2S_4$ cage with the bold bonds of Ag_4S_4 ring.

In the structure of compound **3**, it is indicated that linear cyanamido(-) groups $(N{\equiv}C\text{-}NR)^-$ coordinate with Ag(I).[85] The average single C-N bond distance is 1.281(2) Å and the triple bond distance is 1.152(3) Å. The mean value of the N≡C-N angle is 177.1º, which is significantly close to a linear bond[86,87]. The Ag-N bond length of Ag-NCN complexes has been reported in a wide rang from 2.143 Å to 2.733 Å[88,89]. All

our metal nitrogen bond lengths (2.177(7)–2.549(7) Å) fall in that range. The other two unusual bonding modes of Ag(5) or Ag(6)-N(6)-C(3)-N(5) and Ag(4) or Ag(3)-N(9)-C(5)-N(10) are located in the middle cage (section **B**). The NCN units are considered to adopt the carbodiimido(-) structure (N^-=C=NR)[85] as the dominant canonical form, so that the terminal nitrogen can exhibit bridging coordinated with two Ag(I) atoms (**Scheme 5.4**). The angles of N=C=N are 175.7(8)º and 177.3(9)º, which are similar to the published value of 176.6º.[68] However, interestingly, the N(6)-C(3) (1.162(9) Å) and N(9)-C(5) (1.170(9) Å) bond distance is very close to the general C≡N (1.16 Å) and is shorter than that of C(3)-N(5) (1.287(9) Å) and C(5)-N(10) (1.283(9) Å)[90]. The Ag-N-C angles have various values from 110.3(5)º to 171.8(6)º. The mean values for the two large angles Ag(6)-N(16)-C(8) and Ag(3)-N(4)-C(2) is 171.5(3)º, which is close to linear. These two angles are connected through cage **B** at opposite directions in space. In the middle cage **B**, the angle of Ag(3)-N(9)-Ag(4) and Ag(5)-N(6)-Ag(6) are 82.6(2)º and 87.1(2)º respectively, both being acute.

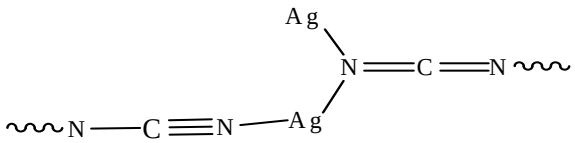

Scheme 5.4

In compound **3** the Ag(3) and Ag(6) (marked in **Figure 5.7**) are tetrahedral surrounded by donor atoms, whereas the other Ag(I) atoms (Ag(1), Ag(2), Ag(4), Ag(5), Ag(7), Ag(8)) all have trigonal geometry with two sulphurs and a terminal nitrogen as donors. Ag(3) and Ag(6) are two connection points, which links section **A** and section **C** with the middle cage. The tetrahedral Ag(I) bonds to two S and two N atoms with four separate ligands: Ag(3)-S = 2.618(2), 2.678(2) Å, Ag(3)-N = 2.177(7), 2.349(7) Å and Ag(6)-S = 2.627(2), 2.667(2) Å, Ag(6)-N = 2.189(7), 2.399(7) Å. The S-Ag(3)-N angle range is 97.7(2)º to 113.3(2)º; the S-Ag(6)-N angle range is 96.0(2)º to 116.0(2)º, so these two Ag(I) atoms have distorted tetrahedral coordination geometry. Each sulphur atom asymmetrically bridges two silver atoms. The average distances for 3-, 4- coordinated silvers are 2.500(2) and 2.641(2) Å respectively, which confirm the Ag-S distance increases as the coordination number of Ag increased[91].

As shown in **Chart 5.3**, a common structural element is a central Ag_4 core (although with different parameters), where the Ag atoms are bridged by S atoms of four ligands to give an eight-membered Ag_4S_4 ring[92]. The three Ag_4S_4 rings (**Chart 5.1 (b)**

and **5.2 (b)**) are presented in each section A, B and C, have four Ag atoms and four S atoms which are coplanar. The dihedral angle between the 4 planar Ag and 4 planar S are 88.5º, 31.4º and 13.1º, in section **A**, **B** and **C**, respectively. In section **A** and **C** Ag_4S_4 rings are much flatter than that in **B**.

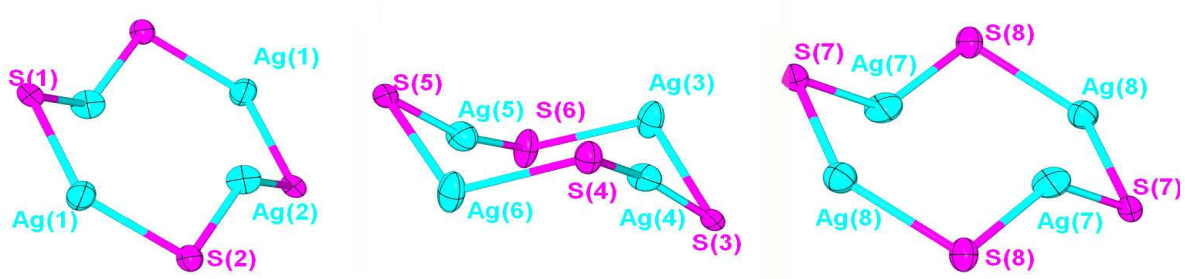

A **B** **C**

Chart 5.3 A perspective view of the Ag_4S_4 core in section **A**, **B** and **C** with thermal ellipsoids at 50% probability level (only the Ag_4S_4 ring is shown for clarity).

The internuclear Ag(5)–Ag(6) and the Ag(3)–Ag(4) separations are respectively 3.411(2) Å and 3.234(3) Å, which although longer than in metallic silver [2.889(6) Å] is shorter than twice the van der Waals radius of this metal (3.440 Å)[93]. The other Ag–Ag distances fall in the range from 3.569(3) Å to 3.931(3) Å and this indicates that a significant interaction does not occur between these atoms.

The standard reference value for P=S double bonds is 1.92 Å, and for P-S single bonds is 2.10 Å[94]. Partial double bonds occur between the P and S (1.994(3) to 2.010(3) Å)[94]. All angles of the C-N-P unit fall within the range 123.3(6)º to 126.0(6)º, which are larger than the angles in neutral free ligands (compound **1** and **2**) (124.4 (2)º and 123.2(2)º) (**Table 5.8**), but they are smaller than the average C-N-P angle value 130.4º for [Cu(I)(**L4**–*S,S*)]$_9$ in compound **4** (**Table 5.10**).

The novel octanuclear Ag(I) complex described has no precedent.

The packing of compound **3** simplified and shown in **Figure 5.8**. The extended molecular chains (see **Figure 5.7**) are packed parallel along the b-axis. The open channel formation between the molecular chains is also presented.

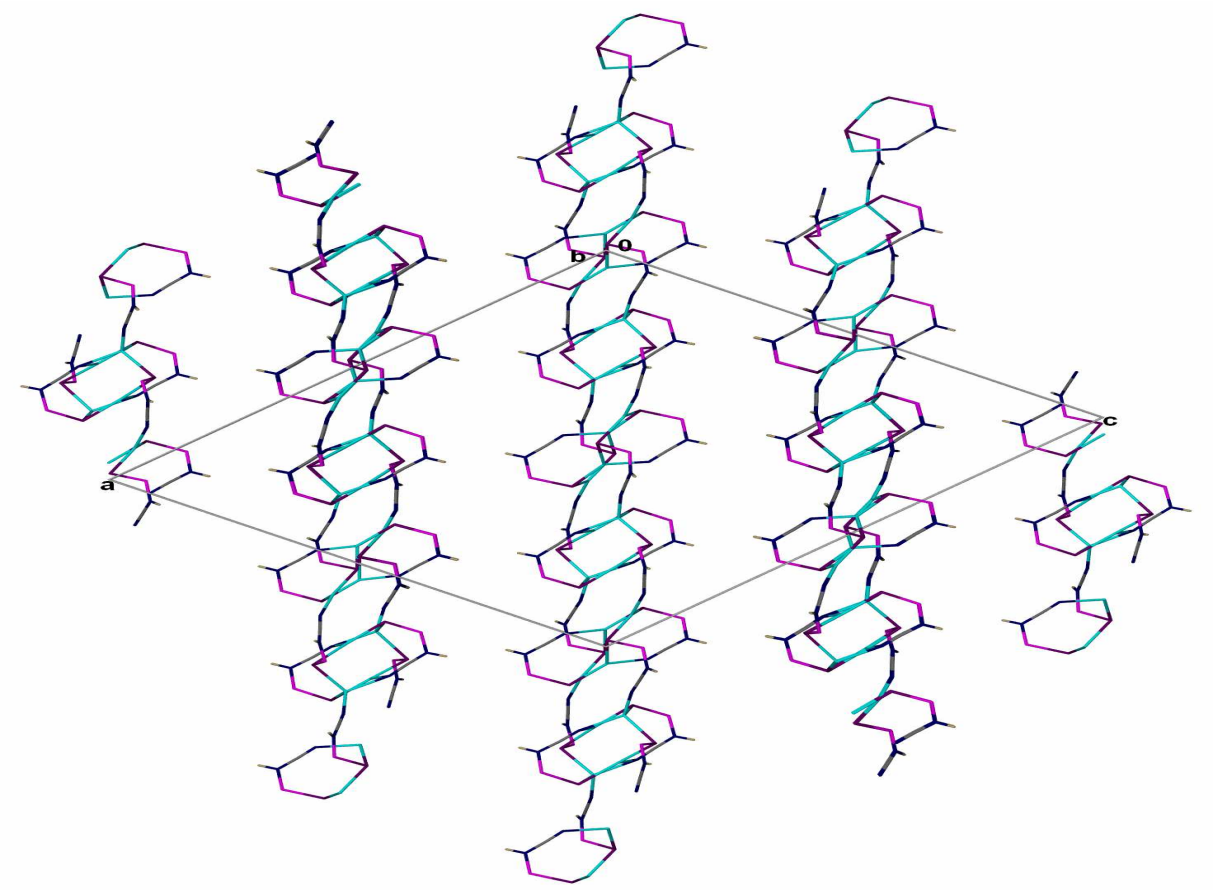

Figure 5.8 Packing diagram of [Ag(**L4**–*S*,*N*)]$_8$ along the b-axis. The isopropyl groups are omitted for clarity.

Table 5.9 Selected bond lengths (Å) and bond angles (º) for compound **3**.

Bond lengths (Å)					
Ag1-N7	2.227(8)	Ag1 S1	2.520(2)	Ag5 S6	2.433(2)
Ag2-N2	2.218(7)	Ag1-S2	2.532(2)	Ag5-S5	2.443(2)
Ag4-N9	2.547(7)	Ag2-S1	2.498(2)	Ag6-S4	2.627(2)
Ag5-N6	2.549(7)	Ag2-S2	2.545(2)	Ag6-S5	2.667(2)
Ag7-N14	2.198 (7)	Ag3-S6	2.618(2)	Ag7-S7	2.480 (2)
Ag8-N12	2.244(8)	Ag3-S3	2.678(2)	Ag7-S8	2.581(2)
Ag3-N4	2.177(7)	Ag4-S4	2.437(2)	Ag8-S7	2.493(2)
Ag3-N9	2.349(7)	Ag4-S3	2.450(2)	Ag8-S8	2.556(2)
Ag6-N16	2.189(7)	Ag6-N6	2.399(7)		
S1-P1	1.999(3)	S4-P4	1.996(3)	S7-P7	2.009(3)
S2-P2	2.005(3)	S5-P5	1.992(3)	S8-P8	1.998(3)
S3-P3	2.001(3)	S6-P6	1.993(3)		
P1-N1	1.584(7)	P4-N8	1.591(7)	P7-N13	1.572(7)
P2-N3	1.570(6)	P5-N10	1.587(6)	P8-N15	1.578(7)
P3-N5	1.588(6)	P6-N11	1.566(8)		
N1-C1	1.261(1)	N7-C4	1.159(1)	N13-C7	1.273(9)
N2-C1	1.139(9)	N8-C4	1.285(1)	N14-C7	1.151(9)
N3-C2	1.284(9)	N9-C5	1.170(9)	N15-C8	1.280(1)
N4-C2	1.163(9)	N10-C5	1.283(9)	N16-C8	1.159(9)
N5-C3	1.290(9)	N11-C6	1.279(1)		
N6-C3	1. 588(9)	N12-C6	1.162(1)		
Bond angles (º)					
N7-Ag1-S1	115.3(1)	N4-Ag3-N9	124.7(3)	S6-Ag5-S5	164.9(8)
N7-Ag1-S2	118.7(2)	N4-Ag3-S6	113.3(2)	S6-Ag5-N6	101.0(2)
S1-Ag1-S2	126.1(7)	N9-Ag3-S6	97.7(2)	S5-Ag5-N6	94.1(2)
N2-Ag2-S1	112.6(2)	N4-Ag3-S3	111.5(2)	N16-Ag6-N6	131.5(2)
N2-Ag2-S2	112.3(2)	N9-Ag3-S3	98.1(2)	N16-Ag6-S4	116.0(2)
S1-Ag2-S2	135.1(6)	S6-Ag3-S3	109.8(7)	N6-Ag6-S4	96.0(2)
N14-Ag7-S7	119.9(2)	S4-Ag4-S3	164.5(7)	N16-Ag6-S5	106.9(2)
N14-Ag7-S8	106.5(2)	S4-Ag4-N9	96.1(2)	N6-Ag6-S5	92.2(2)
S7-Ag7-S8	133.1(7)	S3-Ag4-N9	99.1(2)	S4-Ag6-S5	111.8(6)
N12-Ag8-S7	115.8(2)	N12-Ag8-S8	109.6(2)	S7-Ag8-S8	134.5(7)
Ag2-S1-Ag1	98.7(7)	C1-N1-P1	126.0(6)	N2-C1-N1	177.1(9)
Ag1-S2-Ag2	101.5(7)	C2-N3-P2	124.9(5)	N4-C2-N3	178.1(9)
Ag4-S3-Ag3	78.1(6)	C3-N5-P3	124.6(5)	N6-C3-N5	175.7(8)
Ag4-S4-Ag6	92.0(7)	C4-N8-P4	123.3(6)	N7-C4-N8	177.4(9)
Ag5-S5-Ag6	83.6(6)	C5-N10-P5	126.5(6)	N9-C5-N10	177.3(9)
Ag5-S6-Ag3	92.5(8)	C6-N11-P6	123.8(6)	N12-C6-N11	177.4(9)
Ag7-S7-Ag8	91.7(7)	C7-N13-P7	125.7(6)	N14-C7-N13	177.4(8)
Ag8-S8-Ag7	100.1(7)	C8-N15-P8	125.5(6)	N16-C8-N15	175.2(9)
C4-N7-Ag1	163.6(7)	C5-N9-Ag4	116.4(5)	C5-N9-Ag3	152.6(6)
C1-N2-Ag2	136.8(6)	C3-N6-Ag5	110.3(5)	Ag6-N6-Ag5	87.1(2)
C7-N14-Ag7	145.9(6)	C3-N6-Ag6	156.7(6)	Ag3-N9-Ag4	82.6(2)
C6-N12-Ag8	163.1(7)	C8-N16-Ag6	171.8(6)		

5.2.3.3 Crystal and molecular structure of $[Cu(I)(L4–S,S)]_9$ (4)

X-ray diffraction studies on compound **4** shows that the Cu(I) is bonded to the deprotonated ligand forming an interesting cluster of the type $[Cu(I)(\mathbf{L4}–S,S)]_9$ in the solid state as shown in **Figure 5.9** (b). Selected bond lengths and angles are given in **Table 5.10**. The structure was solved in the triclinic space group $P\bar{1}$.

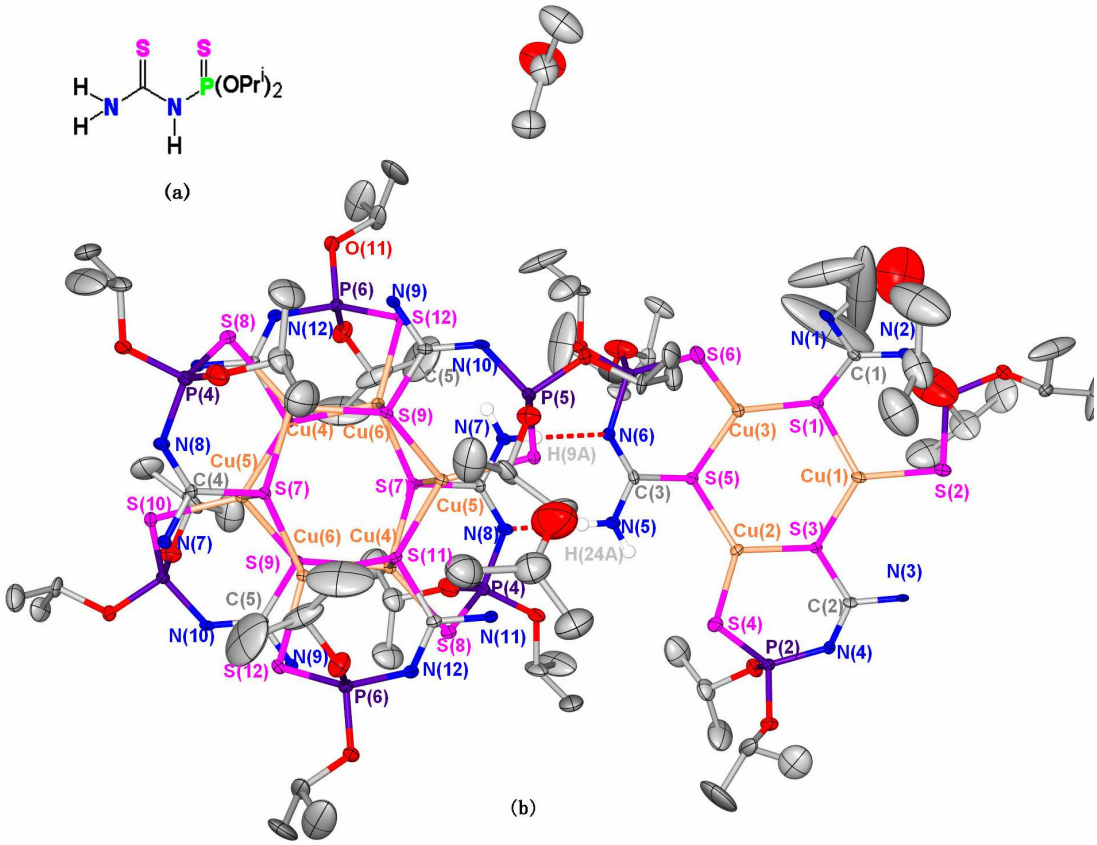

Figure 5.9 (a) Pre-ligand (**HL4**) structure. (b) Molecular structure of $[Cu(I)(\mathbf{L4}–S,S)]_9$ (compound **4**) showing the atom numbering scheme. Hydrogen atoms are omitted for clarity. Ellipsoids enclose 50% of the electron density.

Compound **4** is a neutral Cu(I) complex. X-ray diffraction studies show that the metal cation is bonded to the deprotonated ligand through the sulphur atoms of thiocarbonyl and thiophosphoryl groups forming the 6-membered heterometallocyclic chelate ring [CuL] (**Scheme 5.5**). The [CuL] moieties, by using their sulphur atoms as donors and by increasing the coordination number of Cu(I), form independent trimer $[Cu_3L_3]$ (**Chart 5.4** (a)) and hexamer $[Cu_6L_6]$ (**Chart 5.4** (b)) units.

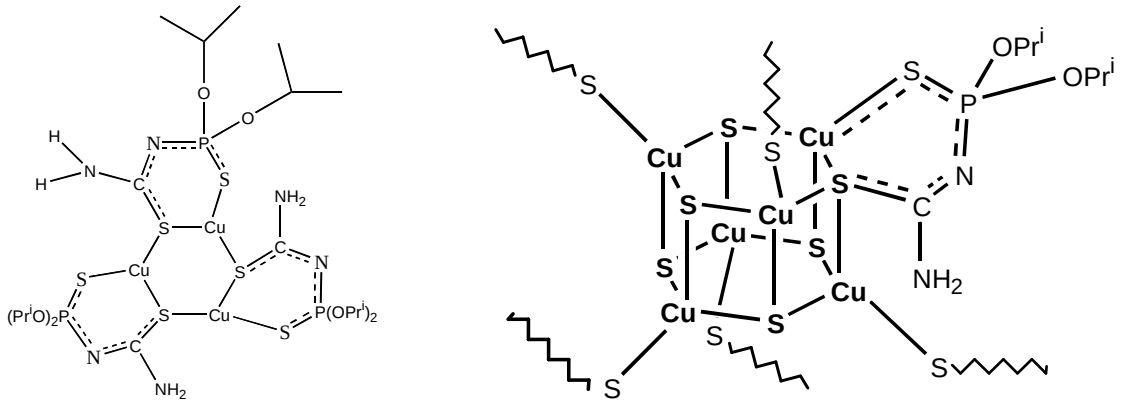

(a) (b)

Chart 5.4 (a) Structure of a hexagonal Cu_3S_6 core of the trimer $[Cu_3L_3]$. (b) Structure of a hexagonal-prismatic Cu_6S_{12} core of the hexamer $[Cu_6L_6]$ (certain ligands are omitted for clarity).

The molecular structure consists of the trimer $[Cu_3L_3]$ that alternates with a hexamer $[Cu_6L_6]$ moiety. The two moieties are interlinked by two hydrogen bonds: N(5)-H(24A)···N(8) and N(7)-H(9A)···N(6). Four acetone solvent molecules occur as guests in the X-ray crystal structure as well. In the centre of the trimer there is a 6-membered Cu_3S_3 ring. The hexamer consists of two symmetrical 6-membered rings which are connected by six Cu-S bonds. All the internal angles in the 6-membered rings are obtuse, and they are present in a stable chair conformation.

Two different coordination geometries were formed with the Cu atoms: the hexamer contains Cu(I) in a distorted tetrahedral geometry formed by four sulphur donors with the S-Cu-S angle around 95.0°; the trimer is formed by trigonal CuS_3 moieties, and the average of the S-Cu-S angle is 120.0º. The average of the tetrahedral Cu-S (2.490(1) Å) bond lengths is significantly longer than the trigonal Cu-S (2.220(1) Å) situation[95].

The Cu(4)–Cu(6) (2.817 Å) and the Cu(5)–Cu(6) (2.789 Å) distance are close to twice the van der Waals radius of Cu, 2.80 Å[96]. The other Cu–Cu distances fall in the interval 2.909-3.399 Å, showing no indication of metal-metal interactions.

Another important non-planar 6-membered heteroatom-contaning ring is formed by the deprotonated chelated ligand coordinating with Cu(I) through a -S-C-N-P-S- unit (**Scheme 5.5**).

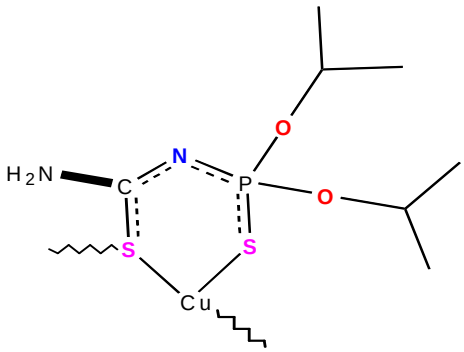

Scheme 5.5

The 6-membered ring is best described as having a pseudo-boat conformation with P being out of the plane[39,43]. Within the chelate rings, the SCNPS unit has partial delocalization of the bond, because all the C-S, P-S, P-N [94] and C-N bond lengths are between the values of single and double bond distances. The bridging C-S bond distances are significantly longer [1.754(5) to 1.766(5) Å], compared to those found in other Cu(I) complexes with thiourea[97-101] and thioamide[43,44,97,98] ligands. Hydrogen bonding occurs between the trimer and hexamer within the thiourea moiety, hence, the C-S bonds are elongated. The C-N distances do not show the usual bond lengths and all are shorter than the average single C(sp^2)-N(sp^2) bond length of 1.41 Å, and longer than the double bond length of 1.27 Å[102]. Bond lengths of C-NP (1.328(6) to 1.334(6) Å) are slightly longer than C-NH_2 (1.313(6) to 1.315(6) Å). The longer bond length is possibly due to the intra-molecular hydrogen bonding, e.g. N(7)-H(9A)···N(6). Comparison of the angle of P-N-C (from 126.8(3)º to 130.8(3)º) with the free ligand (124.4(2)º) (**Table 5.8**) shows that it is significantly larger in compound **4**. A hydrogen atom is lost from this nitrogen, so that affects the result, and this will be described in the next section (**Scheme 5.6**).

The isopropyl groups are disordered as shown by the large ellipsoids. P-O bond lengths are seemingly longer (1.555(4) to 1.586(5) Å) compared with their similar free thio-phosphorylated thiourea ligand[44], but it is not out of the range when the ligand coordinates with the metal (1.591(2) Å, 1.584(2) Å)[45].

The Cu(I) coordination to *N*-(thio)phosphorylated (thio)urea ligands has been isolated in the past.[44,46] To the best of our knowledge this, however, represents the first example of a hexagonal-prismatic core [Cu_6S_{12}] among Cu(I) chelates with (*S,S*) or (*O,S*) donor sets. In 1997, Herrmann[46] reported a structure of {Cu(I)[$(C_6H_5O)_2P(S)NC(S)N(C_2H_5)_2$]}$_3$ which contains only a [Cu_3S_6] nucleus. In the 6-membered Cu_3S_3 single ring, an acute internal angle is present (Cu-S-Cu = (76.8º).

The geometry around the Cu atom is trigonal planar. $(Ph_3P)_2Cu$(L-*S,S*) crystals have been isolated by Verat and co-workers[44], but mononuclear complexes occur in the solid state.

The packing of compound **4** is shown along the a-axis (**Figure 5.10**). The alternating trimer and hexamer packing are connected by intermolecular N-H···N hydrogen bonds which leads to a two-dimensional layer. The hydrogen bonding forms a closed cavity which is layered along the b-axis direction (**Figure 5.10**), and the other closed cavity framework extends along the direction of the c-axis (**Figure 5.11**). There could be hydrophobic interactions within the cavities. **Figure 5.11** also shows the open channel formation. A zoomed-in situation on the central packing of **Figure 5.11** is shown in **Figure 5.12**. The hexamer moiety has hydrogen bonds to connect with the six trimer rings, and it shows chains spread out radially. This is an unusual supramolecular "honeycomb" aggregate of the polynuclear Cu(I) chelate of *N*-thiophosphoryl thiourea. There are six hydrogen bonds (N-H···N) which are less than 2.95 Å, so they are classified as intermediate[103].

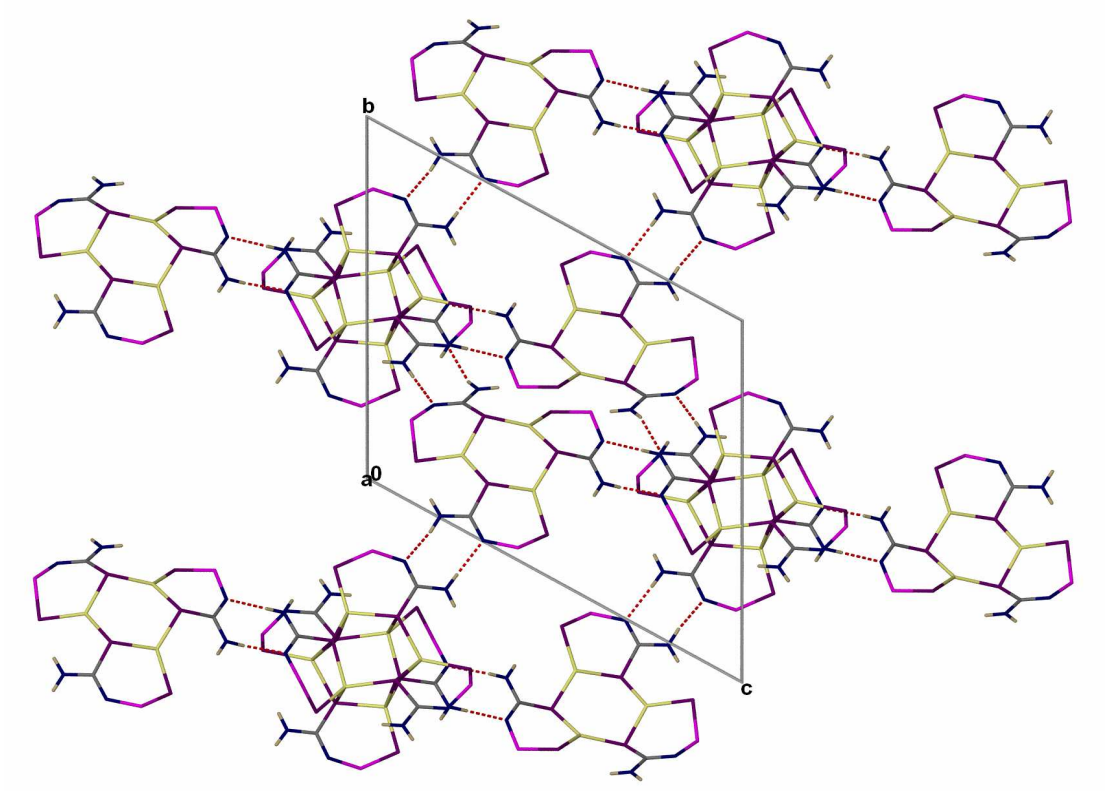

Figure 5.10 Packing of the unit cell of [Cu(I)(**L4**–*S,S*)]$_9$ along the a-axis. The isopropyl groups are omitted for clarity.

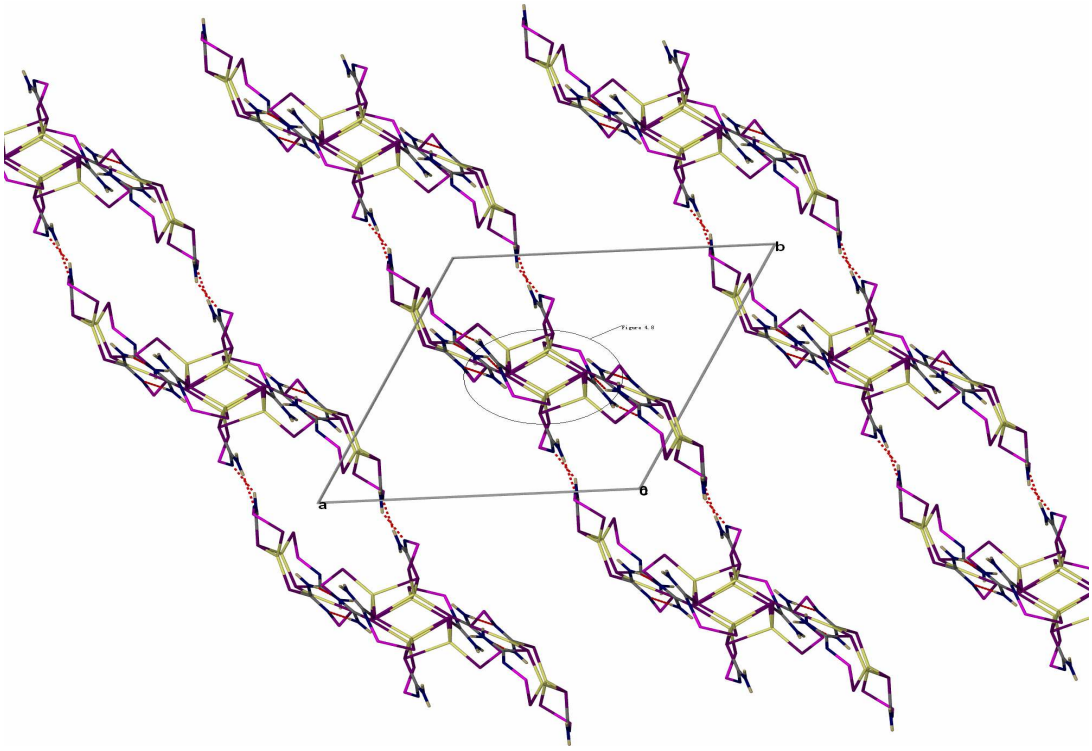

Figure 5.11 Packing of the unit cell of [Cu(I)(**L4**–*S,S*)]$_9$ along the c-axis. The isopropyl groups are omitted for clarity.

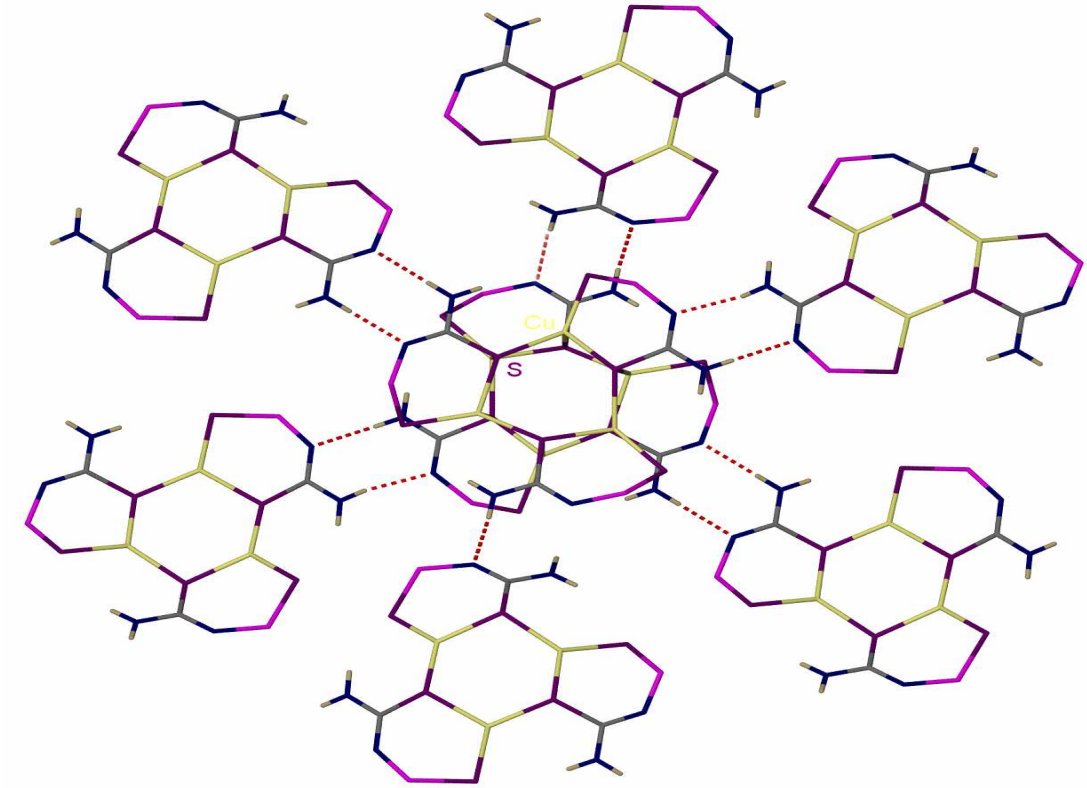

Figure 5.12 H-bonding and "honeycomb" 3D structure in the crystal of complex **4**.

Table 5.10 Selected bond length (Å) and angles (^{O}) for compound **4**.

Bond lengths (Å)					
Cu1-S3	2.216(1)	Cu2-S5	2.202(1)	Cu3 -S1	2.196(1)
Cu1-S1	2.218(1)	Cu2-S3	2.222(1)	Cu3-S5	2.220(1)
Cu1-S2	2.252(1)	Cu2-S4	2.225(1)	Cu3-S6	2.226(1)
Cu4-S8	2.252(1)	Cu5-S10	2.256(1)	Cu6-S12	2.263(1)
Cu4-S7	2.277(1)	Cu5-S9	2.290(1)	Cu6-S11	2.294(1)
Cu4-S9	2.314(1)	Cu5-S11	2.328(1)	Cu6-S7	2.345(1)
Cu4-S11	2.530(1)	Cu5-S7	2.493(1)	Cu6-S9	2.482(1)
S1-C1	1.764(5)	S5-C3	1.766(5)	S9-C5	1.758(5)
S2-P1	2.000(2)	S6-P3	1.981(2)	S10-P5	1.984(2)
S3-C2	1.762(5)	S7-C4	1.754(5)	S11-C6	1.76(5)
S4-P2	1.992(2)	S8-P4	1.976(2)	S12-P6	1.988(2)
P1-N2	1.603(4)	P3-N6	1.608(4)	P5-N10	1.614(4)
P2-N4	1.610(4)	P4-N8	1.618(4)	P6-N12	1.616(4)
N1-C1	1.334(6)	N5-C3	1.318(6)	N9-C5	1.328(6)
N2-C1	1.315(6)	N6-C3	1.315(6)	N10-C5	1.316(6)
N3-C2	1.331(6)	N7-C4	1.323(6)	N11-C6	1.329(6)
N4-C2	1.316(6)	N8-C4	1.313(6)	N12-C6	1.316(6)
Bond angle (º)					
S1-Cu1-S2	114.0(5)	S5-Cu2-S3	113.9(5)	S1-Cu3-S5	117.2(5)
S3-Cu1 S1	117.7(5)	S5-Cu2-S4	130.2(5)	S1-Cu3-S6	127.0(5)
S3-Cu1 S2	128.4(5)	S3-Cu2-S4	115.9(5)	S5-Cu3-S6	115.8(5)
S9-Cu4 S11	105.6(5)	S9-Cu5-S7	108.1(5)	S9-Cu6-Cu5	51.1(3)
S9-Cu4 Cu6	56.9(4)	S9-Cu5-S11	95.1(5)	S9-Cu6-Cu4	51.3(3)
S9-Cu4 Cu5	119.2(4)	S9-Cu5-Cu6	57.5(4)	S7-Cu6-S9	106.7(5)
S8-Cu4 S9	127.2 (5)	S9-Cu5-Cu4	120.2(4)	S7-Cu6-Cu5	57.3(4)
S8-Cu4 S7	112.5(5)	S7-Cu5-Cu6	52.4(3)	S7-Cu6-Cu4	120.9(4)
S8-Cu4 S11	108.5(5)	S7-Cu5-Cu4	49.1(3)	S12-Cu6-S9	108.6(5)
S8-Cu4 Cu6	127.6(4)	S11-Cu5-S7	104.0(5)	S12-Cu6-S7	126.2(5)
S8-Cu4 Cu5	113.6(4)	S11-Cu5-Cu6	118.4(4)	S12-Cu6-S11	110.9(5)
S7-Cu4 S9	96.3(5)	S11-Cu5-Cu4	56.5(4)	S12-Cu6-Cu5	127.8(4)
S7-Cu4 S11	104.4(5)	S10-Cu5-S9	110.7(5)	S12-Cu6-Cu4	112.8(4)
S7-Cu4 Cu6	119.0(4)	S10-Cu5-S7	109.3(5)	S11-Cu6-S9	107.8(5)
S7-Cu4 Cu5	55.9(4)	S10-Cu5-S11	127.8(5)	S11-Cu6-S7	95.0(5)
S11-Cu4 Cu6	50.5(3)	S10-Cu5-Cu6	113.8(4)	S11-Cu6-Cu5	121.0 (4)
S11-Cu4 Cu5	50.1 (3)	S10-Cu5-Cu4	128.5(4)	S11-Cu6-Cu4	58.3(4)
Cu1-S3-Cu2	110.7(5)	Cu4-S7-Cu5	75.00(4)	Cu5-S9-Cu4	119.7(5)
Cu2-S5-Cu3	109.5(6)	Cu4-S7-Cu6	119.53(6)	Cu5-S9-Cu6	71.4(4)
Cu3-S1-Cu1	108.2(6)	Cu4-S9-Cu6	71.83(4)	Cu5-S11-Cu4	73.4(4)
Cu6-S11-Cu4	71.3(4)	Cu6-S11-Cu5	119.63(6）	Cu6-S7-Cu5	70.3(4)
C1-N2-P1	126.8(3)	C3-N6-P3	130.8(3)	C5-N10-P5	128.5(3)
C2-N4 P2	129.8(4)	C4-N8-P4	129.6(4) . .	C6-N12-P6	128.0(3)

5.2.3.4 Crystal and molecular structure of [Cu(I)(L6–*S,S*)]$_3$ (5)

The X-ray structure of compound **5** is shown in **Figure 5.13** (c), and selected bond lengths and angles are given in **Table 5.11**. The structure was solved in the monoclinic space group *P2$_1$/n.*

The neutral complex **5** is built up of three deprotonated ligands with three Cu(I) cations by dichelated (*S,S*) donor coordination. The crystal structure shows a [Cu (**L6**–*S,S*)]$_3$ cluster, and a hydroxy tetrahydrofuran solvent molecule (**Section 5.2.1.3**). A hydrogen bond (O(8)-H(6A)···O(2)) connects these two entities. The intermolecular contacts (O···O) are longer than 2.95Å[103].

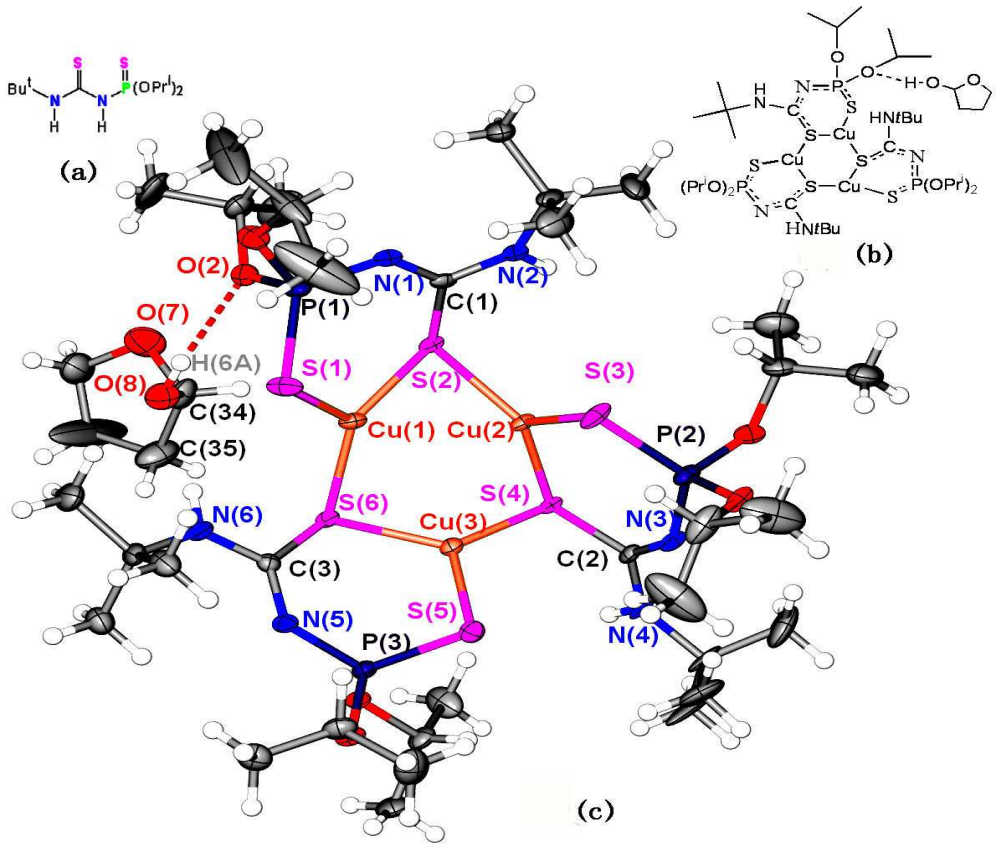

Figure 5.13 (a) Pre-ligand (**HL6**). (b) The simplified crystal structure. (c) Molecular structure of [Cu(I)(**L6**–*S,S*)]$_3$ (compound **5**) showing the atom numbering scheme. Ellipsoids enclose 50% of the electron density.

In the centre of the molecule, Cu(I) atoms and bridging S atoms form a 6-membered ring. The structure of compound **5** is similar to the trimer of compound **4** (**Section 5.2.3.3**). All the copper atoms coordinate with two μ$_2$-bridging S atoms of thiocarbonyl groups and a monodentate S of a thiophosphoryl group to form a

distorted trigonal geometry. The S-Cu-S angles appose in the interval 114.25(5)º to 124.58(6)º. The Cu(2)-Cu(3) separation of 2.764 Å is close to twice the van der Waals radius of Cu, 2.80 Å [96]. The other Cu–Cu distances lie within 2.900 Å to 3.062 Å, which is long for a metal-metal interval. The asymmetric ring has a very stable distorted chair configuration. In this ring six internal angles are included: three acute sulphur angles Cu(3)-S(2)-Cu(1) = 81.09(6)º, Cu(1)-S(4)-Cu(2) = 76.84(5)º, Cu(2)-S(6)-Cu(3) = 87.17(5)º and three obtuse copper angles S(2)-Cu(1)–S(3) = 123.93(5)º, S(6)-Cu(2)-S(4) = 123.34(6)º, S2-Cu3-S6 = 124.58(6)º, which are differences to compound **4** (see **Section 5.2.3.3**). The 6-membered ring in the structure of compound **4** did not have acute angles. All the Cu-S bond distances are variable in the short range (2.208(1) Å to 2.262(2) Å). The average of the tetrahedral Cu-S (2.493(2) Å) bond length is significantly longer than the trigonal Cu-S (2.223(2) Å) bond distance.

The deprotonated nitrogen atoms in C-N-P have the angles C(1)-N(1)-P(1) of 134.4(4)º, C(12)-N(3)-P(2) of 129.8(4)º and C(23)-N(5)-P(3) of 127.0(3)º. The average size of the angles are larger than in the free ligand (S)C-N(H)-P(S), but the C-N, N-P bond distances are similar. After deprotonation the lone electron pair appears on the nitrogen atom, and it occupies more space, so that strain causes the C-N-P angle to open up in the non-planar 6-membered heteroatom ring (see **Scheme 5.5**). Therefore, the C-N-P angle is extended (**Scheme 5.6**).

Compound **5** Free ligand

Scheme 5.6

Cu(I) coordination with sulphur donor atoms has been published before: in the form of an 8-membered ring of four Cu(I) atoms with bridging sulphurs[104], a [CuS_2N] cluster[105] and 6-membered ring complex Cu(I) with bidentate S-bridging ligands[43,45]. A similar single 6-membered ring structure as in our situation has been reported by Herrmann and coworkers in 1997, viz. tris[*N,N*-diethyl-*N'*-diphenoxythiophosphoryl-thioureato-Cu(I)[46]. The only differen-ces are that our ligand contains isopropyl groups rather than their benzyl units and that our ligand contains tertiary butyl group

instead of two ethyl groups substituted on the terminal nitrogen atom. In Herrmann's structure, the average angle of N-P-S is 122.6º, which is significantly larger than the same angle of 120.4º in our compound **5**. The average S-P and P-N bond lengths are slightly longer than those in the Herrmann structure, but we still postulate partial double bond character in the S-P-N-C-S moiety.

The packing of compound **5** is shown in **Figure 5.14** along the a-axis. Each molecule is oriented in opposite directions to the previous one with hydrogen bonding alternating in an up and down fashion in a layer along the b-axis.

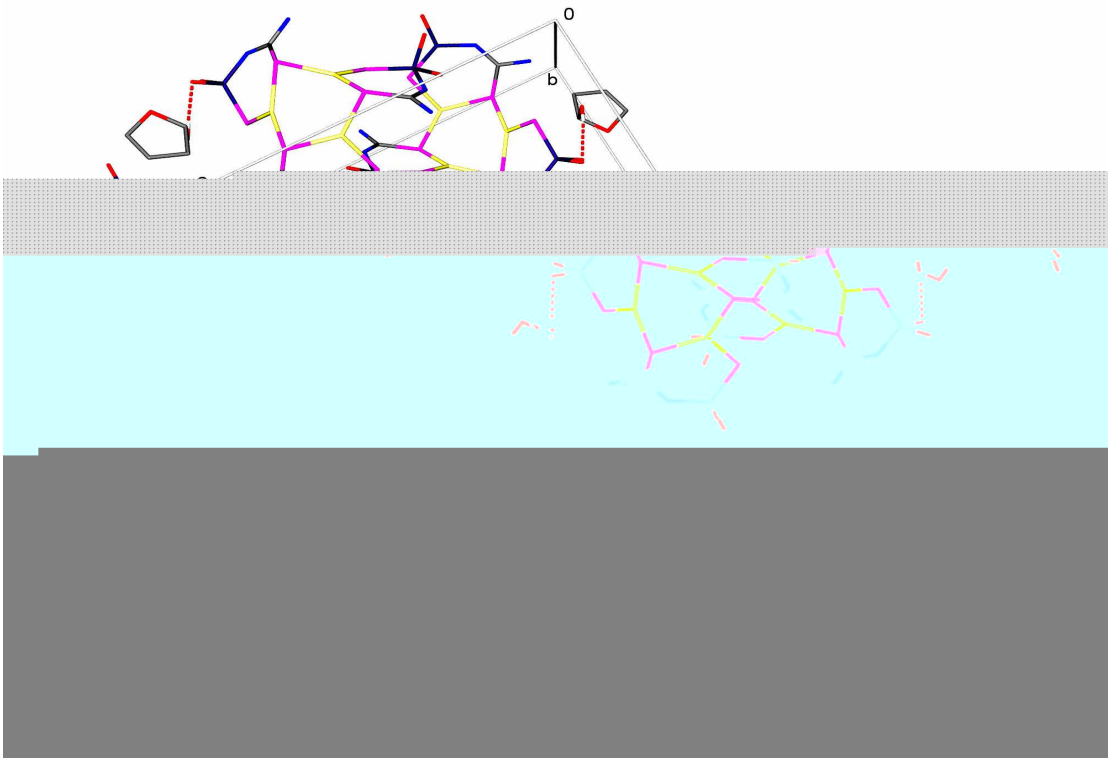

Figure 5.14 Unit cell and packing pattern of compound **5** viewed along the a-axis. The isopropyl groups and some hydrogen atoms are omitted for clarity.

Table 5.11 Selected bond lengths (Å) and angles (º) for compound **5**.

Bond lengths (Å)					
Cu1-S2	2.211(2)	Cu2-S4	2.208(2)	Cu3-S6	2.218(2)
Cu1-S6	2.223(2)	Cu2-S3	2.228(2)	Cu3-S4	2.239(2)
Cu1-S1	2.262(2)	Cu2-S2	2.250(2)	Cu3-S5	2.255(2)
S1-P1	1.969(2)	P2-N3	1.696(4)	P3-N5	1.615(4)
P1-N1	1.616(4)	P2-S3	2.002(2)	P3-S5	1.979(2)
N1-C1	1.315(6)	C2-N3	1.287(6)	C3-N5	1.313(6)
C1-N2	1.327(6)	C2-N4	1.339(6)	C3-N6	1.339(6)
C1-S2	1.780(5)	C2-S4	1.807(5)	C3-S6	1.784(5)
O7-C34	1.417(7)	O7-C37	1.436(8)	O8-C34	1.406(7)
Bond angles (º)					
S2-Cu1-S6	124.6(6)	S4-Cu2-S3	116.1(6)	S6-Cu3-S4	123.4(6)
S2-Cu1-S1	114.3(5)	S4-Cu2-S2	123.9(5)	S6-Cu3-S5	115.9(5)
S6-Cu1-S1	120.9(5)	S3-Cu2-S2	120.0(5)	S4-Cu3-S5	120.4(5)
P1-S1-Cu1	92.7(7)	C1-S2 Cu1	104.9(2)	C2-S4-Cu2	108.8(2)
P2-S3-Cu2	97.7(7)	C1-S2 Cu2	104.2(2)	C2-S4-Cu3	98.8(2)
P3-S5-Cu3	91.4(7)	Cu1-S2-Cu2	81.1(6)	Cu2-S4-Cu3	76.8 (5)
N1-P1-S1	118.2(2)	N3-P2-S3	122.6(2)	N5-P3-S5	119.7(2)
C1-N1-P1	126.9(3)	C1-N2-C4	128.3(4)	C2-N3-P2	134.4(4)
N1-C1-N2	120.3(4)	N3-C2-N4	120.9(4)	N5-C3-N6	121.0(4)
N1-C1-S2	126.7(4)	N3-C2-S4	127.4(4)	N5-C3-S6	125.5(4)
N2-C1-S2	112.9(4)	N4-C2-S4	111.6(4)	N6-C3-S6	113.5(3)

5.3 Conclusions

Three unique polynuclear Ag(I) and Cu(I) clusters that contain deprotonated *N*-(thio)pho-sphorylated (thio)urea ligands bridging in different modes have been described.

An octanuclear Ag(I) complex with distorted trigonal and tetrahedral geometries around Ag(I) are reported. Different coordination geometries around the Ag(I) atom exist, because of tautomerism between the carbodiimido and cyanamido groups. The molecules pack producing three different alternating cavities which are connected by unique 16-membered rings. A novel AgS_2N_2 cage is created, which is seen for the first time.

Compound **4** is a nonanuclear Cu(I) complex with trigonal and distorted tetrahedral geometries. The structure of compound **4** has a hexamer alternating with a trimer, which is connected by hydrogen bonding. Hydrogen bonding led to a two-

dimensional layer and created two closed cavities. The hexagonal-prismatic core [Cu_6S_{12}] structure is unprecedented in the literature. This is an unusual supramolecular "honeycomb" aggregate of the polynuclear Cu(I) chelate.

Finally, a trinuclear Cu(I) complex with a hydroxy tetrahydrofuran molecule connected by hydrogen bonding have been determined.

Table 5.12 The crystallographic data and structure refinement for compound **1** and **2**.

	1	**2**
Empirical formula	$C_{26}H_{40}N_2O_8P_2$	$C_{13}H_{18}BrNO_4P$
Formula weight	570.54	363.16
T/K	100(2)	100(2)
λ/Å	0.71073	0.71073
Crystal system	Monoclinic	Monoclinic
space group	*C2/c*	$P2_1/n$
a/Å	22.831(2)	8.6106(12)
b/Å	8.8312(9)	19.786(3)
c/Å	14.984(2)	9.8491(1)
α/°	90.00	90.00
β/°	91.03(2)	95.36(2)
γ/°	90.00	90.00
V/Å^3	3020.7(5)	1670.7(4)
Z	4	4
D_c/g cm^{-3}	1.255	1.444
Absorption coefficient/ì,mm^{-1}	0.191	2.567
F(000)	1216	740
Crystal size/mm	0.63 × 0.05 × 0.05	0.30 × 0.20 × 0.15
Θ-range for data collection/°	1.78 to 26.39	2.06 to 26.46
No. of reflection collection	8551	9035
No. independemt reflection	3068	3405
Refinement method	Full-matrix least-3quares on F^2	Full-matrix least-3quares on F^2
data / restraints / parameters	3068/0/180	3405/0/185
Goodness-of-fit on F^2	1.040	1.034
Final R indices [I>2σ>I]	*R1* = 0.0487	*R1* = 0.0450
	wR2 = 0.1217	*wR2* = 0.1135
R indices (all data)	*R1* = 0.0569	*R1* = 0.0628
	wR2 = 0.1270	*wR2* = 0.1231

Table 5.13 The crystallographic data and structure refinement for compound **3**, **4**, **5**.

	3	**4**	**5**
Empirical formula	$C_{56}H_{120}Ag_8N_{16}O_{16}P_8S_8$	$C_{54}H_{120}Cu_6N_{12}O_{16}P_6S_{12}$	$C_{37}H_{72}Cl_0Cu_3N_6O_8P_3S_6$
Formula weight	2640.88	2145.40	1204.90
T/K	100(2)	100(2)	100(2)
λ/Å	0.71073	0.71073	0.71073
Crystal system	Monoclinic	Triclinic	Monoclinic
space group	$P2_1/c$	$P\bar{1}$	$P2_1/n$
a/Å	28.204(4)	16.488(2)	14.448(7)
b/Å	14.694(2)	18.705(2)	15.407(7)
c/Å	25.550(4)	19.593(3)	25.575(11)
α/°	90.00	115.49(2)	90.00
β/°	112.08(3)	95.36(2)	91.10(8)
γ/°	90.00	111.707(2)	90.00
V/Å^3	9812(2)	4832.5(11)	5692(4)
Z	4	2	4
D_c/g cm^{-3}	1.788	1.474	1.406
Absorption coefficient/ì,mm^{-1}	1.923	1.712	1.462
F(000)	5280	2224	2512
Crystal size/mm	0.63 × 0.05 × 0.05	0.30 × 0.20 × 0.15	0.17 × 0.15 × 0.08
Θ-range for data collection/°	1.60 to 26.50	1.39 to 26.56	1.93 to 26.55
No. of reflection collection	55455	52808	32467
No. independent reflection	20165	19905	11760
data / restraints / parameters	20165/0/1041	19905/6/982	11760 / 0 / 590
Goodness-of-fit on F^2	1.090	1.121	1.133
Final R indices [I>2σ>I]	*R1* = 0.0761	*R1* = 0.0648	*R1* = 0.0696
	wR2 = 0.1475	*wR2* = 0.1333	*wR2* = 0.1475
R indices (all data)	*R1* = 0.1188	*R1* = 0.0872	*R1* = 0.0900
	wR2 = 0.1653	*wR2* = 0.1418	*wR2* = 0.1562

Chapter 6

Study of the transport, extraction and co-ordination chemistry of di, tri, and tetra-benzyl *N*-substituted cyclen derivatives with a series of transition and post-transition metal ions

6.1 Introduction

The successful application of several 1,4,7,10-tetraazacyclododecane (cyclen) precursors to the synthesis of macrocyclic complexes stems mainly from their use as models for protein-metal binding sites in biological systems[106] and as selective complexing agents for metal ions[84-86], such as therapeutic reagents for the treatment of metal ion toxicity[107,108].

Recently, varieties of multi-armed macrocyclic polyamines and their derivatives have been prepared as a new type of metal carrier. Because of the presence of a central cavity, macrocyclic ligands have been chosen as selective hosts for a wide range of guest molecules and ions. Introduction of an additional ligating group into a polyamine ring could change its properties and can be effectively modified, so that unique host-guest complexes are formed and interesting chemical functions are developed[109]. Often the rates of formation and dissociation of their metal complexes are modified by the incorporation of pendant arms, hence, compounds of this class can act as unique carriers of various metal cations. Thus, macrocyclic systems have been employed as selective extractants (ionophores) for transition and post-transition metal ions in a range of solvent extraction and bulk membrane transport studies[16]. In 1991, Tsukube *et.al*.[110] reported a series of multi-armed macrocylic poly-amines, which have amide, ester, and related functional groups introduced into the side arms of the macrocyclic polyamines producing 9-, 12-, 14- and 15-membered rings. They acted as cation transport agents towards alkali-metal and alkaline-earthmetal ions.

Substituted tetraazamacrocycles, derivatives of cyclam and cyclen, constitute a wide family of ligands acting as receptors for a large range of metallic cations. Their versatility with regard to coordination of the metals is under the control of a number of factors including the functionalisation of the coordinating nitrogen. Indeed *N*-functionalisation has been revealed to be a remarkable tool for the synthesis of ligands possessing enhanced selectivity towards metal-ion coordination[111]. Selective

methods for the *N*-substitution of cyclen were a crucial step in most syntheses of cyclen-based ligands and bifunctional chelating agents.

In our studies, **Figure 6.1** shows the *N*-benzylated cyclen derivatives, which were successfully synthesized in this work, viz. 1,4-dibenzyl-1,4,7,10-tetraazacyclododecane (compound **N2**) 1,4,7-Tris(benzyl)-1,4,7,10-tetraazacyclo-dodecane (compound **N3**) and 1,4,7,10-tetrabenzyl-1,4,7,10-tetraazacyclododecane (compound **N4**). All were synthesized from cyclen, through a protection / functionalization / deprotection method.

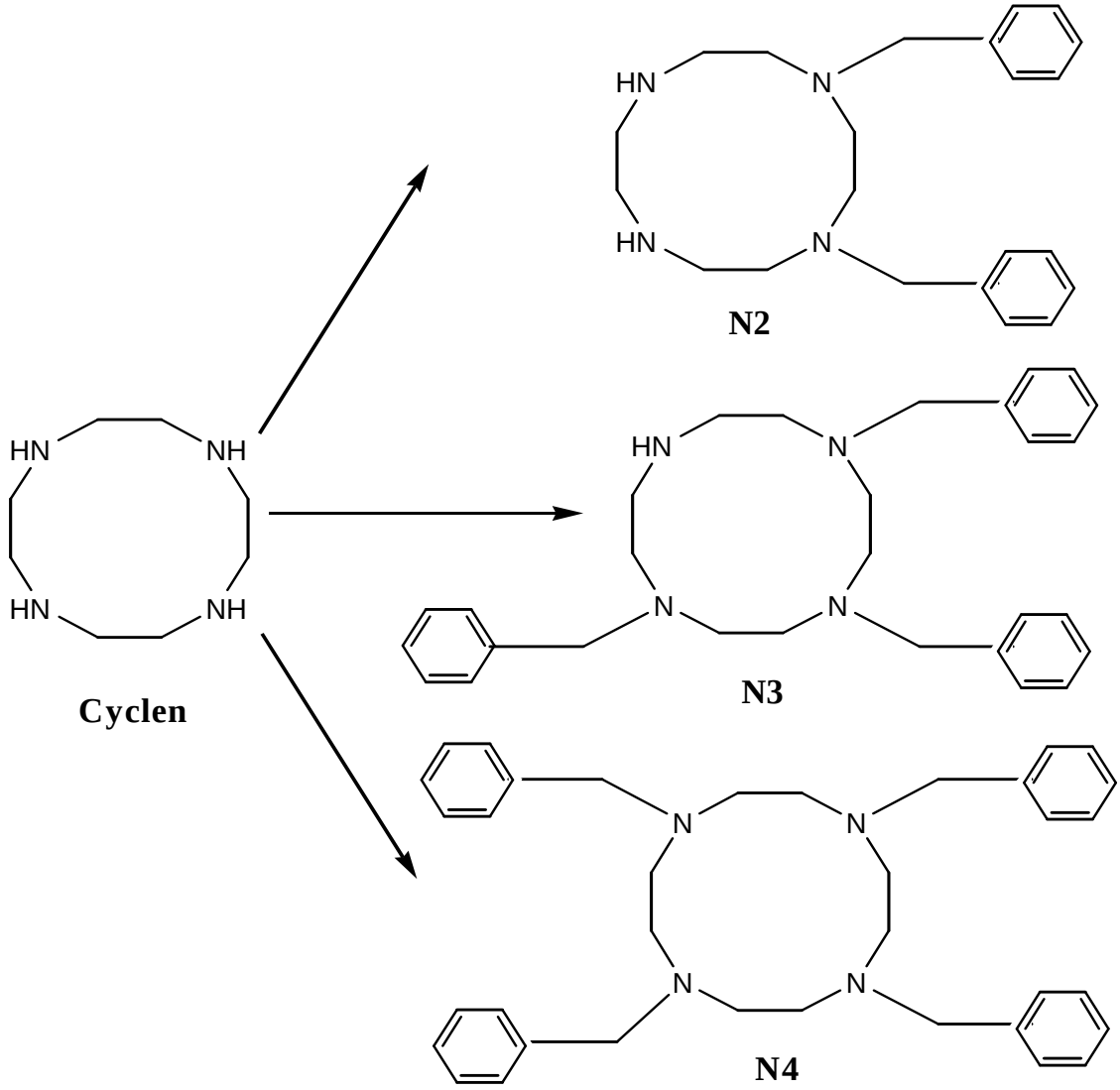

Figure 6.1 Scheme for the synthesis of the cyclen derivatives.

Although different nitrogens in cyclen have been protected regioselectively to afford mono-, *cis*-di-, *trans*-di- and tri-nitrogen protected cyclen compounds in the past

years, these studies were performed by the most profitable pathway for *cis*-di-, tri- and tetra-benzyl on nitrogen atoms of cyclen. 1,4-dibenzyl- and 1,4,7,10-tetrabenzyl-1,4,7,10-tetraazacyclo-dodecane were synthesized according to the method described by F. Bellouard[60] and D. Kong[53]. The tri-benzyl substituted compound was synthesized using J. Yoo's[58] method mainly, but modified slightly. The identity and purity of the ligands were verified with the help of melting point determination, ^{1}H and ^{13}C NMR spectra and Mass spectrometry.

The modification of macrocyclic ligands to control selectivity has also been the subject of much interest. *N*-substitution of the donor atoms has the potential to generate the biggest steric and electronic effects, due to the closeness of the site of substitution for the metal ions[97]. A series of *N*-benzylated cyclen ligand derivatives of di, tri, and tetra-benzyl *N*-substituents (**Figure 6.1**) have been successfully synthesized. We used the individual ligands as ionophores in bulk liquid membrane transport and extraction studies. The comparative study of the effects of such substitution on the metal binding properties towards the selected seven metal ions Co(II), Ni(II), Cu(II), Zn(II), Cd(II), Ag(I) and Pb(II) has been noted. Based on the published paper of similar transport and extraction with *N*-benzylated cyclam derivative ligands by Dong *et al.*[16,112], our work has been deployed. The method (**Section 2.1**) and calculations (**Section 3.1.2 and Section 4.1.2**) for the transport and the extraction of these ligands is exactly the same as reported for the *N*-(thio)phosphorylated (thio)amides and *N*-(thio)-phosphorylated (thio)urea ligands. The present report represents an extension of this study.

6.2 Results and discussion

6.2.1 Synthesis and characterization of three *N*-benzylated cyclen derivatives

6.2.1.1 Preparation of 1,4-dibenzyl-1,4,7,10-tetraazacyclododecane (compound N2)

The use of diprotective groups had been envisaged for selective dialkylation of cyclen tetraazamacrocycles. The reaction pathway is shown in **Scheme 6.1**. Equimolar amounts of diethyl oxalate and cyclen were allowed to react in absolute ethanol in an airtight flask at 25 ^{o}C. This condition was very strictly adhered to so that the cyclenoxamide **6.2a** was obtained in high yield of 96%. Acylation of cyclen with diethyl oxalate led to **6.2a**, which was used as the intermediate reagent to protect the nitrogens N^{1} and N^{4} of cyclen. However, molecular mechanics calculations predicted that the oxamide group should properly fit the distance between the two adjacent nitrogens. The formation of the corresponding six-membered ring is preferred[60].

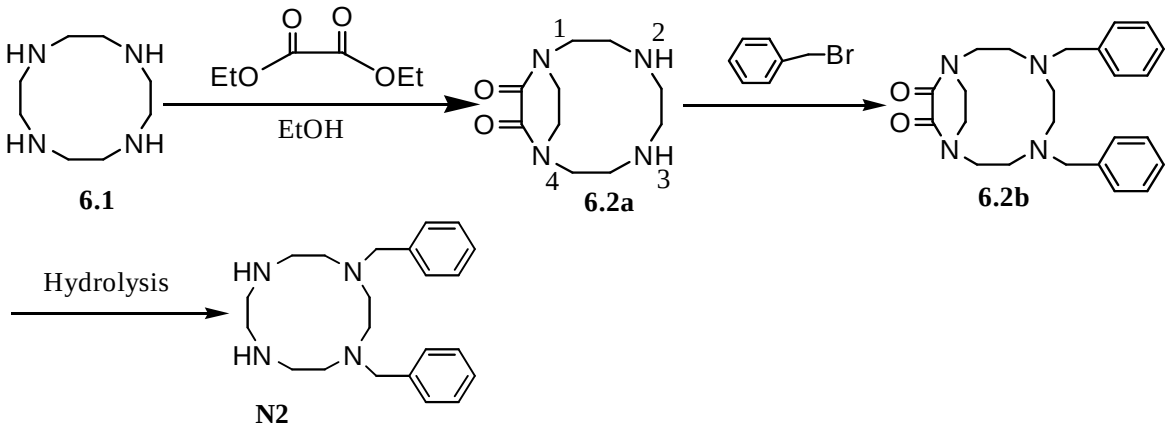

Scheme 6.1

The oxamide intermediate was a very powerful binucleophile. Under S_N2 conditions, **6.2a** was efficiently converted to the corresponding N^{1},N^{4}-dialkylated compound **6.2b**. These were readily hydrolysed under acidic or basic conditions into the corresponding N^{1},N^{4}-dialkylated cyclen, compound **N2**. NaOH (10 mol dm^{-3}) was employed for deprotection. After subsequent purification, these derivatives were isolated in good yield (87%). The resulting product had a cis-configuration, which

was proved by X-ray structure for single crystals of the dibenzylated dioxocyclen. This would be discussed in **Section 6.2.31**.

6.2.1.2 Preparation of 1,4,7-Tris(benzyl)-1,4,7,10-tetraazacyclododecane (compound N3)

The major process for this synthesis was protecting three amine nitrogens in cyclen with an aldehyde group, and then further alkylation to protect the fourth nitrogen with a benzyl chloroformate (Cbz). After the selective removal of the three formyl groups and the monoprotected cyclen compound was formed, then the benzyl substitution step could be done. The Cbz group is deprotected under more severe acidic conditions[59]. The synthetic procedure for compound **N3** is shown in **Scheme 6.2**.

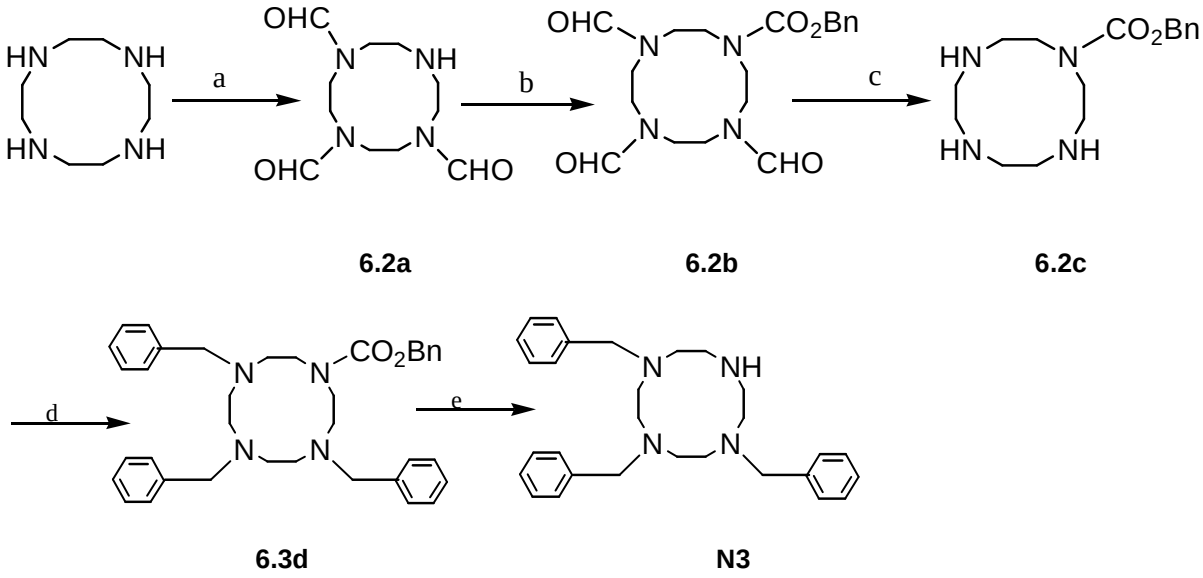

Scheme 6.2: Reagents and conditions: (a) $Cl_3CCH(OH)_2$, EtOH, 60 ^oC; (b)benzyl chloroformate, pH 10, H_2O; (c) 1 mol dm^{-3} HCl, 50 ^oC; (d)$C_6H_5CH_2Br$, $(Pr^i)_2Net$, $CHCl_3$, 60 ^oC; (e) H_2 10% Pd/C, EtOH.

The preparation of the triprotected cyclen compound, 1,4,7-triformylcyclen (**6.2a**) method is successfully carried out according to Boldrini's[113] method. A mixture of cyclen and 6 equiv of chloral hydrate in absolute ethanol was stirred for 4 h at 60 ^oC. The large excess of chloral hydrate did not affect the result of the formation, but the reaction proceeded less satisfactorily in water. The product was isolated by column chromatography using $CHCl_3$–isopropylamine 5:1 as was done with the previous cyclenoxamine synthesis. This eluent was better than that given in the original paper[113], which was CH_2Cl_2–MeOH–NH3, 9:1:0.1, because ammonia was not easily kept in the liquid phase, and the water solution reduced the product yield. In the

second protection step, **6.2b** was formed by adding excess benzyl chloroformate (4.5 equiv). It was important to keep the reaction pH at 10 by adding saturated Na_2CO_3 solution. The hydrate group was then easily deprotected in 1 mol dm^{-3} hydrochloric acid at 50 ℃, in order to form the monoprotected cyclen, mono-*N*-Cbz-cyclen (**6.2c**). The tri-benzyl substituted reaction could then be deployed. *N,N*-diisopropylethylamine ($(Pr^i)_2Net$) was simultaneously present as a catalyst giving a high yield of **6.3d**, at 90%[59]. After reiterative practises, $CHCl_3$ was confirmed as the best solvent in this reaction[114]. In Ohrenberg *et al.*'s work[104], the reaction is carried out in acetonitrile, in which it is difficult to produce a good yield. The Cbz group was deprotected by hydrogenation over Pd/C and strong base treatment (10 mol dm^{-3} NaOH).

6.2.1.3 Preparation of 1,4,7,10-tetrabenzyl-1,4,7,10-tetraazacyclododecane (compound N4)

Scheme 6.2 shows the synthetic reaction for compound **N4**. NaOH was the deprotonation reagent and used in the ratio of 4:1 to cyclen. The reaction was monitored by TLC until the $PhCH_2Cl$ disappeared.

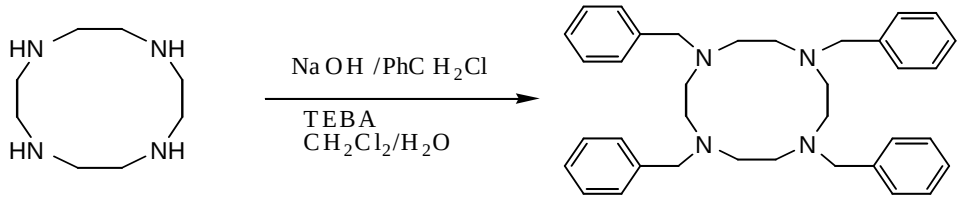

N4

Scheme 6.3

The tetra-alkylation of cyclen was prepared using triethylbenzylammonium chloride (TEBA) as a transphase catalyst. The catalyst is a basic salt, which is an electron donor reagent to remove the protons on the four nitrogens in the cyclen molecule. However the yield was not successful even in the presence of an excess of cyclen. The 1:1 ratio of CH_2Cl_2–EtOH mixture solution was the perfect choice for recrystallization of the final product, so that increases the product's yield.

6.2.1.4 Spectroscopic characterization of compound N2

The ^1H and ^{13}C NMR data for compound 1,4-dibenzyl-1,4,7,10-tetraazacyclododecane (compound **N2**) were recorded in D_2O and are summarized in **Table 6.1**. Compound **N2** has C_s symmetry. The mirror plane is presented by the dotted line (**Table 6.1**). This CH_2 was characterized by its five resonances in the ^{13}C

NMR spectrum (δ 41.1, δ 42.9, δ 47.3, δ 50.1, δ 56.6). The protons H^2 and H^3 have a similar shift, so they overlap and couple with each other forming a multiplet peak at δ 3.03. Around H^5 there is a high electron density, which caused on upfield shift at δ 3.75.

Table 6.1 ^{1}H and ^{13}C **NMR** data for compound **N2** in D_2O.

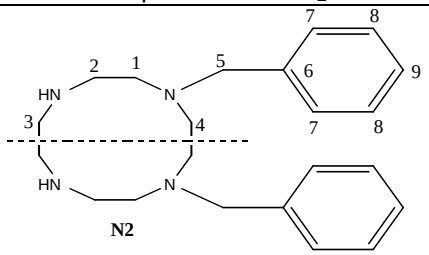

N2

1,4-Dibenzyl-1,4,7,10-tetraazacyclododecane

Assignment	**δ/ppm**
^{1}H **NMR**	
$H^{2,3}$	3.03 (8H, m)
H^1	3.09 (4H, m)
H^4	3.16 (4H, s)
H^5	3.75 (4H, s)
H^9	7.23 (2H, m)
H^8	7.25 (4H, m)
H^7	7.39 (2H, m)
^{13}C **NMR**	
C^2	41.1 (s)
C^3	42.9 (s)
C^4	47.3 (s)
C^1	50.1 (s)
C^5	56.6 (s)
C^9	129.3 (s)
C^8	130.4 (s)
C^7	132.2 (s)
C^6	137.3 (s)

Mass spectrometry

The structure of compound **N2** was confirmed by electrospray ionization mass spectrometry (ESI-MS), showing the fragment $[M]^+$ (100%) at m/z 353 as the base peak in the mass spectrum.

6.2.1.5 Spectroscopic characterization of compound N3

The ^{1}H and ^{13}C NMR spectra for compound 1,4,7-tribenzyl-1,4,7,10-tetraazacyclododecane (compound **N3**) were recorded in $CDCl_3$ and the results are tabulated in **Table 6.2**. Along the dotted line, compound **N2** exhibits C_s symmetry

(**Table 6.2**). In the ^{13}C NMR spectrum, three resonances show the three asymmetrical carbon atoms in the cyclen ring, viz. δ 44.5, δ 50.8, δ 57.3. C^5 and C^6 are in the benzyl groups, which are attached to N atoms. Their ^{13}C peaks exist upfield, however, C^6 is located in a high electron density position. Therefore the C^5 and C^6 resonances occur at δ 58.3 and δ 65.4, respectively.

Table 6.2 ^1H and ^{13}C **NMR** data for compound **3** in $CDCl_3$.

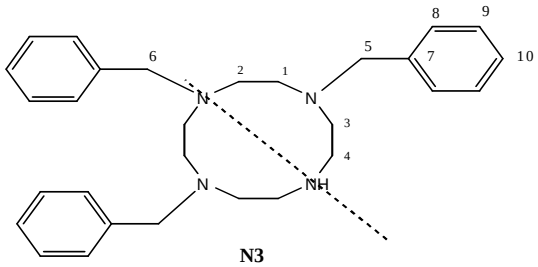

N3

1,4,7-tribenzyl-1,4,7,10-tetraazacyclododecane

Assignment	**δ/ppm**
^1H **NMR**	
NH	1.94 (1H, b)
H^3	2.78 (4H, s)
$H^{1/2}$	2.96 (8H, m)
H^4	
H^5	3.47
H^6	3.74
H^{10}	6.64
H^9	7.20
H^8	7.34
H^7	7.44
^{13}C **NMR**	
$C^{1/2}$	44.5 (s)
C^3	50.8 (s)
C^4	57.3 (s)
C^5	58.3 (s)
C^6	65.4 (s)
C^7	128.6(s)
C^8	129.3(s)
C^9	130.5(s)
C^{10}	131.8 (s)

Mass spectrometry

The structure of compound **N2** was confirmed by electrospray ionization mass spectrometry (ESI-MS), showing the fragment $[M]^+$ (100%) at m/z 443 as the molecule peak in the mass spectrum.

6.2.1.6 Spectroscopic characterization of compound N4

The ^1H and ^{13}C NMR data for compound **N4** were recorded in $CDCl_3$ and are summarized in **Table 6.3.** 1,4,7,10-tetrabenzyl-1,4,7,10-tetraazacyclododecane (compound **N4**) is a highly symmetrical molecule. The symmetrical protons in the cyclen ring are chemically equivalent. The16 H in the ^1H NMR was shown as a single peak at δ 2.93. The secondary carbon of N-CH_2-Ar in the ^{13}C NMR was further down field at δ 58.9 in the CH_2 range. Whereas all the carbons in the 12-membered cyclen ring do not stay in the same plane, the ring was most likely puckered in solution. There are two ^{13}C NMR chemical shifts present upfield at δ 46.7 and δ 40.5. The two carbons (C^1, C^2) in the cyclen ring body are difficult to assign but most likely these two shifts are responsible for this.

Table 6.3 ^1H and ^{13}C **NMR** data for compound **N4** in $CDCl_3$.

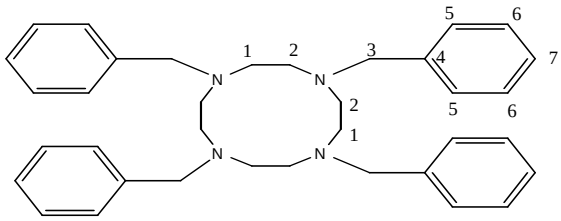

N 4

1,4,7,10-Tetrabenzyl-1,4,7,10tetraaza-cyclododecane

Assignment	**δ/ppm**
^1H **NMR**	
$H^{1,2}$	2.93 (16H, s)
H^3	3.60 (8H, s)
H^5	7.11 (4H, m)
H^7	7.27 (8H, m)
H^6	7.34 (8H, m)
^{13}C **NMR**	
$C^{1,2}$	40.7 (s)
$C^{1,2}$	46.5 (s)
C^3	58.9 (s)
C^7	128.3 (s)
C^6	130.3 (s)
C^5	133.4 (s)
C^4	137.7 (s)

Mass spectrometry

The structure of compound **N4** was confirmed by electrospray ionization mass spectrometry (ESI-MS), showing the fragment $[M]^+$ (100%) at m/z 533 as the base peak in the mass spectrum.

6.2.2 Study of the competitive metal ion transport and extraction involving benzyl *N*-substitution of cyclen

Competitive metal transport experiments have been done with the chloroform membrane phase (50 ml) containing ligands **N2, N3** and **N4** (**Figure 6.1**) as the ionophore at 2×10^{-3} mol dm^{-3}. The aqueous source phase (10 ml) contained equimolar concentrations of the nitrate salts of Co(II), Ni(II), Cu(II), Zn(II), Cd(II), Ag(I) and Pb(II) at 1×10^{-2} mol dm^{-3}. The transport was carried out using the 1:1 ratio of ligand to metal ion. The main transport process is the deprotonated ligand with metal ion to form a neutral complex at the interface of the two phases. After the metal-ligand complex diffuses to the interface of the membrane / receiving phase, because of the acidic aqueous receiving phase, the metal ions are stripped into the receiving phase, and the protonated ligands can recirculate in the organic phase. Under the conditions employed, the J-values are shown in **Table 6.4**. J-values of less than 2.2 $\times10^{-7}$ mol/24 h are considered as falling within the experimental error of zero.

Table 6.4 J-values for the competitive metal ion transport by **N2**, **N3** and **N4** (data includes ± 5% experimental error).

	N2	**N3**	**N4**
Metal ion transport: J values (mol/h x 10^{-7})			
Ag(I)	–	–	–
Cu(II)	0.43	0.97	–
Co(II)	0.42	–	0.30
Cd(II)	–	–	0.73
Ni(II)	–	–	0.26
Pd(II)	0.45	–	0.56
Zn(II)	0.56	–	0.53
	N2	**N3**	**N4**
$^{Ag}T_m$%	57	70	64
$^{Cu}T_m$%	27	17	12
$^{Co}T_m$%	17	16	14
$^{Cd}T_m$%	4	–	–
$^{Ni}T_m$%	14	11	14
$^{Pb}T_m$%	38	12	4
$^{Zn}T_m$%	11	–	–

The experimental conditions are: pH of source phase = 5.5, pH of receiving phase = 1.0 and concentration of ligand = 0.002 mol dm^{-3}.

Based on *N*-benzylated cyclam derivative ligands by Dong *et al*[112], we expected Ag(I) to be transported by this series of *N*-benzylated cyclen derivative ligands. Inconsistently, all ligands did not show transport of any Ag(I) metal ion under the experimental conditions. Considering the other J-values in **Table 6.4**, all of them are still not high enough. We have calculated the percentage of metal ion transport into the receiving phase. They are all less than 2%, which is within experimental error of zero. It means the *N*-benzylated 12-membered cyclen ring does not transport metal ions like the 14-membered cyclam ring, although the cyclam derivatives have also relatively low transport ability[112].

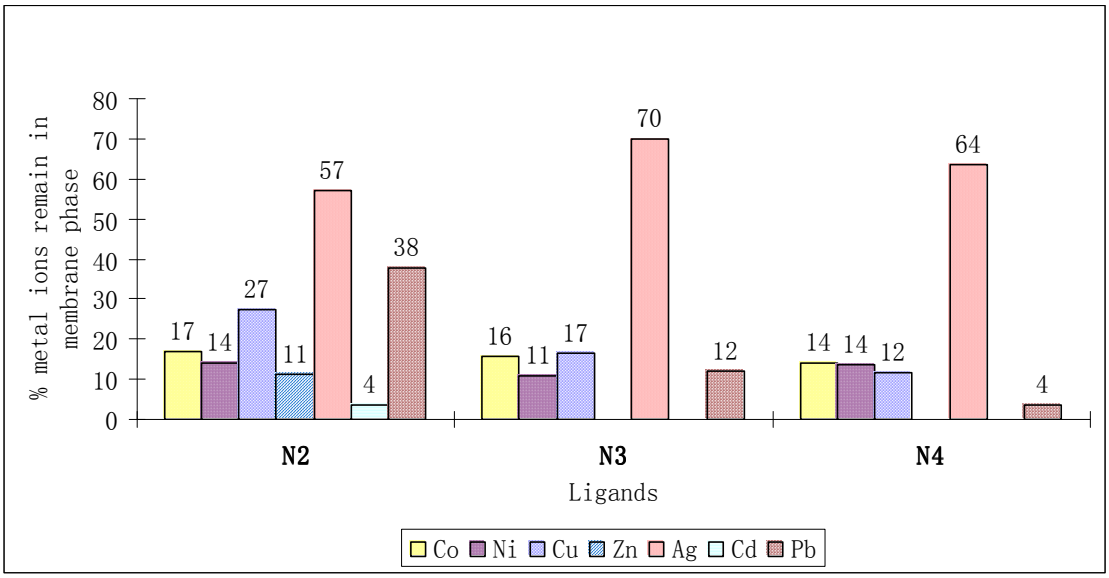

Figure 6.2 Comparison of the percentage of the different metal ions which remain in the membrane phase for ligands **N2**, **N3** and **N4**. **pH of the source phase = 5.5**, **pH of receiving phase = 1.0**, and the **concentration of the ligand** is **2 x 10 $^{-3}$ mol dm^{-3}**.

Figure 6.2 shows the percentage of metal ions which remain in the membrane phase. Ag(I) has the highest percentage of metal ion in the membrane phase. **N3** is the best ligand with the percentage of 70.13%, then **N4** with 63.64%, and then **N2** which has 57.12% (**Table 6.4**). Each of them has nearly an equal difference of 7%. These interesting results illuminate how the number of benzylate substituted groups affects the Ag(I) transport efficiency into the membrane phase.

Cu(II), Co(II), Ni(II) and Pb(II) have also been transported into the membrane phase albeit a small amount by each ligand. **N2** has the higher efficiency with Cu(II) and Pb(II) compared with the other ligands, and even 37.61% Pb(II) has been transported to the membrane phase. From **Figure 6.2**, we can see that **N2** ligand is an unusual

ligand in that it transports all the metal ions into the membrane phase, viz. Co(II), Ni(II), Cu(II), Zn(II), Ag(I), Cd(II) and Pb(II). It is the most unselective ligand.

Comparison of the percentage of Ag(I) remaining in the membrane phase ($^{Ag}T_m$%) of **N2**, **N3** and **N4** at a ligand concentration of 2×10^{-3} mol dm^{-3} (See **Table 6.4**) shows the following order: **N3** > **N4** > **N2**. No ligands showed transport of any metal ion into the receiving phase under the experimental conditions.

We use the same reagents as in the competitive transport studies for the extraction experiments. The source phase contains equal concentrations of Co(II), Ni(II), Cu(II), Zn(II), Cd(II), Ag(I) and Pb(II) at 1×10^{-2} mol dm^{-3} with pH at 5.5. The chloroform phase has the concentration of the ligand at 2 x 10^{-3} mol dm^{-3} with palmitic acid (4×10^{-3} mol dm^{-3}). In order to mirror the conditions of transport, the mole ratio of metal and ligand is 1:1. All experiments involved shaking the extraction vial for 24 h at 25ºC. **Figure 6.3** shows all the results of percentage of each of the different metal ions in competitive extraction studies. Any apparent extraction of metal ion of less than 2% relative is assumed to be within the experimental error of zero and hence ignored in the treatment of the results.

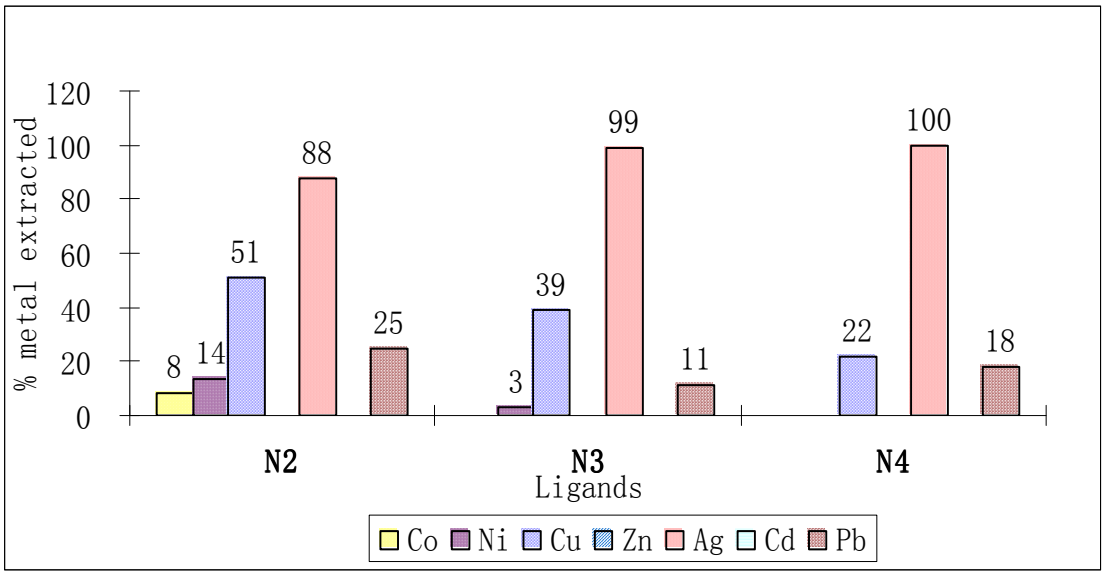

Figure 6.3 Comparison of the percentage extraction of the different metal ions in competitive extraction studies involving **N2**, **N3** and **N4**. **pH of the aqueous phase = 5.5** and the **concentration of the ligand** is **2 x 10^{-3} mol dm^{-3}**.

Comparison of the extraction percentage results of the three cyclen derivatives distinctly shows that Ag(I) ions were extracted much more than the other metal ions. From the dibenzyl, tribenzyl until the tetrabenzyl substituted cyclen, there is an

increase in the Ag(I) ions extracted, and the percentages are 88%, 99% and 100%, respectively. Comparison of **Figure 6.3** and **Figure 6.4** indicates that Ag(I) metal ion showed the highest selection. The worst ligand was **N2** as is confirmed by these results. **N3** and **N4** do not show much difference with the extraction results. Although Ag(I) was transported to the organic phase, nothing was transported to the receiving phase, because the *N*-benzylated cyclen ligand derivatives most likely have a high stability constant with Ag(I), hence taking it into the organic phase and not releasing the metal ion into the receiving phase.

The original cyclen has a high stability with Cu(II) metal ion, which was tested previously. Dong *et al.*[112] reported that the solvent extraction was successively reduced for *N*-benzylated derivatives of cyclam with Cu(II). The dibenzyl substituted compound was the highest for Cu(II) metal ions at 51%. There is a gradual decrease in the extraction percentage of Cu(II) metal ion from **N2** to **N4** which is at 22%. The inductive effect of the benzyl group activates the efficiencies and selectivity. The different efficiency for Ag(I) ion is not very large, but for Cu(II) it is much more effective. **N4** extraction showed the highest amount for Ag(I), but the least amount for Cu(II), on the other hand **N2** reversed this selectivity with Ag(I) and Cu(II). The extraction results are consistent with the transport results. **N2** extracted the most and different metal ions for these ligands.

At a ligand concentration of 2×10^{-3} mol dm^{-3}, the extraction efficiency of **N2**, **N3** and **N4** for Ag(I) is in the order: **N4** > **N3** > **N2**. Under the same conditions the Cu(II) extraction has the following order: **N2** > **N3** > **N4**. The selectivity for Ag(I) compared to Cu(II) has the order: **N4** > **N3** > **N2**.

There are four nitrogen atoms in the heterocyclic cyclen ring, and the number of protons is decreased with the substituted functional group addition. With a substituted group on the nitrogen atoms, the pKa values would have changed compared to the pKa values of cyclen on its own. Therefore there is an electronic effect to controlling the selectivity and efficiency of competitive metal transport and extraction. Under these extraction conditions, we had a composition of 1:1 metal ion to ligand ratio, so the protonation constants would also play an important role.

6.2.3 X-ray structure determination

6.2.3.1 Crystal and molecular structure of dibenzylated dioxocylen (6)

The organic compound **6** was synthesized as described in **Section 5.3.1**, and was isolated in the crystalline form from THF in a closed thin glass pipette at room temperature after two weeks. It was an intermediate product when making the dibenzylated cyclen.

The X-ray diffraction structure of compound **6** is represented in **Fig. 4.5**, and selected bond lengths and angles are given in **Table 4.4**. The structure was solved in the monoclinic space group $P2_1/n$.

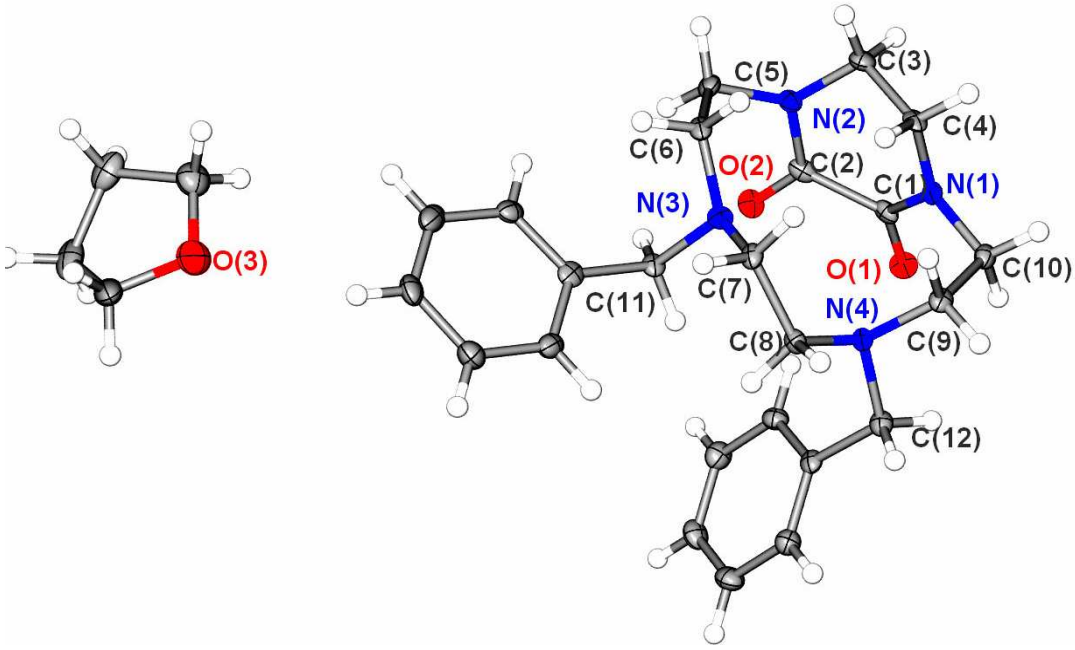

Figure 6.4 Molecular structure of dibenzylated dioxocylen showing the atom numbering scheme. Ellipsoids enclose 50% of the electron density.

This structure consists of a dibenzylated dioxocyclen molecule and a THF molecule. The oxamide group is attached with N(1) and N(2), and two benzyl groups replace the two protons on N(3) and N(4). This structure confirmed the *cis*-configuration of the dibenzyl substituted cyclen. There are four N atoms in the cyclen ring. The average bond length of N(1)-C(1) and N(2)-C(2) is 1.359(4) Å, which is 0.105 Å shorter than the N-C single bond length in the cyclen ring. These results may be

attributed to the sp^2 hybridization of the *N*-atoms to form the partial double bonds between N(1)-C(1) and N(2)-C(2). N(3)-C(11) and N(4)-C(12) are slightly longer than the N-C bond length in the cyclen ring, where the cyclen connects with the benzyl group. In the oxamide group, the C-O bond length is in the range from 1.230(4) Å to 1.227(4) Å. All the C-C bonds are normal from 1.505(5) Å to 1.532(5) Å.

The dibenzylated dioxocyclen structure has been published by Bellouard *et al.*[60]. The solvent molecule is water in Bellouard's structure, whereas THF was included with compound **6**. The spacegroup is $P2_1/a$ for Belluard's crystal, while $P2_1/n$ was the space group for compound **6**.

The packing of compound **6** is shown as a molecular layer along the a-axis in **Figure 6.5**. Along the c-axis, the molecules have the oxygen atoms pointing in the same direction, but moving along the b-axis they are pointing in opposite directions.

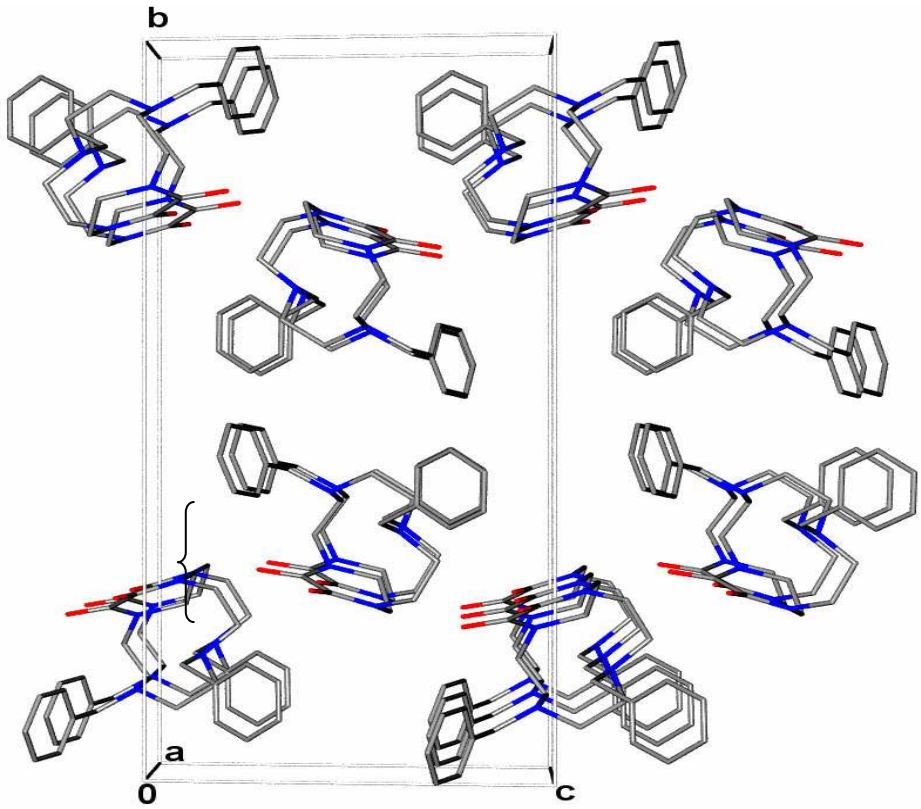

Figure 6.5 Packing of the unit cell of dibenzylated dioxocylen along the a-axis. The isopropyl groups are omitted for clarity.

Table 5.5 Selected bond lengths (Å) and angles (°) for compound **6**.

Bond lengths (Å)					
N1-C1	1.357(4)	N2-C2	1.361(4)	N3-C7	1.466(4)
N1-C4	1.463(4)	N2-C5	1.457(4)	N3-C6	1.469(4)
N1-C10	1.457(4)	N2-C3	1.468(4)	N3-C11	1.481(4)
O1-C1	1.230(4)	N4-C12	1.467(4)	C3-C4	1.505(5)
O2-C2	1.227(4)	N4-C8	1.468(4)	C5 C6	1.537(5)
O3-C28	1.419(5)	N4-C9	1.470(4)	C7 C8	1.527(4)
O3-C25	1.426(5)	C1-C2	1.548(5)	C9 C10	1.532(5)
Bond angles (°)					
C1-N1-C4	122.1(3)	C12-N4-C8	110.8(3)	N2-C3-C4	111.1(3)
C1-N1-C10	118.8(3)	C12-N4-C9	108.9(2)	N1-C4-C3	110.8(3)
C4-N1-C10	116.5(3)	C8-N4-C9	112.9(2)	N2-C5-C6	110.8(3)
C2-N2-C5	119.0(3)	O1-C1-N1	123.7(3)	N3 C6 C5	111.1(3)
C2-N2-C3	117.7(3)	O1-C1-C2	118.7(3)	N3-C7-C8	114.3(3)
C5-N2-C3	118.5(3)	N1-C1-C2	117.1(3)	N4-C8-C7	114.6(3)
C7-N3-C6	113.8(2)	O2-C2-N2	124.4(3)	N4-C9-C10	111.2(3)
C7-N3-C11	114.0(3)	O2-C2-C1	118.5(3)	N1-C10-C9	110.8(3)
C6-N3-C11	113.2(3)	N2-C2-C1	116.9(3)	N3-C11-C13	116.5(3)
				N4-C12-C19	113.8(3)

6.2.3.2 Crystal and molecular structure of dibenzylated cyclen Cu(II) complexes (7)

This compound was synthesized by reacting $Cu(ClO_4)_2 \cdot 6H_2O$ with ligand **N2** as described in **Section 6.4.3**. Compound **7** was dissolved in methanol at 60 °C. It was slowly cooled down to room temperature, and the same amount of ether was added to isolate the crystalline form. Single crystals of the complex were obtained after one week in a closed thin glass pipette stored at 4 °C. This condition has a less open evaporation surface area, and lower surrounding temperature. It could be that one requires slow evaporation of the solvent, in order to grow these good quality crystals.

The X-ray diffraction structure of compound **7** is represented in **Figure 6.6**, and the selected bond lengths and angles are given in **Table 6.6**. The structure was solved in the monoclinic space group $P2_1/n$.

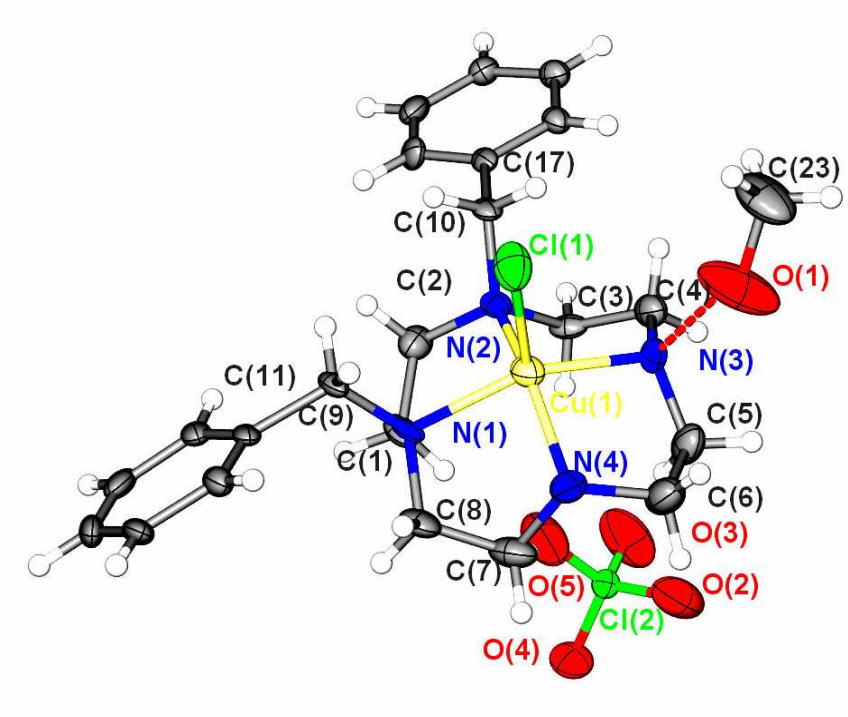

Figure 6.6 Compound **7**. Molecular structure of dibenzylated cyclen complexed to Cu(II) showing the atom numbering scheme. Ellipsoids enclose 50% of the electron density.

The crystal structure of **7** consists of a $[Cu(L)Cl]^+$ cation and a ClO_4^- anion, and a methanol solvent molecule with O(1)-H(23)···N(3) hydrogen bonding. The macrocyclic ligand skeleton of the present compound has the *cis*-configuration in the solid state. The copper complex cation is five-coordinate, bound to four N atoms of the macrocycle and to a chloride anion. The coordination geometry around the copper cation is an ideal square pyramidal with Cl^- ion in an apical position. There is a very ideal least squares plane through these four nitrogen donor atoms (deviations: N(1) 0.00343 Å, N(2) -0.00338 Å, N(3) 0.00345 Å and N(4) -0.00350 Å). The cyclen ring backbone is bent away from the plane of the nitrogen atoms in a direction opposite to that of the copper ion. The two benzyl groups attached to the N1 and N2 atoms of the cyclen ring is directed away form the cyclen ring with the benzyl group somewhat above the copper ion, the C(11)-C(9) bond in the benzyl groups are roughly parallel to the Cu(1)-N(1) and C(17)-C(10) is roughly parallel to the Cu(1)-N(2) bond (**Figure 6.6**)

Cu(II) coordinates with the four nitrogens in the ring. In our structure, Cu(II) is out of the 12-membered cyclen plane by 0.541(3) Å. The average Cu-N bond length is 2.055 Å, which is within the range of the Cu-N in CCDC (1.998(7)-2.059 Å).[46] Also, Cu-Cl has a distance, which falls within the normal range (CCDC), 2.450(3) Å.[47] The

Cl^- in this crystal structure moves around freely. This is shown by the CrystalExplorer surface graph[115]. The central blue area around Cl^-, which faces us, is the possible range of movement for Cl^- (**Figure 6.7**). The four N-Cu-Cl angles are not the same and range from 102.8(20)º to 107.82(19)º, which indicates the Cu-Cl cannot be fixed perpendicular to the N_4 plane.

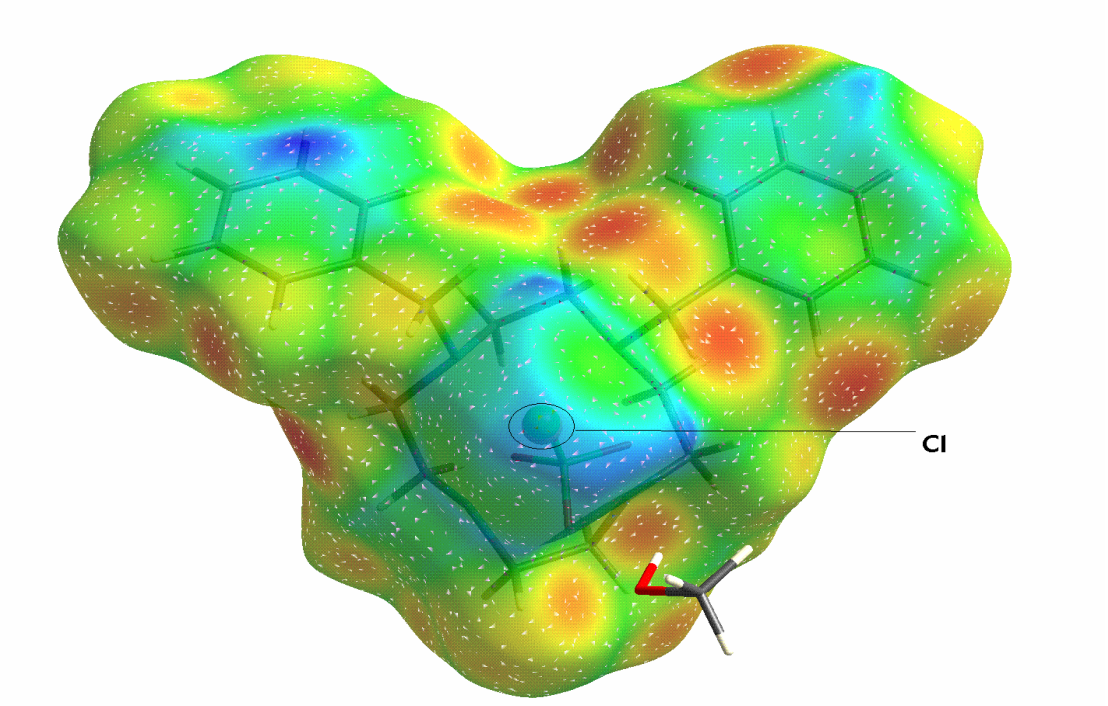

Figure 6.7 Surface graph of compound 7 (The blue region indicates the possible free atom movement. The central atom shown is Cl^-).

The free $(ClO_4)^-$ anion which surrounds the Cu(II) complex has a classic tetrahedral geometry. There is a methanol solvent molecule, which has a longer O1-H23···N3 hydrogen bond which is 2.972(5) Å, with an angle of 168.3°.

The Cu(II) with the parent cyclen and various substituents has been reported previously[34-36,45,46], but our structure with 2 substituted benzyl groups has not been reported. The larger the macrocyclic ring, the closer Cu(II) is to the N_4 plane. This is illustrated by the following: For the 12-membred dibenzylated cyclen Cu(II) is 0.541 Å from the N_4 plane; in the 14-membred azamacrocycle, Cu(II) is 0.310 Å away from the N_4 plane[51]; in the 18-membered Cu(II) hexaazamacrotetracyclic complex, Cu(II) is 0.146 Å from the copper to N_4 plane[109].

The packing of compound **7** is shown in **Figure 6.8** along the a-axis. Each molecule occurs in the reverse direction with the apical Cl anion alternating in an up-down direction along the c-axis. The aromatic rings are interlinked along the c-axis.

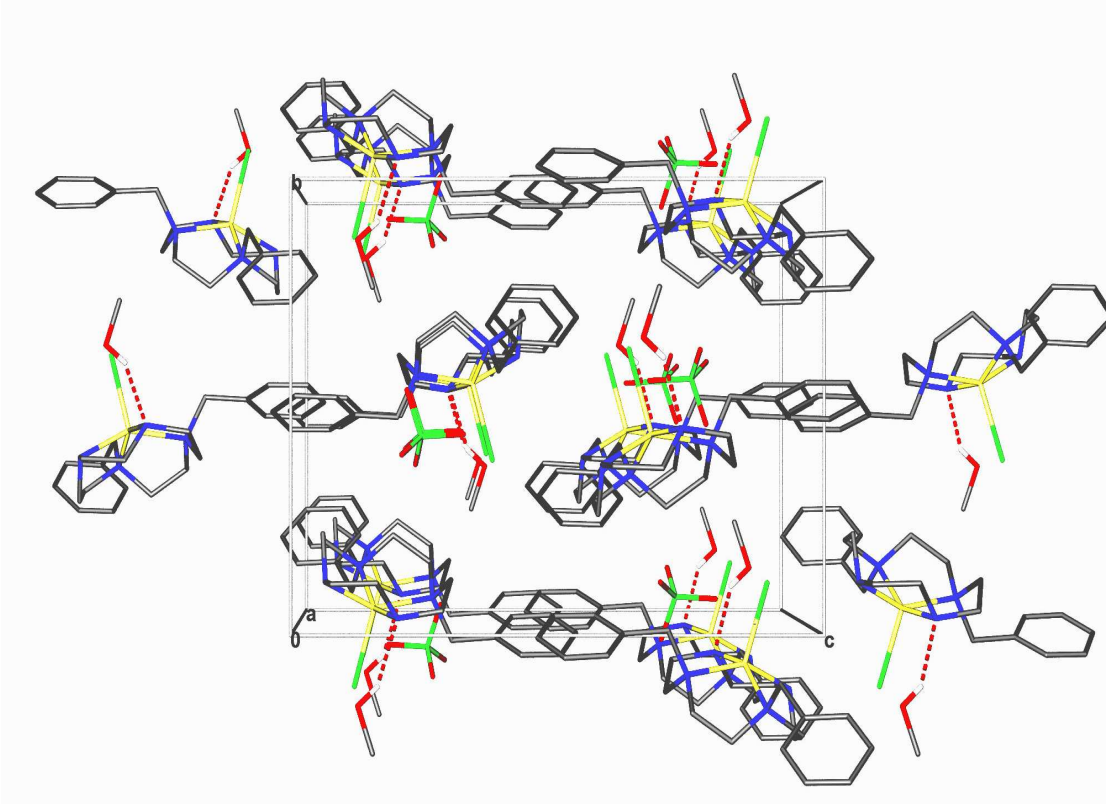

Figure 6.8 Packing of the unit cell of dibenzylated cyclen Cu(II) complex along the a-axis. The isopropyl groups are omitted for clarity.

Table 6.6 Selected bond lengths (Å) and angles (º) for compound **7**.

Bond length (Å)					
Cu1-N4	2.029(8)	N1-C1	1.471(11)	N2-C3	1.460(10)
Cu1-N3	2.037(7)	N1-C9	1.498(10)	N2-C2	1.497(11)
Cu1-N1	2.058(6)	N1-C8	1.511(11)	N2-C10	1.500(9)
Cu1-N2	2.098(7)	O1-C23	1.411(15)	Cl2-O5	1.397(9)
Cu1-Cl1	2.450(3)	Cl2-O2	1.405(8)	Cl2-O3	1.411(9)
N3-C5	1.465(12)	N3-C4	1.489(11)	N4-C7	1.488(13)
N4-C6	1.495(12)	Cl2-O4	1.422(7)		
Bond angles (º)					
N4-Cu1-N3	85.7(3)	C1-N1-C9	113.7(7)	C2-N2-Cu1	106.6(5)
N4-Cu1-N1	86.4(3)	C1-N1-C8	110.6(6)	C10-N2-Cu1	113.9(5)
N3-Cu1-N1	151.1(3)	C9-N1-C8	111.3(6)	C5-N3-C4	114.0(7)
N4-Cu1-N2	147.7(3)	C1-N1-Cu1	101.5(5)	C5-N3-Cu1	104.5(5)
N3-Cu1-N2	86.5(3) .	C9-N1-Cu1	114.2(4)	C4-N3-Cu1	107.1(5)
N1-Cu1-N2	85.5(3)	C8-N1-Cu1	104.8(5)	C7-N4-C6	115.0(8)
N4-Cu1-Cl1	104.5(3)	C3-N2-C2	112.7(6)	C7 N4-Cu1	102.7(6)
N3-Cu1-Cl1	102.8(2)	C3-N2-C10	112.0(6)	C6-N4-Cu1	108.6(6)
N1-Cu1-Cl1	106.05(19)	C2-N2-C10	110.8(6)		
N2-Cu1-Cl1	107.82(19)	C3-N2-Cu1	100.3(5)		
				O5-Cl2-O2	113.2(8)
N1-C1-C2	110.6(7)	N4-C6-C5	109.4(8)	O5-Cl2-O3	107.4(8)
N2-C2-C1	110.5(7)	N4-C7-C8	106.0(7)	O2-Cl2-O3	108.3(6)
N2-C3-C4	111.2(7)	C7-C8-N1	111.1(7)	O5-Cl2-O4	108.4(5)
N3-C4-C3	110.6(7)	N1-C9-C11	114.5(6)	O2-Cl2-O4	110.5(5)
N3-C5-C6	110.2(8)	N2-C10-C17	116.0(6)	O3-Cl2-O4	108.9(6)

6.2.3.3 Crystal and molecular structure of Isopropylammonium (isopropylamino)-oxoacetate monohydrate (8)

Chagas disease, which is caused by Trypanosoma cruzi, is an endemic parasitic disease in Latin America, specially in the Southern part of Mexico[116]. The Trypanosoma cruzi enzyme designated α-hydroxyacid dehydrogenase (HADH), exhibits two molecular forms (I and II). The trypanocidal activity of *N*-isopropyl oxamate (NIPOx) on cultured epimastigotes (*in vitro*) and marine trypanosomiasis (*in vitro*) is used in different T. cruzi strains. It is an effective and selective inhibitor of HADH-isozyme II[117].

Compound **8** was serendipitously synthesized during a chromatographic partition of cyclenoxamide. The cyclen and diethyl oxalate were added in equal molar ratios as starting materials to form the cyclenoxamide at room temperature with stirring for 48 h[60]. The reaction stoichiometry should be one to one, so the excess diethyl oxalate was separated by chromatography on silca ($CHCl_3$–isopropylamine, 5:1). The diethyl oxalate reacted with isopropylamine to produce compound **8** at room temperature. Crystals were obtained by the slow evaporation method. After two weeks, colourless, flat crystals were deposited. Compound **8** was characterised by proton NMR in deuterated chloroform as follows: δ 1.12 (6H, d, CH~3~ for anion); δ 1.13 (6H, m, CH~3~ for cation); δ 3.40 (1H, m, CH for cation); δ 4.18 (1H, m, CH for anion); δ 7.35 (1H, d, NH for anion); δ 7.97(1H, br., NH for cation).

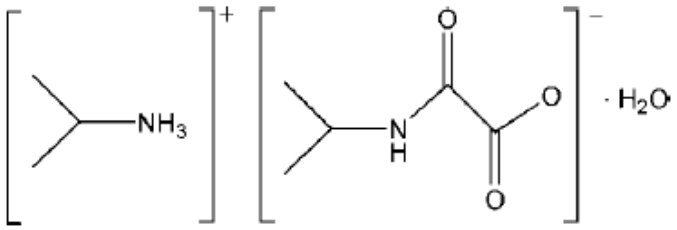

Scheme 6.1

Compound **8** is a salt, consisting of the *N*-isopropyloxamate anion, an isopropyl ammonium cation and a water molecule (**Scheme 6.1**).

The X-ray diffraction structure of compound **8** is represented in **Figure 6.9**, and the selected bond lengths and angles are given in **Table 6.8**. The structure was solved in the triclinic space group $P\bar{1}$.

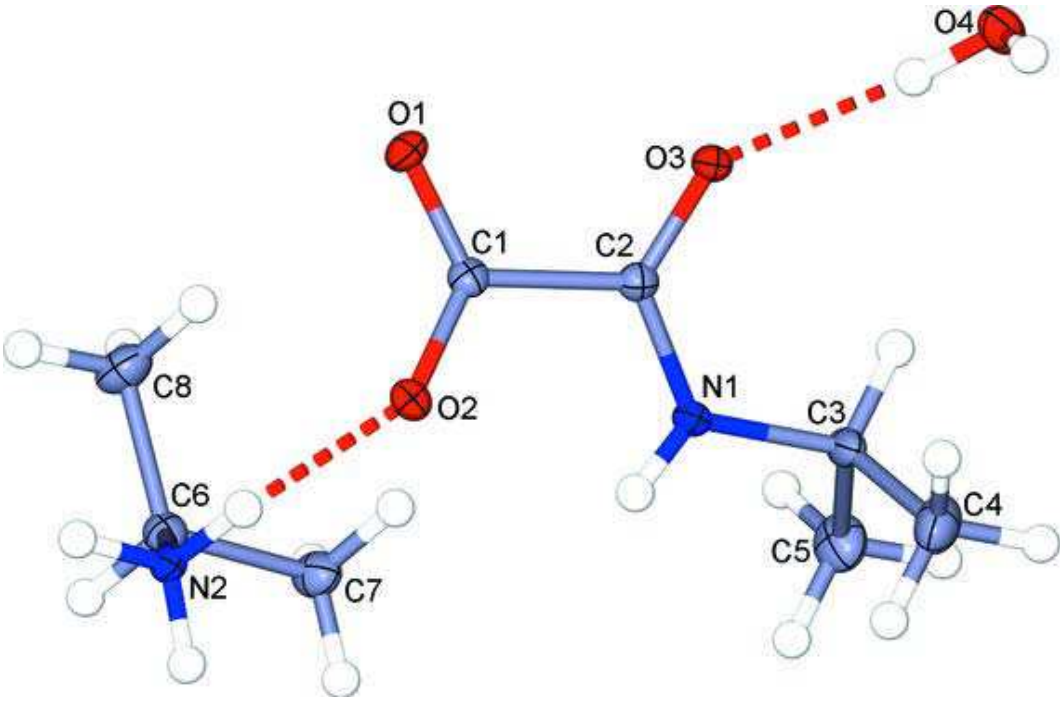

Figure 6.9 Compound **8**. Molecular structure shows the atom numbering scheme. Ellipsoids enclose 50% of the electron density.

Figure 6.9 illustrates that compound **8**, comprises $C_3H_{10}N^+ \cdot C_5H_8NO_3^- \cdot H_2O$. It is a salt from water and connected by intramolecular hydrogen bond N(2)-H(2)···O(2), and intermolecular hydrogen bond O(4)-H(10)···O(3). The hydrogen bonding details are summarized in **Table 6.7**. The C(1)-C(2) bond was 1.55 Å which is longer than the typical C(sp^2)-C(sp^2) bond length. This is most likely due to the stretching by hydrogen bonds at the two sides of the bond. There is a partial double bond between the C(2) and N(1) (1.33 Å) in the amide group.

Table 6.7 Hydrogen-bond geometry (Å, º).

D-H···*A*	*D*-H	H···*A*	*D*···*A*	*D*-H···*A*
O4-H9···O2^{i}	0.820(3)	2.060(3)	2.864(2)	170(3)
O4-H10···O3	0.880(2)	1.960(2)	2.840(2)	173.5(2)
N1-H1···O4^{ii}	0.840(2)	2.140(2)	2.918(2)	153.7(2)
N2-H2A···O2	0.88	1.89	2.7957(19)	175
N2-H2B···O3^{ii}	0.88	2.02	2.8808(19)	157
N2-H2C···O12^{iii}	0.88	1.91	2.8182(18)	172

Symmetry codes: (i) -x+1, -y+1, -z (ii) x-1, y, z (iii) - x,-y, -z.

Intermolecular N—H··· O and O—H···O hydrogen bonds lead to two-dimensional layers. The layers are stacked in the c-axis direction with hydrophobic interactions between the methyl groups (**Figure 6.10**).

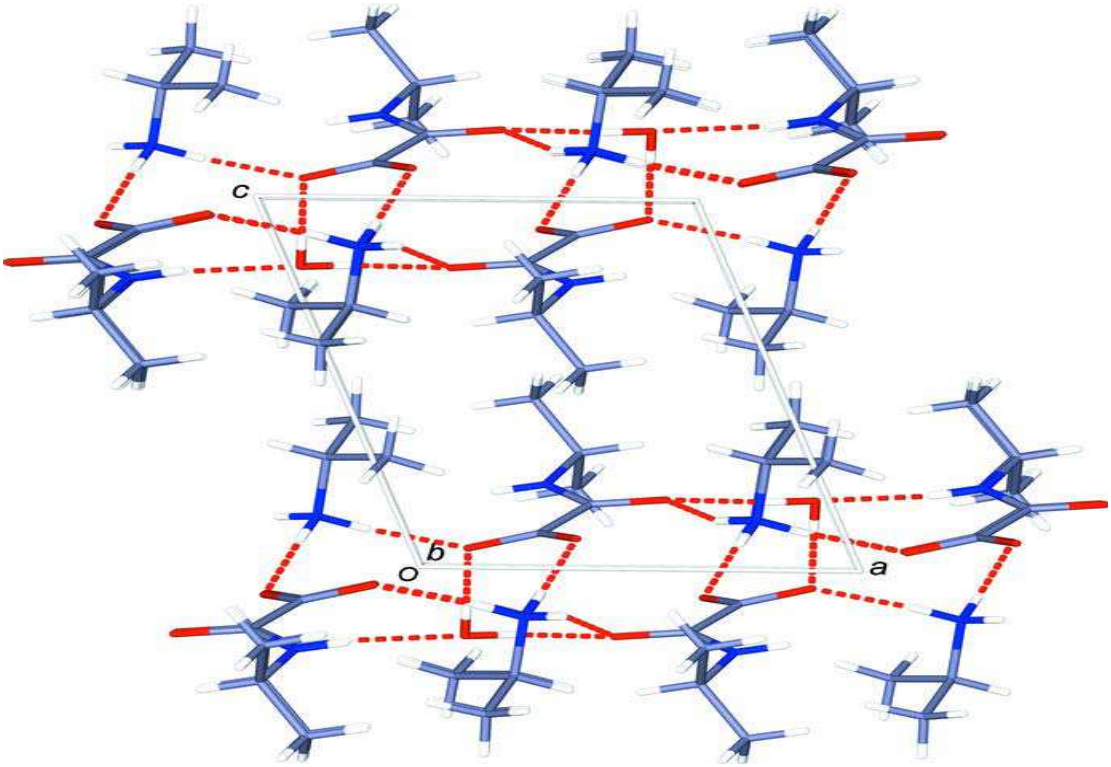

Figure 6.10 The molecular packing in compound **8** with hydrogen bonds shown as red dashed lines along the b-axis.

Table 6.8 Selected bond lengths (Å) and angles (^{O}) for compound **8**.

Bond distances (Å)					
O1-C1	1.245(2)	C1-O2	1.255(2)	C1-C2	1.549(2)
N1-C2	1.3262(2)	N1-C3	1.326(2)	N1-C3	1.462(2)
C2-O3	1.239(2)	C3-C4	1.518(2)	C3-C5	1.518(2)
C6-C7	1.518(2)	C6-C8	1.519(2)		
Bond angles (º)					
C2-N1-C3	123.8(1)	C2-N1-H1	118.0(1)	C3-N1-H1	118.1(1)
O1-C1-O2	128.2(1)	O1-C1-C2	115.5(1)	O2-C1-C2	116.4(1)

Table 6. 9 The crystallographic data and structure refinement for compound **6, 7** and **8**.

	6	**7**	**8**
Empirical formula	$C_{28}H_{38}N_4O_3$	$C_{23}H_{34}Cl_2N_4O_5Cu$	$C_3H_{10}N^+ \cdot C_5H_8NO_3^- \cdot H_2O$
Formula weight	478.62	580.98	208.26
T/K	100(2)	100(2)	100(2)
λ/Å	0.71073	0.71073	0.71073
Crystal system	Monoclinic,	Monoclinic	Triclinic
space group	$P2_1/n$	$P2_1/n$	$P\bar{1}$
a/Å	8.2951(14)	11.227(1)	7.1720(4)
b/Å	26.918(5)	13.032(1)	9.1540(5)
c/Å	11.527(2)	17.836(2)	9.4720(5)
α/°	90.00	90.00	104.37(8)
β/°	101.116(3)	92.536(2)	105.94(8)
γ/°	90.00	90.00	94.73(8)
V/Å^3	2525.5(7)	2606.9(4)	571.60(5)
Z,	4	4	2
D_c/g cm^{-3}	1.259	1.480	1.21
Absorption coefficient/ì,mm^{-1}	0.083	1.084	0.096
F(000)	1032	1212	228
Crystal size/mm	0.63 × 0.25 × 0.10	0.30 × 0.20 × 0.15	0.38× 0.19 × 0.08
Θ-range for data collection/°	1.95 to 26.47	1.94 to 26.43	2.32 to 26.48
No. of reflection collection	13669	15016	6062
No. independent reflection	5186	5353	2324
data / restraints / parameters	5186/0/316	5353/0/318	2324/0/144
Goodness-of-fit on F^2	1.251	1.067	1.156
Final R indices [I>2σ>I]	*R1* =0.0939 *wR2* =0.2076	*R1* = 0.1121 *wR2* = 0.3076	*R1* = 0.045 *wR2* =0.106
R indices (all data)	*R1* = 0.1089 *wR2* = 0.2146	*R1* = 0.1497 *wR2* = 0.3350	*R1* = 0.0494 *wR2* = 0.1060

6.3 Conclusion

The series of *N*-benzylated cyclen ligand derivatives were employed for the transport and extraction of metal ions. In order to enhance the solubility in chloroform compared with the original cyclen ligand, we successively benzylated the parent ligand. From the transport results, there was no metal ion transported into the receiving phase, but high extraction results and a large amount of Ag(I) ions remaind in the membrane phase under these experimental conditions. Since the series of *N*-benzylated cyclen derivatives appear to have a high stability with all the metal ions, these metal ions are not stripped into the receiving phase.

The extraction results shows that the Ag(I) metal ions were extracted with the order of **N4**>**N3**>**N2**, but the Cu(II) had the reverse order. Therefore **N4** had the highest selectivity for Ag(I) compared with Cu(II). **N2** extracted the most as well as all the different metal ions for these ligands, which was confirmed from both sets of results. In further work, the stability constant data for the ML^{2+} complexes of Co(II), Ni(II), Cu(II), Zn(II), Cd(II), Ag(I) and Pb(II) with the single-ring macrocycles could be determined by potentiometic titrations. These results would hopefully give a better understanding of the number and nature of the metal ions present across all three transport phases with the use of mass balance equations[53].

The benzyl *N*-substituted cyclen derivatives form complexes with metal ions, but not very easily. They need high temperatures to combine, and the low temperature could decrease the solubility. This could prevent the formation of crystalline complexes.

From the molecular structure of the dibenzylated cyclen Cu(II) complex, we know the metal ion coordinates with four N donor atoms in the cyclen ring. The cavity does not change in these different derived compounds. Ideally we have tried to make a series of Ag(I), Cu(II), Co(II), Ni(II) and Pb(II) metal complexes, in order to see bonding modes, which are based on the extraction results obtained.

Future work would involve trying to crystallize metal complexes with each of the di, tri and tetrabenzyl *N*-substituted cyclen derivatives so as to examine bonding modes. The stability constants of the three *N*-substituted cyclen derivatives should be determined.

Chapter 7

Conclusions

Twenty-six *N*-(thio)phosphorylated (thio)amide and *N*-(thio)phosphorylated (thio)urea ligands were studied for potential application as specific carriers (ionophores) for the transport of seven transition and post-transition metal ions through a bulk liquid membrane set up. The metal ions included Ag(I), Cu(II), Co(II), Cd(II), Ni(II), Pb(II), and Zn(II).

The ligands were classified based on their substituted functional groups. Most deprotonated ligands transported Ag(I) metal ions into the membrane phase, but they did not transport Ag(I) to the receiving phase. The morpholine substituted ligands (**HL7**, **HL17**) had the least solubility in the organic phase. These ligands bled into the aqueous phase, therefore, they are not suitable as metal ion carriers. Bulky alkyl substituted functional groups hinder the metal ion formation with the ligand, which reduces the transport process. Of the studies, where the ligands which had extended electron donor atoms of N and O in the bipodal ligand chain (see **Section 3.2.7**), they could increase the complex formation constant, but they were difficult to strip the Ag(I) metal ions into the receiving phase.

Deprotonated **HL1** had a high transport efficiency, at 36% Ag(I), because of the favourable equilibrium between coordination and releasing the Ag(I). This ligand only had a benzyl group substituted on *N*-phosphorylated (thio)amide. **HL11** and **HL16** were the other two effective ligands for Ag(I) transport, although they had less transport efficiency. **HL1**, **HL11** and **HL16** all exhibite the (*S,O*) donor sites. **HL4** had 94% Ag(I) which remained in the organic phase, so it has a possibility of the highest formation constant with Ag(I). The **HL4** structure has the (*S,S*) donor site. **HL5** has a (*O,O*) site, and no combination ability with Ag(I). This series of studies shows that the Ag(I) complex stabilities probably have the following order: *S,S*-chelating > *S,O*-chelating > *O,O*-chelating.

A little Cu(II) was also transported by a few ligands: **HL1** and **HL20** stripped 6–7% Cu(II) into the receiving phase. **HL4**, **HL9** and **HL16** transported only 2% Cu(II). **HL15** had the most Cu(II) remaining in the membrane phase. Pyridine was a good substituent group for Ag(I) metal ion coordination, while only the *o*-unsaturated nitrogen ligand (**HL15**) had a possibility for increasing the formation constant with

Cu(II). When the unsaturated nitrogen is on the *m*-position (**HL18**), Ag(I) was only transported into the membrane phase.

Comparing the selectivity of Ag(I) to Cu(II), **HL1** performed the best, but nevertheless, L11 only transported Ag(I) without any of the other metals. L20 only transported Cu(II) into the receiving phase.

Parallel to the transport studies, competitive metal ion extraction studies were carried out and were consistent with the transport results. The extraction results showed that most ligands extract 100% Ag(I), except **HL1**, **HL7 HL5** and **HL17**. **HL1** most likely had a moderate stability constant with Ag(I). **HL5**, **HL7** and **HL17** extracted the least amount of Ag(I), because they lacked the formation ability. The extraction also occurred with a little amount of Ni(II) and Cd(II) . There were only four (thio)amide ligands with bulk substituents that were able to extract Co(II), i.e. **HL1**, **HL7**, **HL11** and **HL17**. **HL8** was an unusual ligand. It extracted a variety of metal ions: Ag(I), Co(II), Cd(II), Ni(II), Pb(II) and Zn(II), but not Cu(II). It is the most unselective ligand.

From the structures of the metal complexes, it shows that the coordination possibilities vary with the series of *N*-(thio)phosphorylated (thio)urea and *N*-(thio)phosphorylated (thio)amide ligands. Deprotonated **HL4** and **HL6** were used as coordinated ligands forming complexes with silver and copper metal ions. Two neutral ligand structures were determined and their R-factors were lower than 0.0500. Comparison of the characterization of neutral ligands and coordinated ligands was done using NMR, IR and X-ray structure crystallography. A unique octanuclear $[Ag(I)(\mathbf{L4}\text{-}S,N)]_8$ complex **3** was obtained by ligand rearrangement. Ag(I) with donor atoms had two geometries: distorted trigonal and tetrahedral, because of two resonance structures between the carbodiimido ($N^-=C=N^-$) and cyanamido ($N\equiv C\text{-}N^{2-}$) groups. There were three different cavities alternating with two unusual 16-membered rings in the crystal packing structure **(Figure 5.10**). Perhaps these cavities could be useful for storing gases or solvent of crystallization. A novel AgS_2N_2 cage is reported for the first time. An unprecedented nonanuclear $[Cu(I)(\mathbf{L4}\text{-}S,S)]_9$ complex **4** was isolated. The crystal structure exhibited a $[Cu_3L_3]$ trimeric moiety and a $[Cu_6L_6]$ hexameric moiety, which were connected by hydrogen bonding. Hydrogen bonding led to a two-dimensional layer and created two closed hydrophobic cavities. Cu(I) with sulphur donor atoms had trigonal coordination geometry in the trimer, and distorted tetrahedral geometry in the hexamer. The hexagonal-prismatic core $[Cu_6S_{12}]$ structure had an unusual supramolecular “honeycomb” aggregate of the polynuclear Cu(I) chelate, which has no precedent. The trinuclear $[Cu(I)(\mathbf{L6}\text{–}S,S)]_3$

complex **5** showed a single [Cu_3L_3] trimeric moiety with a hydroxy tetrahydrofuran molecule connected by hydrogen bonding.

The series of *N*-benzylated cyclen derivative ligands were successfully synthesized with good yield. Di-, tri- and tetra-benzyl-1,4,7,10-tetraazacyclododecane (cyclen) were confirmed by ^{1}H and ^{13}C NMR spectroscopy, and mass spectrometry. They were also employed for the transport and extraction studies, but they were not good ligands for transport of any metal ion. Since the series of *N*-benzylated cyclen derivative ligands most likely had high formation constants with all the metal ions, they were not easily stripped into the receiving phase. *N*-benzylated cyclen derivatives extracted large amounts of Ag(I) metal ions. The extraction results showed that the Ag(I) metal ions were extracted in increasing order with the di, tri, and tetra-benzyl substituents, with four benzyl substituents extracting 100% Ag(I). Cu(II) metal ions were extracted less than Ag(I) and followed the reverse order. Therefore **N4** had the highest selectivity of Ag(I) compared to Cu(II).

The transport and extraction results showed that a slight variation in the structure of the ligands brought about a significant change in the transport behaviour. The reason for this is different ligand structures have different formation constants (logK values) with metal ions.

The dibenzylated dioxocylen (**6**) was an intermediate product of dibenzyl cyclen. The X-ray structure of compound **6** confirmed the *cis*-formation of the benzyl substituent. In the dibenzylated cyclen Cu(II) complex (**7**) structure, the central Cu(II) metal ion with four N atoms had an ideal square pyramidal coordination geometry. Cu(II) had a distance of 0.541(3) Å from the N-plane. An organic compound of isopropylammonium (isopropylamino)-oxoacetate mono-hydrate (**8**) was crystallized. The packing in the crystal shows that intermolecular N-H··· O and O-H···O hydrogen bonds lead to two-dimensional layers. The layers are stacked along the c-axis with hydrophobic interactions between the methyl groups.

For the future, the monobenzyl cyclen and *trans*-dibenzyl cyclen should be synthesized, in order to complete the *N*-benzyl cyclen system. More metal complexes with each of the di-, tri- and tetra-benzyl *N*-substituted cyclen ligands should be crystallized in order to examine bonding modes. The stability constants of the three *N*-substituted cyclen derivatives should be determined. The stability constants are important factors for transport studies.

References:

[1] N. Alizadeh, S. Salimi, A, Jabbari, *Sep. and Purif. Technol.*, 2002, **28,**174.

[2] J. Kim, A. J. Leong, L. F. Lindoy, J. Kim, J. Nachbaur, A. Nezhadali, G. Rounaghi, G. Wei, *J. Chem. Soc., Dalton Trans*. **2000**, *19*, 3453.

[3] A. Drapala, P. Wieczorek, *Desalination.* **2002***, 148*, 235.

[4] M. M. Naim, A. A. Monir, *Desalination.* **2003**, *153*, 361.

[5] P. R. Danesi, *Sep. Sci. Technol.* **1984**, *19*, 857.

[6] M. L. Goyette, T. L. Longin, R. D. Noble, C. A. Koval, *J. Membr. Sci.* **2003**, *212*, 225.

[7] A. Gherrou, H. Kerdjoudj, R. Molinari, E. Drioli, *Sep. Sci. Technol.* **2001**, *36*, 2289.

[8] C. Hill, J. F. Dozol, S. Eymard, B. Tournois, *J. Membr. Sci.* **1996**, *114*, 73.

[9] J. S. Bradshaw, J. D. Maas, R. M. Izatt, J. J. Christensen, *J. Am. Chem. Soc*. **1980**, *102*, 467.

[10] J. D. Lamb, R. M. Izatt, P. A. Robertson, J. J. Christensen, *J. Am. Chem. Soc.* **1980**, *102*, 2452.

[11] R. M. Izatt, D. V. Dearden, P. R. Brown, J. S. Bradshaw , J. D. Lamb, J. J. Christenson, *J. Am. Chem. Soc.* **1983**, 105, 1785.

[12] H. Tsukube, *Tetrahedron Lett.* **1982**, *23*, 2109.

[13] R. Wakita, M. Matsumoto, Y. Nakatsuji, M. Okahara, *J. Membr. Sci.* **1991**, *57*, 297.

[14] S. Ameerunisha, P. S. Zacharias, *J. Chem. Soc., Perkin Trans.* **1995**, *2*, 1679.

[15] S. S. Lee, I. I. Yoon, K. Park, J. H. Jung, L. F. Lindoy, A. Nezhadali, G. Rounaghi, *J. Chem. Soc., Dalton Trans.* **2002**, 2180-2182.

[16] Y. Dong, S. Farquhar, K. Gloe, L. F. Lindoy, B. R. Rumbel, P. Turner. K. Wichmann, *J. Chem. Soc., Dalton Trans.* **2003**, 1556-1558.

[17] M. Shamsipur, M. H. Mashhadizadeh, *Sep. Purif. Technol.* **2000**, *20*, 147.

[18] L. F. Lindoy, *The Chemistry of Macrocyclic Ligand Complexes*, Cambridge University Press, Cambridge, **1989**, p9.

[19] J. D. Chartres, M. A. Groth, L. F. Lindoy, G. M. Meehan, *J. Chem. Soc., Dalton Trans.* **2002**, *3*, 371-375.

[20] L. F. Lindoy, *Pure Appl. Chem.* **1997**, *69*, 2179.

[21] M. Shamsipur, G. Azimi, M. H. Mashhadizadeh, S. S. Madaeni, *Anal. Sci.* **2001**, *17*, 491-494.

[22] L. F. Lindoy, *Pure Appl. Chem.*, **1997**, *69,* 2179.

[23] M. Shamsipur, M. H. Mashhadizadeh, *Sep. Purif. Technol*. **2000**, *20*, 147.

[24] A. Safavi, E. Shams, *J .Membr. Sci*. **1998**, *144*, 37.

[25] K. Saito, S. Murakami, A. Muromatsu, *Polyhedron* **1993**, *12*, 1587.

[26] H. Sakamoto, J. Ishikawa, T. Mizuno, K. Doi, M. Otomo, *Chem. Lett.* **1993**, 609.

[27] E. Lachowicz, B. Rozanska, F. Teixidor, H. Meliani, M. Barboiu, N. Hovnanian, *J. Membr. Sci*. **2002**, *210*, 279-290.

[28] H. M. Cho, C. S. Lee, C. S. Yang, S. S. Shin, K. Kim, *Bull. Korean Chem. Soc.* **1996**, *17*, 1109-1111.

[29] F. Z. Aamrani, A. Kumar, L. Beyer, A. Florido, A. M. Sastre, *J. Membr. Sci.* **1999**, *152*, 263-275.

[30] Z. G. Muhammed, *Sep. Sci. Technol.* **1990**, *25*, 1785.

[31] A. Gherrou, H. Kerdjoudj, R. Molinari, E. Drioli, *Sep. and Purif. Technol*. **2002**, *28*, 235-244.

[32] H. G. Berhe, S. A. Bourne, M. W. Bredenkamp, C. Esterhuysen, M. M. Habtu, K. R. Koch, R. C. Luckay, *Inog. Chem. Comm.* **2006**, *9*, 99-102.

[33] M. M. Habtu, S. A. Bourne, K. R. Koch, R. C. Luckay, *New J. Chem*. **2006**, *30*, 1155-1162.

[34] (a) R, Levinson Atomic Absorption Spectroscopy,1982, (b) S. B. Smith Jr., G. M. Hieftje, *Appl. Spectrosc.* **1983**, *37*, 419-424.

[35] E. Kimura, *Pure Appl. Chem.* **1993**, *65*, 355.

[36] D. A. Safin, F. D. Sokolov, N. G. Zabirov, V. V. Brusko, D. B. Krivolapov, I. A. Litvinov, R. C. Luckay, R. A. Cherkasov, *Polyhedron* **2006**, *25*, 3330-3336.

[37] M. P. Kutyreva, N. G. Zabirov, V. V. Brusko, N. A. Ulakhovich. *Anal. Sci.* **2001**, *17*, 1049.

[38] J. D. Birdsall, J. Green, Q. T. Ly, J. Novosad, M. Necas, A. M. Z. Slawin, J. D. Woollins, Z. Zak, *J. Inorg. Chem.* **1999**, 1445-1452.

[39] O. Crespo, V. V. Brusko, M. C. Gimeno, M. L. Tornil, A. Laguna, N. G. Zabirov, *J. Inorg. Chem.* **2004**, 423-430.

[40] L. G. Shaidarova, A. V. Gedmina, V. V. Brusko, N. G. Zabirov, N. A. Ulakhovich, H. K. Budnikov, *Russ. J. Appl. Chem.* **2002**, *75*, 919.

[41] M. P. Kutyreva, N. A. Ulakhovich, Yu. I. Salnikov, V. V. Brusko, F. D. Sokolov, N. G. Zabirov, *Russ. J. Inorg. Chem.* **2004**, *49*, 1520.

[42] M. G. Zimin, R. M. Kamalov, R. A. Cherkasov, A. N. Pudovik, *Phosphorus and Sulfur*, **1982**, *13*, 371-378.

[43] V. N. Solovév, A. N. Chekhlov, N. G. Zabirov, R. A. Cherkasov, I. V. Martynov, *zh. Strukt, Khim. (Russ.)* **1990**, *31*, 117.

[44] A. Y. Verat, F. D. Sokolov, N. G. Zabirov, M. G. Babashkina, D. B. Krivolapov, V. V. Brusko, I. A. Litvinov, *Inorg. Chimi. Acta* **2006**, *359*, 475-483.

[45] F. D. Sokolov, D. A. Safin, M. G. Babashikna, N. G. Zabirov, V. V Brukso, N. A. Mironov, D. B. Krivolapov, I. A. Litvinov, R. A. Cherkasov, B. N. Solomonov, *Polyhedron* **2007**, *26*, 1550-1560.

[46] E. Herrmann, R. Richter, N. Chau, *Zanorg. Allg. Chem.* **1997**, *623*, 403-408.

[47] A. Ziegler, V. P. Botha, I. Haiduc, *Inorg. Chim. Acta* **1975**, *15*, 123-128.

[48] V. F. Toropova, T.A. Lazareva, F.M. Batyshina, M. G. Zimin, *Zh. Anal. Khim*. **1982**. *37.* 1739-1743.

[49] S. Bourne, R. K. Koch, *J. Chem. Soc., Dalton Trans*. **1993**, *13*, 2071.

[50] H. Muller, R. Rother, *Anal. Chim. Acta* **1973**, *66*, 49.

[51] Y. Kojima, Y. Seki, S. Yasuda, K. Hirotsu, H. Miyake, *Acta Cryst.* **1998**, 1602.

[52] K. W. Aston, S. L. Henke, A. S. Modak, D. P. Rily, K. R. Sample, R. H. Wesis, W. L. Neumann, *Tetrahedron Lett.* **1994**, *35*, 3687-3960.

[53] D. Kong, L. Meng, L. Song, Y. Xi, *Transition Metal Chemistry* **1999**, *24*, 553.

[54] S. Aoki, H. Kawatani, T. Goto, E. Kimura, M. Shiro, *J. Am. Chem. Soc.* **2001**, *123*, 1123.

[55] L. L. Chappell, D. A. Voss Jr., W. D. Horrocks Jr., J. R. Morrow, *Inorg. Chem.* **1998**, *37*, 3989.

[56] A. Bianchi, L. Calabi, C. Giorgi, P. Losi, P. Mariani, D. Palano, P. Paoli, P. Rossi, B. Valtancoli, *J. Chem. Soc., Dalton Trans.* **2001**, *6*, 917.

[57] F. Denat, S. Brandes, R. Guilard, *Synlett*, **2000**, 561.

[58] J. Yoo, D. E. Reichert, M. J. Welch, *Chem. Commun.,* **2003**, 766-767.

[59] J. Yoo, D. E. Reichert, M. J. Welch, *J. Med. Chem.* **2004**, *47*, 6625-6637.

[60] F. Bellouard, F. Chuburu, N. Kervarec, L. Toupet, S. Triki, Y. Le Mest, H. Handel, *J. Chem. Soc., Perkin Trans.* **1999**, *1*, 3499–3505.

[61] C. J. Anderson, M. J. Welch, *Chem. Rev.* **1999**, *99*, 2219.

[62] D. C. Buster, M. M. Castro, C. F. Geraldes, C. R. Malloy, A. D. Sherry, T.C. Siemers, *Magn. Reson. Med.* **1990**, *15,* 25.

[63] J. Platzek, P. Blaszkiewicz, H. Gries, P. Luger, G. Michl, A. Müller-Fahrnow, B. Radüchel, D. Sülzle, *Inorg. Chem.* **1997**, *36*, 6086.

[64] S. Aimem J. R. Morrow, C. R. Lake, M. R. Churchill, *Angew. Chem. Int. Ed. (Engl.)* **1994**, *33*, 773.

[65] B. F. Baker, H. Khalili, N. Wei, J. R. Morrow, *J. Am. Chem. Soc.* **1998**, *38*, 119.

[66] J. W. Sibert, A. H. Cory, J. G. Cory, *Chem. Commun.* **2002**, 154.

[67] X. Liang, J. A. Parkinson, M. Weishaeupl, R. O. Gould, S. J. Paisey, H. S. Park, T. M. Hunter, C. A. Blindauer, S. Parsons, P. J. Sadler, *J. Am. Chem. Soc.* **2002**, *124*, 9105.

[68] SMART Data Collection Software (version 5.629), Bruker AXS Inc. (Madison), WI, **2003**.

[69] SAINT, Data Reduction Software (version 5.629), Bruker AXS Inc. (Madison), WI, **2003**.

[70] R. H. Blessing, *Acta Crystallogr., Sect. A*, **1995**, *51*, 33-38.

[71] SADABS (version 5.629), Bruker AXS Inc. (Madison), WI, **2002**.

[72] G. M. Shelrick, SHELX-97. Program for Crystal Structure Analysis, University of Göttingen (Germany), **1997**.

[73] L. J. Barbour, *J. Supramol. Chem.* **2003**, *1*, 189-191.

[74] J. L. Atwood, L. J. Barbour, *Cryst. Growth Des.* **2003**, *3*, 3-8.

[75] B. I. Douglass, B. F. Dain, *J Am. Chem. Soc*., **1934**, *56*, 719.

[76] M. Schuster, *Fresenius J. Aal. Chem.*, **1992**, *342*, 791

[77] G. R. Pearson, *J. Am. Chem. Soc.* **1963**, *85*, 3533.

[78] A. E. Martell, R. D. Hancock, *Metal complexes in aqueous solutions,* Plenum Press: New York, **1996**, p9-10.

[79] K. R. Koch, S. Bourne, *J. Mol. Struct.* **1998**, *441*, 11.

[80] K. R. Koch, Y. Wang, A. Coetzee, *J. Chem. Soc., Dalton Trans*. **1999**, *6*, 1013-1014.

[81] I. L. Finar, *Organic Chemistry*, Longman Press: London, **1973**, p464.

[82] I. L. Finar, *Organic Chemistry*, Longman Press: London, **1973**, p360.

[83] F. D. Sokolov, D. A. Safin, N. G. Zabirov, V. V. Brusko, B. I. Khairutdinov, D. B. Krivolapov, I. A. Litvinov, *Eur. J. Inorg. Chem.* **2006**, 2027.

[84] G. Baldinozzi, B. Malinowska, M. Rakib, G. Durand*, J. Mater. Chem.* **2002**, *12*, 268–272

[85] Y. Tanabe, S. Kuwata, Y. Ishii, *J. Am. Chem. Soc.* **2002**, *124*, 6528-6529.

[86] D. Britton, Y. M. Chow. *Acta Crystallogr.* **1977**, *B33*, 697-699.

[87] B. Jürgens, H. A. Höppe, W. Schnick, *Solid State Sciences* **2002**, *4*, 821-825.

[88] Y. Tanabe, S. Kuwata, Y. Ishii, *J. Am. Chem. Soc.* **2002**, *124*, 6528-6529

[89] D. Britton, *Acta Cryst.*, **1987**, *C43*, 2442-2443

[90] Y. Kim. Y. Kwak, S. Lee, J. *Organometallic Chemisry* **2000**, *603*, 152-160.

[91] R. M. Silva, M. D. Smith, J. R.Gardinier, *Inorg. Chem.* **2006**, *45*, 2132-2142.

[92] E. Barreiro, J. S. Casas, M. D. Couce, A. Sánchez, R. Seoane, J. Sordo, J. M. Varela*,* E. M. V′azquez-L′opez*, Dalton Trans.*, **2007**, *3075*, 3074-3085.

[93] A. Bondi, *J. Phys. Chem.*, **1964**, *68*, 441.

[94] M. Perakyla, T. A. Pakkanen, J. P. Bjorkroth, E. Pohjalab, H. O. Leirasb, *J. Chem. Soc., Perkin Trans*. **1992**, 2.

[95] J. A. García-Vázquez, A. Sousa-Pedrares, M. Carabel, J. Romero, A. Sousa, *Polyhedron,* **2005**, *24*, 2043-2054.

[96] J. E Huheey, E. A. Keiter, R. L. Keiter, *Inorganic Chemistry: Principles of Structure and Reactivity* Harper Collins College Publishers: New York, **1993**.

[97] M. R. Truter, *J. Chem. Soc*. **1960**, 997.

[98] W. Walter, S. Harter, J. Voss, *Acta Crystallogr.* **1976**, *B32***,** 2876.

[99] N. R. Kunchur, M. R. Truter, *J. Chem. Soc*. **1958**, 2551.

[100] M. M. Elcombe, J. C. Taylor, *Acta Crystallogr.* **1968**, *A24*, 410.

[101] H. W. Dias, M. R. Truter, *Acta Crystallogr.* **1964**, *A17*, 937.

[102] A. Marchi, L. Marvelli, M. Cattabriga, R. Rossi, M. Neves, V. Bertolasi, V. Ferretti, *J. Chem. Soc., Dalton Trans.* **1999**, *12*, 1937-1943.

[103] G. Aullön, D. Bellamy, L. Brammer, E. A. Bruton*,* A. G. Orpen, *Chem. Commun*. **1998**, 653.

[104] C. Ohrenberg, M. M. Saleem, C. G. Riordan, G. P. A. Yap, A. K. Verma, A. L. Rheingold, *Chem. Commun.* **1996**, 1801-1802.

[105] J. A. García-Vázquez, A. Sousa-Pedrares, M. Carabel, J. Romero, A. Sousa, *Polyhedron,* **2005**, *24*, 2043-2054.

[106] E. Kimura, *Pure Appl. Chem.* **1993**, *65*, 355.

[107] S. Blain, P. Appriou, H. Chaumeil, *Anal. Chim. Acta* **1990**, *232*, 331.

[108] H. Tsubuke, T. Yoden, T. Iwachido, M. Zenki, *J. Chem. Soc., Chem. Commun.* **1991**, 1069.

[109] K. Y. Choi, *J. Chem. Cry.* **2005**, *35*, 419.

[110] K. Tesukube, *Japan KEK.* **1991**, 11-15.

[111] A. Bianchi, M. Micheloni, P. Paoletti, *Coord. Chem. Rev.* **1991**, *110*, 17.

[112] Y. Dong, G. A. Lawrance, L. F. Lindoy, P. Turner, *Dalton Trans.* **2003**,1567-1576.

[113] V. Boldrini, G. B. Giovenzana, R. Pagliarin, G. Palmisano, M. Sisti, *Tetrahedron Lett.* **2000**, *41*, 6527.

[114] C. Li, W. T. Wong, *Tetrahedron* **2004**, *60*, 5595-5601.

[115] CrystalExplorer 2.1, the University of Western Australia, Perth, Australia, **2007**.

[116] E. Dumonateil, *Salud Pública Méx.* **1999**, *41*, 322–327.

[117] A. M. Chena, S. Elizondo, L. Ropríguez-Páez, E. Nogueda, I. Baeza, C. Wong, *J. Enzym. Inhib. Med. Chem.* **2005***, 20*, 189-197.

Appendix 1

N-(thio)phosphorylated (thio)amides and *N*-(thio)phosphorylated (thio)urea ligands

1 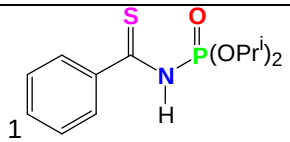	8 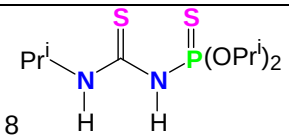	15 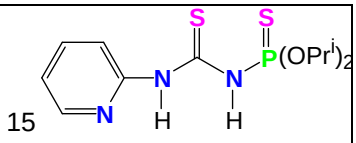
2 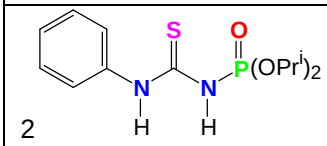	9 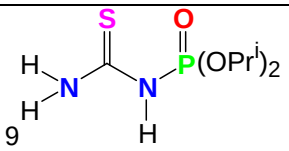	16 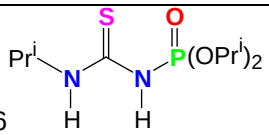
3 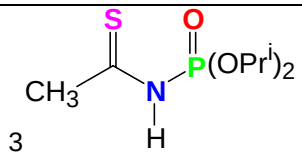	10 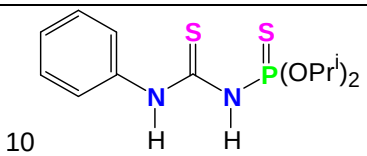	17 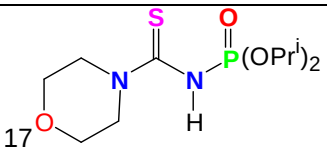
4 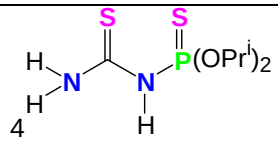	11 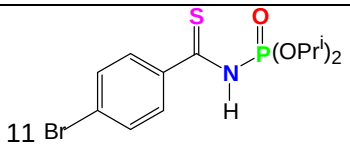	18 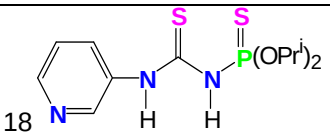
5 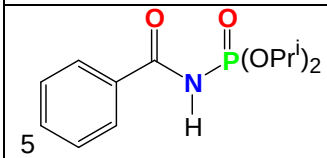	12 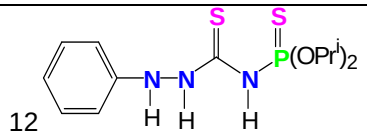	19 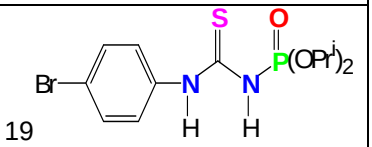
6 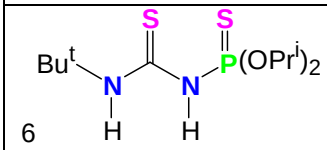	13 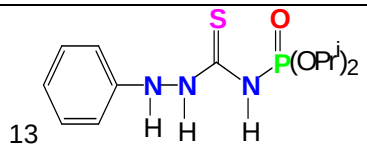	20 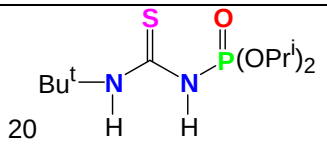
7 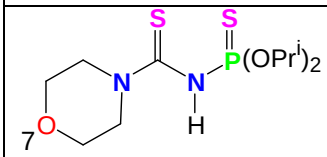	14 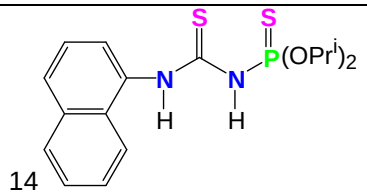	21 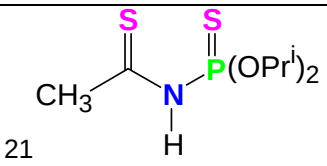

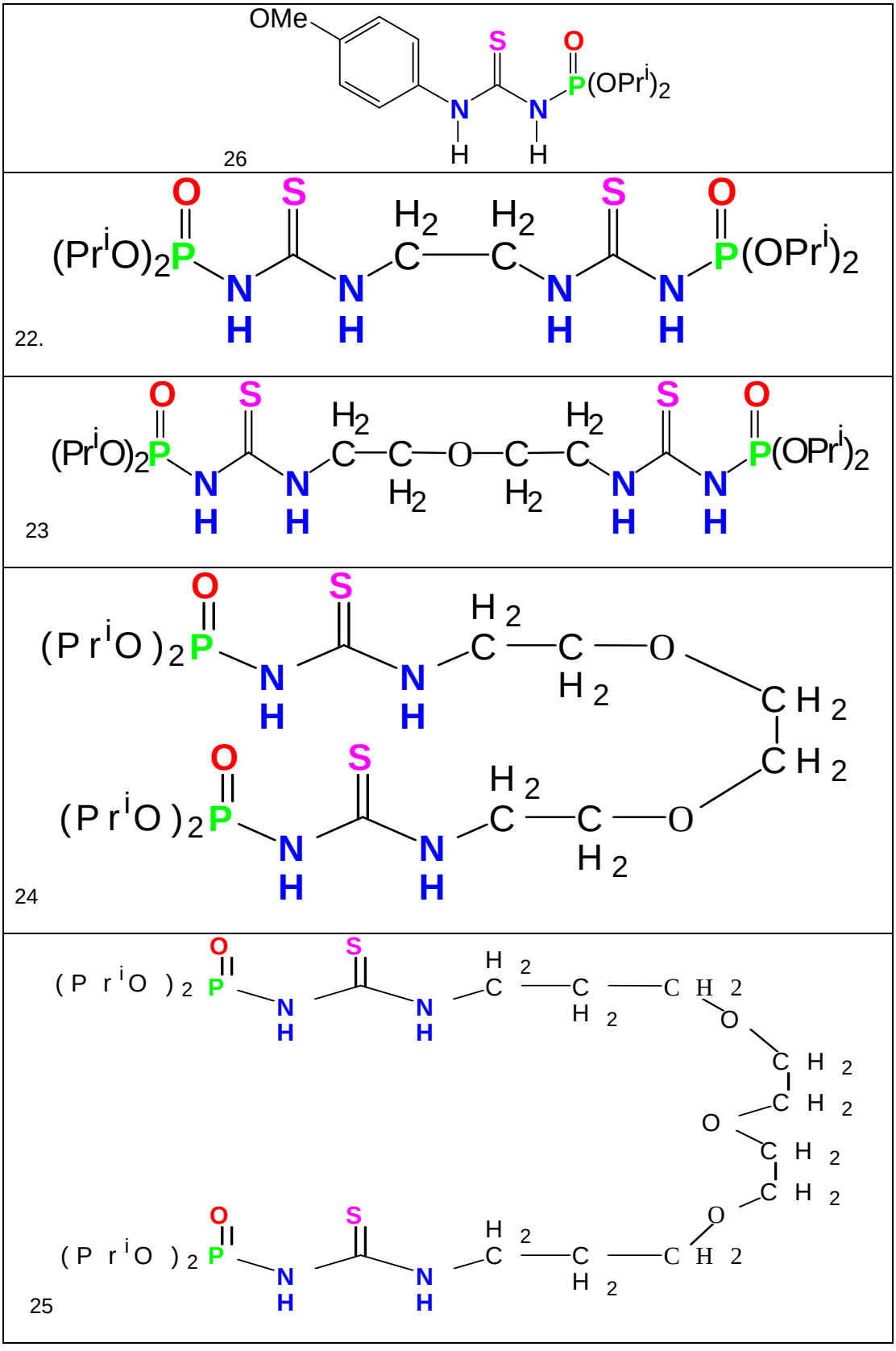
OMe
S
O
P(OPr^i)$_2$
N
H
26
(Pr^{i}O)$_2$P
H$_2$
22.
23
24
25